DRAG FORCES IN LIQUID HELIUM II

Colin N. B. Martin

A Thesis Submitted for the Degree of PhD
at the
University of St Andrews

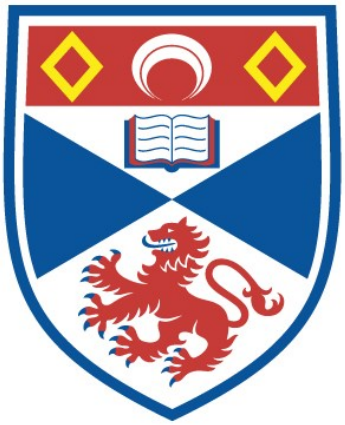

1969

Drag forces in liquid helium II

A thesis presented by

Colin N.B. Martin

to the University of St. Andrews

in application for the degree of

Doctor of Philosophy.

September, 1969

Declaration

I hereby declare that the following thesis is based upon research work carried out by me, that it is my own composition and that it has not previously been presented for a higher degree.

The research has been performed in the Department of Natural Philosophy of the United College of the University of St. Andrews and in the School of Mathematics and Physics of the University of East Anglia under the supervision of Professor D. V. Osborne.

Certificate

I certify that Colin E. B. Martin has spent six terms in the Department of Natural Philosophy of the United College of the University of St. Andrews, and three terms in the School of Mathematics and Physics of the University of East Anglia, engaged in research under my direction, that he has fulfilled the conditions of Ordinance No. 16 of the University Court of St. Andrews and that he is qualified to submit the accompanying thesis in application for the degree of Doctor of Philosophy.

[redacted]

Research Supervisor.

Statement

The study of the drag forces in liquid helium II was undertaken by me following my admission in October 1963 as a research student under Ordinance General No. 12 and as a candidate for the degree of Doctor of Philosophy under Ordinance No. 16 at the United College of the University of St. Andrews.

Personal Preface

I graduated in 1963 as Batchelor of Science of the University of St. Andrews with a second class honours in Physics. In September of that year I began research in the Department of Natural Philosophy of the United College of the University of St. Andrews under Dr. D. V. Osborne. In June 1965 I moved to the University of East Anglia, where Dr. Osborne had taken up an appointment as Dean of the new School of Mathematics and Physics. In November 1966 I finished the experimental work and since then have been working as a Scientific Officer in the Properties of Fluids division of the Fluids Group at the National Engineering Laboratory in East Kilbride.

Acknowledgements

The author wishes to acknowledge the excellent supervision of Professor D. V. Osborne, who provided ideas, help and encouragement whenever they were needed.

For the three years from October, 1963 to September, 1966, the author was supported by a grant from the Science Research Council.

CONTENTS

Page

Page

3. RESULTS

SUMMARY

Measurements of drag forces on spheres and a cylinder in open rectangular channels in liquid helium II heat flow and superflow were made at temperatures between 1.3°K and the λ-point. The drag forces were measured by the deflection of a torsion system suspended above the free surface of the liquid from a quartz fibre.

In the heat flow experiments, the drag was found to be similar to that which would be exerted by a classical fluid with the same velocity, viscosity and density as the normal component. Correlations of the drag coefficient $D/(\frac{1}{2}\rho_n v_n^2 A)$ with the Reynolds numbers $\rho_n v_n d/\eta_n$ and $\rho v_n d/\eta_n$ show that the former is much more suitable both in terms of eliminating temperature dependence and agreement with the classical value.

Above 1.6°K, a small decrease in drag with increasing velocity was usually noticed; this was attributed to the onset of turbulence in the superfluid, giving rise to a component of drag in the direction of superfluid flow. Describing the turbulent superfluid as a laminarly flowing fluid with an effective viscosity η_s makes possible an order of magnitude estimate of η_s from the decrease in drag; it is found to lie between 10 and 100 micropoise.

At temperatures nearer the λ-point, the simple two fluid description appears to become less adequate.

In the superflow experiments, the sphere and the cylinder are dragged in the direction of the superfluid flow. Correlations of drag coefficient with Reynolds number suggest values for the effective viscosity of between 20 and 100 micropoise.

In the cylinder superflow experiments, below a critical velocity of 2 ± 1 cm sec^{-1}, no drag was observable. This is attributed to an ideal flow regime and is believed to be the first direct demonstration of D'Alembert's paradox, namely that an inviscid fluid can exert no drag on a body.

1. INTRODUCTION

1.1 LIQUID HELIUM II

The He^4 molecule consists of a nucleus of two protons and two neutrons, with two electrons filling the first orbital shell. Because the electrons are tightly bound to the nucleus, the intermolecular attraction due to the London dispersion forces is weak, and the boiling point of the liquid ($4.2^{\circ}K$) is lower than that of any other substance. In the liquid, the zero point energy is comparable to the energy of binding of the molecules, and increases the molecular separation by a factor of 1.5. As a result, the liquid, except under pressure, remains a liquid down to absolute zero of temperature.

At $2.18^{\circ}K$ under its vapour pressure (the λ-point), the liquid undergoes a phase transition. The warmer phase (helium I) behaves like any other liquid, whereas the cold phase (helium II) displays a number of unique properties. In particular, although rotating cylinder measurements show a viscosity of about 10^{-5} poise, flow in capillaries is so rapid as to indicate a vanishingly small viscosity, or superfluidity; and heat flows so readily that almost no temperature gradient can be sustained in the bulk liquid. Lastly, while it is possible to sustain an appreciable temperature difference along a capillary containing helium II, this is always accompanied by a proportionate pressure difference (the fountain or thermomechanical effect).

These and other phenomena can be explained in terms of the 'two-fluid' picture. The liquid is considered to consist of a 'normal' component, containing all the entropy and having a normal viscosity, and a 'superfluid' component, having no entropy or viscosity. Writing the densities as ρ_n and ρ_s respectively, the total density is $\rho_s + \rho_n = \rho$. At T = 0 there is no entropy and so $\rho_n = 0$, whereas at the λ-point, $\rho_s = 0$. Although homogeneously mixed, the two components can flow relative to each other without dissipation; thus heat is transported by a flow of normal fluid away from the source of heat while the superfluid flows towards it, and an appreciable temperature difference is only established in a confined region, such as a capillary tube, where the normal fluid viscosity restricts its flow.

The theoretical explanation of the two-fluid model lies in quantum theory. As the temperature of the liquid is raised from absolute zero, the first thermal energy must appear in the form of quantised excitations. The first excitations to appear are longitudinal sound waves or phonons. Later, another type of excitation known as a roton is found to occur. Both types of excitation possess momenta and can be treated mathematically as particles. The normal component can thus be regarded as a gas of quantized excitations, in which viscosity arises by momentum exchange on collision.

Calculations of thermodynamic and transport properties based on the statistical mechanics of the assumed excitations give good agreement with experiment below 1.6°K. Above this temperature, owing to the increase in the density of excitations, the agreement becomes poorer, and the λ-transition cannot be explained in these terms. In fact the λ-transition is thought to be analogous to an effect which occurs in an ideal gas of bosons: as the gas is cooled, a temperature is reached at which a finite fraction of the bosons start to 'condense out' into the ground state.

The absence of viscosity of the superfluid arises from the fact that any slowing down of the liquid by a solid boundary will involve an increase in thermal energy of the liquid. This energy must be in the form of quantised excitations, and at low enough velocity, there is not enough kinetic energy of flow to create an excitation. As an associated condition, the superfluid velocity field is usually thought to be irrotional.

For sufficiently low flow velocities, the simple two-fluid picture is very successful in explaining a wide variety of experimental phenomena. In all flow experiments, however, there exists a superfluid critical velocity at which dissipation effects, often indicated by extra pressure or temperature gradients, begin to appear. In this region the two-fluid model must be modified to take account of these effects.

1.2 IDEAL FLOW

The nature of the flow of an incompressible fluid with zero viscosity is relatively easy to treat mathematically. In such flow vorticity is conserved and if the vorticity is initially everywhere zero, the flow can be described as irrotational: it is also called potential flow, because the mathematics used is similar to that used to describe electrical or gravitational fields. It can be shown that in an ideal flow no drag can be exerted on a body (D'Alembert's paradox) and, except for a semi-infinite body, such as an infinitely long cylinder or aerofoil, supporting circulation, no lift can be exerted.

Craig and Pellam (1957) suspended a pair of inclined wings in a superfluid wind-tunnel and showed that below a certain critical velocity there was no detectable lift force on the wings. Koehler and Pellam (1962) suspended a Rayleigh disc in superflow and showed that the torque exerted agreed with that predicted for an ideal fluid. Other experiments (Hussey and Reynolds, 1965; Corke and Hildebrandt, 1968) help to demonstrate the compatibility of ideal fluid theory and the behaviour of superfluid helium.

1.3 CRITICAL VELOCITIES AND SUPERCRITICAL FLOW

1.3.1 General

Landau (1941) estimated that the superfluid velocity necessary for the creation of a roton was 8×10^3 cm sec^{-1}, while a phonon requires a velocity about three times greater. Actual critical velocities were very much smaller than this, ranging between less than 1 mm sec^{-1} for wide channels and about 10 cm sec^{-1} for fine capillaries.

Onsager (1949) and Feynman (1955) showed that vortex motion in the superfluid is permissible if the angular momentum of each helium atom is quantised. In this situation $\nabla \times v_s = 0$ everywhere except at the core of the vortex line, where there is a fluid-dynamical singularity. Good evidence for the existence of such lines has been found in rotation experiments. Estimates of the critical velocity necessary for the creation of quantised vortex lines give more reasonable values, and the predicted dependence of v_{sc} on the channel dimension d, namely that $v_{sc} \times d$ is a slowly increasing function of d, is similar to that found experimentally. Many flow experiments have been carried out to investigate critical velocities and the nature of the flow in the supercritical region in different situations; because of the number of parameters which can be varied (the channel size and shape, the normal and superfluid velocities, the temperature) it is difficult to form a clear and

consistent picture of the implications of all the results. For the particular case of heat flow in wide channels ($d \gtrsim 1$ mm, mass flow $= \rho_s \bar{\underset{\sim}{v}}_s + \rho_n \bar{\underset{\sim}{v}}_n = 0$), however, it is fairly well established that the major source of resistance in the supercritical region is mutual friction between the two components (see e.g. Atkins, 1959).

The equation of motion of the two fluids are (Atkins, 1959, p.171)

$$\rho_s \frac{D\underset{\sim}{v}_s}{Dt} = -\frac{\rho_s}{\rho} \text{ grad } p + \rho_s S \text{ grad } T - \underset{\sim}{F}_{sn} (\underset{\sim}{v}_s - \underset{\sim}{v}_n) - \underset{\sim}{F}_s (\underset{\sim}{v}_s)$$

for the superfluid and

$$\rho_n \frac{D\underset{\sim}{v}_n}{Dt} = -\frac{\rho_n}{\rho} \text{ grad } p - \rho_s S \text{ grad } T + \underset{\sim}{F}_{sn} (\underset{\sim}{v}_s - \underset{\sim}{v}_n) - \underset{\sim}{F}_n (\underset{\sim}{v}_n) + \eta_n (\nabla^2 \underset{\sim}{v}_n + \tfrac{1}{3} \text{ grad.div } \underset{\sim}{v}_n)$$

for the normal fluid. These are similar to the Navier - Stokes equation except for the grad T term and F_{sn} (mutual friction), F_s and F_n; these last three are inserted to account for the extra frictional forces in the supercritical region, and are zero if the velocities are subcritical.

It is found that except in narrow channels the extra frictional forces in heat flow experiments are independent of channel width, which implies that F_s and F_n are negligible compared with F_{sn} in wide channels.

Mutual friction is usually measured by the increase in the temperature gradient necessary to sustain flow in the supercritical region. This temperature gradient is found to obey the relation grad $T \doteq DW^n$ where W in the heat current density, D is a temperature dependent constant, and $n \doteq 3$.

1.3.2 Experiments

Wide channel critical and supercritical heat flow was investigated extensively by Vinen (1957 a, b, c, d). He studied mutual friction by propagating second sound (entropy waves) transversely in a rectangular channel carrying a heat current, and found that the attenuation constant varied as $(W - W_c)^2$ when $W > W_c$, the critical heat flow; W_c is small and can be ignored for large heat currents. He proposed that mutual friction should be regarded as an essentially linear force $F_{sn} = A\rho_s\rho_n (| \underset{\sim}{v}_s - \underset{\sim}{v}_n | - v_c)^2 (\underset{\sim}{v}_s - \underset{\sim}{v}_n)$. His explanation is that in the supercritical state, the superfluid consists of a tangled mass of quantized vortex lines whose length per unit volume varies as the square of the heat current. Mutual friction then arises as a result of collisions between the excitations which comprise the normal fluid, and vortex lines, which will have the same average velocity as the superfluid.

He was able to study the rate of growth and decay of vorticity in the superfluid heat currents around the critical, and from this the nature and magnitude of the critical velocity. For a channel of 2.4 x 6.45 mm cross section at 1.41°K, there appeared to be a sharp transition between a state with no detectable vorticity and fully developed vorticity; at higher temperatures, however, some vorticity was present in the subcritical region, and above 1.55°K no discontinuous

increase in vorticity was observable. In a wider channel (4.00 x 7.83 mm) this 'blurring' started at a temperature which was lower by 0.1°K.

By comparing the nature of the mechanisms which would cause vorticity to increase or decrease he was able to develop a semi-empirical equation for the time dependence of the vorticity which explained the principal features of the results.

Chase (1962) studied the temperature gradient in heat flow in channels of 0.8 mm diameter. The critical velocities are well defined to much higher temperatures, although the rise in the temperature gradient appears to be never actually discontinuous. The temperature dependence of the critical velocity appears to fall into two regions : below 1.7°K, v_{nc}, the velocity of the normal fluid at the critical heat current, is more or less constant, whereas above this temperature it decreases steadily towards zero at the λ-point. He found that in the low temperature region a critical Reynolds number defined by $R_c = \rho v_{nc} \frac{d}{\eta_n}$, where ρ is the total density, η_n the viscosity of the normal fluid, and d the channel diameter, has a value close to 2100: this value is typical of that found for the breakdown of laminar flow of ordinary fluids in pipes. Critical velocities in another set of experiments conducted in channels of varying cross-sectional shapes (Chase, 1963) could also be explained in terms of classical critical Reynolds numbers.

This suggests that the critical velocity observed here is characterized by the onset of turbulence in the normal fluid, although it is not clear why, if this is so, it is necessary to use the total density ρ rather than ρ_n.

In the temperature region above 1.7°K, where v_s/v_n is larger, he suggested that it was now the superfluid velocity which became critical.

A Reynolds number containing the total density was also used by Staas, Taconis and Van Alphen (1961) in a series of flow experiments in wide capillary tubes (82 - 255 microns diameter); they found that the variation of pressure head with flow velocity was similar to that found with an ordinary fluid in the Poiseuille and Blasius regions, but the minimum critical Reynolds number was 1200, about half the minimum classical value. This description was found to hold for a range of situations between isothermal flow ($\underset{\sim}{v}_s = \underset{\sim}{v}_n$) and heat flow ($\rho_s \underset{\sim}{v}_s + \rho_n \underset{\sim}{v}_n = 0$).

Allen, Griffiths and Osborne (1965) observed the forces on a 1 micron diameter quartz fibre hanging in a wide channel carrying a heat flow. At 1.3°K they found two critical velocities. Above the lower one the superfluid was turbulent, whereas above the upper one the normal fluid also appeared to be turbulent.

Vicentini - Missoni and Cunsolo (1965) measured the drift velocities of positive and negative ions in heat currents in wide channels. At

temperatures below 1.35°K they again found two critical velocities, and showed that at large heat current densities the temperature gradient and the normal fluid velocity were not uniform along the channel.

Ricci and Vicentini - Missoni (1967) investigated the velocity fields in heat flow in rectangular channels 4 x 8 mm, again by measuring the drift velocities of positive and negative ions. They found that above a superfluid velocity of 0.07 cm sec^{-1} (independent of temperature) the normal fluid velocity and the temperature gradient varied with distance along the tube in a strongly non-linear manner.

1.3.3 Tough's Analysis

Tough (1966) attempted to correlate the results of various experiments within a uniform description of the onset of different types of dissipation in the flow of helium. He assumed the existence of two critical velocities in heat flow, the lower one being associated with the superfluid and the higher one with a classical Reynolds number involving the normal fluid velocity and the total density. He attempted to justify the use of the total density in terms of coupling of the velocity fields by mutual friction: a perturbation of the normal fluid velocity field must be accompanied by a similar perturbation in the superfluid velocity field, and vice versa; the relative

magnitude will depend on the degree of coupling. If the coupling is strong, then any perturbations in the normal fluid velocity field will in fact involve perturbation of the whole fluid and the stability of laminar flow against such perturbation will depend on a Reynolds number involving the total density. At higher temperatures, the normal fluid velocity becomes smaller in relation to the superfluid velocity, and the effects of the onset of turbulence in the normal fluid are masked by the magnitude of the mutual friction term.

This analysis succeeds in explaining and reconciling a number of experimental results in a qualitative way, although the variety of experiments and the number of parameters which can be varied precludes the possibility of a comprehensive or quantitative correlation.

The non-linear effects mentioned at the end of the previous section (1.3.2) demonstrate that any theory based on the lines so far proposed will be inadequate in describing some real situations, and help to explain some of the quantitative inconsistencies already encountered.

1.3.4 Superfluid Eddy Viscosity

The term F_s in the thermohydrodynamical equations (1.3.1) describes processes inside the superfluid when the critical velocity is exceeded. When a classical fluid becomes turbulent, the extra resistance to flow is sometimes accounted for in terms of an extra effective viscosity, known as the eddy viscosity. F_s is often interpreted as being due to a similar effect in the superfluid. Vinen (1961) made an order of magnitude estimate of the superfluid eddy viscosity η_s in terms of the vortex line theory: he deduced that it was unlikely to be less than about 20 micropoise. Deductions of the magnitude of η_s from experiments vary from a few micropoise (e.g. Brewer and Edwards, 1961) to around 100 micropoise.

Hidder and Fairbank (1962) measured the pressure difference arising from superfluid flow in a tube 1.1 mm in diameter. If their results can be interpreted in terms of a homogeneous superfluid viscosity, then at 1.3°K, $\eta_s = 56.5\ (v_s - v_{sc})$ micropoise if $v_s > v_{sc}$ (v_s, v_{sc} are in cm sec^{-1}). With a critical velocity v_{sc} of 0.115 cm sec^{-1}, this gives η_s as 4.8 micropoise at 0.2 cm sec^{-1}, 22 micropoise at 0.5 cm sec^{-1} and 39 micropoise at 0.8 cm sec^{-1}.

1.4 CLASSICAL DRAG ON SPHERES AND CYLINDERS

1.4.1 The Dimensionless Groups

For incompressible viscous flow, a characteristic flow pattern in a simple geometrical situation - that is one which can be defined by one length parameter - is uniquely defined by the dimensionless Reynolds number $R = \rho vd/\eta$ (Reynolds' principle of similarity). In the case of flow in an infinite pipe or channel, the characteristic dimension d is the diameter of the pipe or channel; for flow round an obstacle of a given shape, d is a dimension of the obstacle: in the case of a sphere or cylinder, d is the diameter.

The drag force on a submerged obstacle can be reduced to a dimensionless form by dividing by the group $\rho v^2 d^2$; this leads to the definition of a dimensionless drag coefficient $C_D = \text{Drag}/\frac{1}{2}\rho v^2 A$ where A is the frontal area exposed by the body to the flow direction.

Since the Reynolds number defines the characteristic flow pattern for a given shape of obstacle, it is to be expected that at a given Reynolds number the drag coefficient will always be the same; in other words the drag coefficient will be a unique function of the Reynolds number.

It is found from experimental measurements that C_D is indeed a unique function of R; Figures 1.1 and 1.2, which are taken from Schlichting (1960), p. 16, show the functional relationships for spheres and cylinders.

1.4.2 Change of Flow Pattern with Reynolds Number

The detailed nature of flow round spheres and cylinders is discussed extensively in Goldstein (1938) and Schlichting (1960). At sufficiently low Reynolds numbers ($R < 0.5$) it is possible to calculate the flow pattern and drag for cylinders and spheres. As the inertial forces become more important than the viscous forces ($R > 1$) calculation becomes too difficult. Experimental observation, however, reveals the main features of the flow pattern and the distribution of tangential and normal forces which constitute the drag.

The net drag consists of two components; the pressure or form drag, which is the net longitudinal force resulting from pressure variations over the surface, and skin friction drag, which is the integral of the longitudinal components of the tangential viscous shearing forces. At low Reynolds numbers (e.g. the Stokes region for a sphere) the drag is entirely due to skin friction. As the Reynolds number increases, the pressure gradient which the boundary layer has to overcome to follow the rear profile of the sphere or cylinder becomes too great, the boundary layer separates from the wall not far behind the plane of maximum cross-sectional area, and an eddying wake is formed. The suction in this wake causes form drag which becomes increasingly more important than skin-friction drag: at a Reynolds number of 10^4 the drag on a cylinder is almost entirely form drag.

At a critical Reynolds number of about 4×10^5, the boundary layer becomes turbulent. Because the turbulent mixing in the boundary layer increases the forward tangential force exerted by the external flow on that part of the boundary layer closest to the wall, the point of separation of the boundary layer moves considerably further back, the diameter of the wake is markedly reduced, and the drag coefficient decreases by a factor of 4.

1.5 DRAG EXPERIMENTS IN LIQUID HELIUM

Laing and Rorschach (1961) measured the rate of fall of spheres of diameter around one inch in liquid helium at Reynolds numbers of around 10^6. The drag coefficient correlated against a Reynolds number involving a total density was between 0.4 and 1.5, somewhat higher than the classical value. The speed of the experiments was too great for the boundary layer to have time to become turbulent, which partly accounts for the high values. No temperature dependence was apparent.

Dowley and Hollis Hallet (1961) measured the drag on a 2 mm diameter sphere in a wind tunnel formed by the annular gap between two concentric cylinders. It was found that the results could be correlated by using an effective density $\rho_e = \rho_n + 0.25\, V^{\frac{1}{2}} \rho_s$. This led to a drag coefficient smaller than that found for classical liquids by a factor of 3 or 4 at Reynolds numbers between 1000 and 2000, although at Reynolds numbers above 6000 the drag coefficient was not much less than the classical liquid value.

Griffiths (1963) measured the drag on a quartz cylinder of 0.9 micron diameter at a Reynolds number less than 0.4 in heat flow. The normal fluid viscosity deduced from the drag was a factor of 5 larger than the accepted values. No convincing explanation was found for this discrepancy.

2. EXPERIMENT

2.1 GENERAL

Measurements were made of the drag exerted on spheres in heat flow and superflow in open rectangular channels. In the heat flow experiments three spheres with diameters of 395,500 and 1075 microns were used in a channel 4.76 mm wide and 2.5 mm deep. In the superflow experiments, one sphere of diameter 890 microns was used in a channel 3.27 mm wide and 2.5 mm deep. The flow velocities ranged up to about 30 cm sec^{-1}, and the drag forces measured varied between about 10 and 8000 microdynes. The temperatures varied between 1.5°K and more than 2.0°K.

Heat flow and superflow measurements were also made on a cylinder of 0.18 mm diameter and immersed length 18 mm in a channel 1.6 mm wide and 20 mm deep.

Details of the individual experiments are given in 3.2.

A torsion system was used to measure the drag. The basic features (Fig. 2.1) were a vertical glass rod, at the base of which was a thin horizontal copper disc (used mainly for electromagnetic damping) and horizontal arms which each carried a sphere or cylinder; one was used for measurements, the other was a 'dummy'. The dummy was used for balance, and to provide a degree of symmetry in electrostatic and magnetic fields, and sometimes as a second body on which to make measurements.

The system was suspended on a quartz fibre (1.5 - 3 cm long, 2½ - 5 microns thick) from a torsion head which could be rotated, raised and lowered.

The Kapitza resistance of brass is sufficiently high for a negligible fraction of the heat supplied to be lost through the walls of the channel (see 3.3.4).

It was necessary to keep the level of the liquid in the channel constant, and this was achieved by using a separate constant level bath within the helium dewar.

The apparatus which is described in the following section was developed after considerable difficulty had been experienced in earlier designs with spurious torsional forces. A description of those difficulties is given in Appendix A.

2.2 APPARATUS

2.2.1 External Apparatus

A conventional system was used for containing and cooling the liquid helium. The helium dewar vessel was made of monax glass, silvered apart from vertical diametrically opposed clear strips, 1 cm wide; the strips were later widened to about 3 cm over a height of about 8 cm from the bottom of the vessel to improve visibility in the experimental region.

The temperature of the liquid helium was deduced from the vapour pressure using the Van Dijk-Durieux (1958) scale. The pressure in the dewar was measured by a mercury manometer and an oil (di-n-butyl-phthalate) manometer in parallel. The oil manometer could be brought into operation at pressures below 38 mm Hg, and the absolute pressure could then be determined with sufficient accuracy down to the minimum pressure of 1.25 cm oil corresponding to a minimum temperature of 1.26°K. A vacustat was used to correct for the non-zero pressure in the evacuated limb of the oil manometer.

Two 2" lengths of flexible bellows pipe were inserted in the pumping line to isolate the cryostat from pump vibrations, and the rate of pumping could be controlled by a 2" valve or a parallel fine control valve.

2.2.2 Constant Level Bath

The constant level bath (Fig. 2.1) was designed, for reasons given in Appendix A, to be as isolated as possible from the rest of the dewar. It consisted basically of an internally electrically conducting pyrex beaker sealed off by a brass cover, or top-plate, which was supported by a $\frac{1}{2}$" thin-walled stainless steel tube.

The top rim of the beaker was ground flat and smooth, as was a rim on the base, and the beaker was pulled up in a cage onto a 1/16" indium ring in a groove in the new bath top-plate. The cage consisted of six lengths of 8 B.A. studding and an annular baseplate. Lugs were used for the studding holes in the top-plate and the baseplate in order to leave as much horizontal area clearance as possible between the bath and the dewar wall. The studding struts were arranged as shown (Fig. 2.2) to allow good visibility. An indium ring was used between the baseplate and the bottom of the beaker to protect the latter from the possibility of local stress.

The method used for making the inside of the Pyrex beaker electrically conducting was that described by Gamer (1953). The beaker was placed inside an oven and brought to 400°C. Stannic chloride crystals in a Pyrex tube were melted in a bunsen flame, and the fumes were blown into the centre of the beaker. The result was a surface conductivity of not more than a few ohms per square, with a negligible loss of transparency.

2.2.3 Constructional Details

Details of the final arrangement of the experiment are shown in Figures 2.1 and 2.2. The channel and magnet are bolted to a 1/16" brass strip, which is in turn bolted to a flanged tube, I.D. 1/8"; this tube is bolted by 3 x 10 B.A. bolts to the bath top-plate. A 1/8" O.D. stainless steel tube with a funnel at the top receives liquid helium from the filling fountain pump and conducts it into the flanged tube. These tubes also carry all the electric wiring for the bath. At the same radius, 45° clockwise, is the emptying fountain pump.

When transferring liquid helium into the dewar it is necessary to ensure that the liquid reaches the space below the bath. A funnel directly below the filling hole receives the tip of the transfer tube, and the tube below conveys the liquid past the bath to the space at the bottom.

The top of the stainless steel ¼" tube is soldered into the brass endpiece, which is screwed and sealed against the cryostat cap as shown. The torsion head, which in the top region is a 1/8" stainless steel rod, passes through an O-ring seal and through two bearings.

A remote control device is used for twisting the torsion head, and the angle of twist can be read from a long pointer attached to the torsion head.

2.2.4 Channels

Three channels were used over the course of the experiments. Details are shown in Figures 2.3 - 2.5. The experiments fall into two categories, heat flow and superflow. In the superflow experiments the fountain effect is used to set up a flow such that the net velocity of the normal fluid in the channel is zero, while the superfluid has a net velocity towards the heater. Channel I was used entirely for normal fluid experiments with spheres. Channel II was used entirely for superflow experiments with spheres and in Channel III both types of experiments were carried out with cylinders.

The heater in Channel I consisted of a bundle of insulated eureka wire compressed into a rectangular slab which fitted against the end wall of the channel. For heat flow experiments in Channel III the heater was 46 gauge eureka wound uniformly on the front of a strip of Melinex polyester film to provide even heating over the depth and breadth of the channel.

In the superfluid channels, the heater was sealed off from the rest of the channel by a sintered glass filter; in Channel II the filters, which were placed at each end of the channel, had a maximum pore size of 15 microns, and were 3 mm thick, and in Channel III, 2 microns and 0.8 mm. In Channel II, no very satisfactory way of sealing round the filter and round the 'cap' was found, and it is

possible that there was some leakage. In Channel III, the gaps were sealed by 1/32" indium washers, and an airflow experiment at room temperature indicated that these were efficient.

The fluid from the heater chamber was directed through a pipe and allowed to drip or pour back into the bath. For flow calibration purposes, the fluid could be collected in a glass bucket, which could be emptied by its own fountain pump. Owing to shortage of space, flow calibration and drag measurement could not both be carried out during the same run.

2.2.5 Purpose of Channel III

If one wishes to measure the small drags which will occur at sub-critical velocities, the spheres used in Channel I give an unsatisfactorily low signal to noise ratio. Increasing the size of the sphere to overcome this will eventually mean increasing the area of the channel, which will in turn reduce the critical velocity and hence the subcritical drag, so that nothing is gained. On the other hand, if the drag on a cylinder in a deep narrow channel is measured, the channel critical velocity is independent of the depth of the channel (Schlichting, 1960, p.386); so the sensitivity can, in principle, be indefinitely increased by deepening the channel and lengthening the cylinder.

2.2.6 Quartz Fibres

The method used for manufacture was that described in Strong (1938), namely blowing the fibre out in an oxy-gas flame. This was straightforward except that the range of thickness (3 - 4 microns diameter) which was usually required was difficult to obtain.

Torsion constants were measured approximately by timing oscillations of a small bar. Strength testing - checking that the fibre would support about twice the weight which it would be required to support - was abandoned when it was realised that the uniformity of a fibre was sufficient for the strength to be determined from the torsion constant.

Initially the fibres were attached at the two ends by using tiny hooks and melting shellac onto the point of attachment. Later a simpler approach was evolved; the fibre was stuck against a stub of copper wire with nail varnish. Judicious application of acetone ensured a clearly defined demarcation between that part of the fibre which can twist and that which is held rigid.

Centering the fibre with respect to the torsion head is done by bending the wire until rotation of the torsion head causes no sideways movement of the fibre as viewed through a cathetometer.

The torsion constant of the inserted length was determined by measuring the period of oscillation T_1 of the suspended system, then adding a ring whose moment of inertia I_2 could be calculated, and again measuring the period T_2. Then if I_1 is the unknown moment of inertia of the suspended system, and k the torsion constant of the fibre:-

$$I_1 = \frac{kT_1^2}{4\pi^2} \; ; \; I_1 + I_2 = \frac{kT_2^2}{4\pi^2}$$

$$\text{so} \quad k = \frac{4\pi^2 I_2}{T_2^2 - T_1^2}$$

2.2.7 Manufacture and Attachment of Spheres and Cylinders

Spheres were made by melting thin bare copper wire in a bunsen flame. The shape and surface achieved by this method, especially for the smallest ones, was very good; the larger ones tended to have small flaws on the surface probably due to oxidation; and to make the largest one, 1 mm diameter, silver was used.

The wire from which the sphere was made was also used as the vertical support for the sphere. The top of this thin support was glued onto a stiffer (36 g) horisontal copper cross arm, which was in turn araldited onto the copper disc. Silver Dag was painted over the araldite and glue to discourage static.

Cylinders were made by drawing out fused quarts in a hot oxy-gas flame; these were then glued directly onto the cross arm.

2.2.8 Electrical Heaters and Superconducting Electromagnet

Electrical heaters were used in the channel, the two fountain pumps and the main helium dewar. A super-conducting electromagnet, consisting of 250 turns of niobium with a soft iron core was also used. A 10 ohm Allen-Bradly carbon resistor in a wheatstone bridge was used as a thermometer to aid manual thermostating.

All components except the Allen-Bradley were supplied from a 6 V DC power supply, had a common earth, were controlled by switches and potential dividers and/or series rheostats, had resistance ratings of between 10 and 80 ohms (except of course the magnet whose resistance fell to zero), were current-monitored and had leads of 34 and 36 gauge eureka or constantan from the cryostat head.

Resistance-free contacts with the niobium of the electromagnet could be obtained by copper-plating or, more satisfactorily, by spot welding platinum: either of these could then be soft soldered.

To avoid having to know the resistance of the channel heater, which varies somewhat with the temperature, the voltage across the heater was measured along with the current. These were the only electrical measurements which required any degree of accuracy.

2.2.9 Electromagnetic Damping

A superconducting electromagnet was used to eliminate 'wobble' of the suspended system, and to damp down torsional oscillations.

A thin horizontal copper disc (Fig. 2.1) was mounted on the bottom of the glass rod, mostly for electromagnetic damping and partly to add to the mechanical stability in the gravitational field. The electromagnet was mounted with its axis vertical and central, a millimetre or so beneath the copper disc, and in fact the magnet could be used as a shelf on which to lower the disc when it was desired to take tension off the quartz fibre.

The field strength at the top centre off the magnet was $\frac{1}{2}.4\pi \cos\phi$. ni oersted where n = no. of turns/cm. $\doteq 100$, $\cos\phi \doteq \frac{3}{4}$ and i is the current in e.m.u.; so $H \doteq 50$ x (current in amps).

Two amps could be passed, but optimum damping usually occurred with 0.2 amps, or $H \doteq 10$ oersted.

2.3 MEASUREMENT

2.3.1 Measurement of Torque

Back lighting from the far side of the dewar, through heat-absorbing glass and a ground glass screen, showed a small pointer on the edge of the copper disc in silhouette; viewing the pointer through a cathetometer with an eyepiece scale then gave the deflection in arbitrary units. The size of these units could be calibrated by comparing degrees of twist of the torsion head to the movement of the scale.

The method of measurement of torque was basically a null one, although small changes in torque were observed directly. For small angular deflections, the movement of the pointer on the eyepiece scale was noted, but after the system had been allowed to twist through some 5°, the torsion head was twisted to bring the pointer back to its original position. Sometimes five or more measurements were made between adjustments of the head, sometimes only one or two. This was done to save the time involved in adjusting the head and waiting for the system to settle again. After the torsion head had been twisted back, a 'null' reading was usually taken at the same heat current as for the previous 'direct' reading. Because these readings almost always agree to within a few per cent, it is justifiable to consider the 'direct' readings as valid, in spite of the change in position of the sphere in the channel which occurs with a net twist of the suspended system.

Three principal difficulties were encountered while measuring drag: the liquid level had to be kept constant, the temperature had to be kept constant and the suspended system had to remain in steady control. Conditions were most difficult while working with the large heat currents; the level went down fast owing to evaporation, necessitating frequent refills with the fountain pump, and this in turn caused temperature fluctuations; and the liquid helium became used up in too short a time. Trying to work near the λ-point was especially wasteful, as the fountain pump becomes inefficient in this region. With sufficient concentration and acquired skill, however, the fluctuations in temperature and level could usually be kept to within a range where they did not constitute a substantial part of the eventual uncertainty in the results.

A second cathetometer, with a vertical eyepiece scale, was used to monitor the level. Except with very large heat currents it was possible to keep the level within $\pm$ 0.2 mm of the required level. The temperature was controlled manually by altering the speed of pumping. This required effort and experience, but an automatic thermostat capable of absorbing the temperature surges resulting from the use of the filling fountain pump would have been very difficult to construct. The temperature could be controlled to less than 0.01°K for most of the range, and less than 0.005°K for the lowest temperatures.

Temperatures or levels which were outside their specified ranges at the time of taking a deflection reading were noted.

Apart from the torque exerted by the fibre and the drag on the cylinder or the sphere, and its supporting wire, several types of forces acted on the suspended system. The possibility of electrostatic forces was theoretically almost eliminated since all surfaces on and in the vicinity of the suspended system were made conducting except for the insulation on the wiring for the heater and its leads, and the fibre itself. Torque resulting from magnetic forces was present but appeared to be independent of the deflection of the system over the range in which measurements were made. Convection currents must have been present in the vapour. Surface tension forces pulled the supporting wire, or with Channel III, the cylinder, against the channel walls if it was allowed to approach them. So great was this effect with Channel III that the cylinder was unstable in the centre of the channel, and the channel had to be made T-shaped (Fig. 2.5) to bring the walls at the surface sufficiently far apart for drag measurements to be made. In the other channels, mechanical constraint limited the range of deflection and kept the wire out of range of the wall.

Although the position of the pointer on the scale could often not be read to less than 0.5 degrees, a distinct lack of repeatability of the equilibrium position of the disc for zero heat current was sometimes found, amounting occasionally to more than 1 degree. This suggests the presence of small electrostatic forces, as this is the only type of force likely to change irreversibly. As might be expected, lack of repeatability also occurred with drag measurements, the order of magnitude being indicated in the graphs (Figs. 3.1 - 3.16); it is probable, however, that different flow patterns in the channel are largely responsible for this. A fuller analysis of the various uncertainties involved in the measurements is given later (3.5).

Drag measurements were obtained by working at constant temperatures and increasing heat flow. The results of one experiment then consisted of deflection readings at about 15 values of heat current. The table below shows readings taken at 1.39° in Channel I with the large (1075) silver sphere.

Experiment No. 29

Manometer Pressure in cm oil	Heater Current in m A	Deflection in Divisions	Torsion Head Reading in Degrees	Level in Divisions
2.5	0	52.0	95	51.2
	4	51.0		
	6	48.8		
	8	50.8	90	
2.55	10	50.8	85	
	11	50.8	80	
	12	52.0	75	50.9
	13	52.7	70	
2.6	14	52.8	65	
	15	51.0	60	
2.6	16	50.8	50	49.2
	18	53.0	40	51.0
	20	50.8	25	49.7

In this particular experiment, because the sphere is large and the temperature low, a large drag is obtained with a moderate heat input and the torsion head has to be twisted for almost every reading. Calibration carried out at zero heat flow and confirmed in other heat

flow experiments, shows that 2 divisions deflection = 3 degrees to within 10%; thus the total deflection can be calculated from the two deflection readings. For these readings only the change in value from that at zero heat current is relevant, the absolute scale readings have no significance.

The level divisions are equivalent to 0.21 mm; thus a fluctuation of 1 division in a total depth of 2.5 mm will cause an 8.4% change in the velocity if the velocity is uniform across the channel. In the graph (Fig. 3.3) corrections have been made for the fluctuations in level. In most other experiments this correction is not necessary, as it is rendered trivial by a combination of better control of level and greater scatter of experimental points.

2.3.2 Superfluid Experiments in Channel II

Channel II was designed for measuring the drag on a sphere in a superflow. The rounded entrance and exit to the channel and its narrowness are designed to raise the velocity at which the superfluid velocity becomes critical. The pipe is arranged to discharge into a 'bucket' for calibration purposes.

The main difficulty with this experiment was that no fluid emerged from the pipe until a finite amount of power was supplied to the heater; also the rate of increase of liquid flow with heat supplied was considerably less than that predicted for an ideal system.

2.3.3 Calculation of Superfluid Velocity

Assuming the temperature of the fluid emerging has not been raised above the ambient temperature, (T), one can imagine that fluid at $0^{\circ}K$ is drawn through to the heater and heated to T. For unit area, mass heated per second $= \frac{W}{ST} = \rho_s v_s$ where v_s is the average superfluid velocity.

Ignoring the small change in total density between $0^{\circ}K$ and T, volume emerging per second

= volume passing through filter per second $= \frac{W}{\rho ST}$ per unit area.

If A is the cross-sectional area of the flow, then

$$W = wA$$

$$\text{so volume/second} = \frac{W}{ST}$$

$$\text{and } v_s = \frac{1}{A}\,\frac{\rho}{\rho_s}\,\frac{W}{\rho ST} = \frac{\rho}{\rho_s}\,v_n$$

where v_n is the equivalent average normal fluid velocity for the same W.

2.3.4 Superfluid Experiments in Channel III

Channel III was designed to be convincingly leaktight both between the heater chamber and the channel and between the heater chamber and the bath, $\frac{1}{32}$" indium ring seals being used in each case. The efficacy of the seal was crudely tested at room temperature by comparing the rate of loss of an overpressure of air through the channel filter and through a slab of filter material. The agreement was good, suggesting that there were no leaks.

In spite of these precautions, the difficulties which were present in Channel II were still present, though on a smaller scale. This can be seen in the calibration graph (Fig. 2.7).

An assessment of the calibration difficulties is given in Appendix C.

3. RESULTS

3.1 GENERAL

3.1.1 Heat Flow

As expected, a force was exerted on the spheres and cylinder in the direction of normal fluid flow. Graphs of drag force against calculated normal fluid velocity are shown (Figs. 3.1 to 3.16) for a number of experiments.

It can be seen that the drag is proportional roughly to the velocity or the square of the velocity. At very high velocities (e.g. Expt. 47, Fig. 3.7) the dependence appears to be less than linear; this is caused by the fact that the normal fluid velocity is calculated from the heat input, whereas at high heat current densities a large temperature gradient is set up, and a proportion of the heat is lost by evaporation and leakage through the walls.

In the graphs above 1.6°K (Figs. 3.1, 3.5, 3.15, 3.16) for drag on spheres a 'kink' in the curve is apparent. This is discussed later (3.4.2) and shown to be probably caused by the onset of superfluid turbulence.

The results of the successful heat flow experiments were corrected for various effects (3.3) and correlated in terms of the dependence of drag coefficient on Reynolds number (3.4.1).

3.1.2 Superflow

It was found that the superfluid exerted a drag on a sphere in the direction of flow of the superfluid; a force was also exerted on the cylinder, except at very low velocities. Drag graphs are shown in Figures 3.12 and 3.13.

For the sphere drag experiments in Channel II, the flow velocity calculated from the assumption that all the heat was being used to drive the superflow was about five times greater than the calibrated velocity, leakage of fluid from the heater chamber was suspected, and the drag velocity graphs tended to be noisy and inconsistent, so no great reliance is to be placed on these results.

For the cylinder experiments in Channel III, the sealing was more effective and the calculated velocity was about twice the calibrated velocity. The low velocity region where no drag was observed is considered to correspond to an ideal flow regime, since an ideal fluid can exert no drag on a body.

3.2 SUMMARY OF EXPERIMENTS

3.2.1 General

The results of 34 drag experiments have been analysed and correlated. 21 experiments on spheres and eight on cylinders are in heat flow, and three experiments on spheres and two on cylinders are in superflow. Details of the experiments are listed below.

All measurements made have been included in the correlations, except when experimental conditions were so difficult as to produce excessive noise in the drag velocity graphs, or when some important parameter (e.g. heater power) was not known with sufficient accuracy.

3.2.2 Dimensions of Spheres, Cylinders and Channels

Spheres	Diameter (microns)	Stem Diameter (microns)
1	395	50
2	500	50
3	1075	180
4	890	50

Height of sphere centres above bottom of channel 1.5 mm.

Cylinder diameter 180 microns

Cylinder immersed length 1.8 cm.

Channels	Width (mm)	Depth (mm) of Liquid
I	4.76	2.5
II	3.27	2.5
III	1.60	20

3.2.5 Drag on Spheres in Heat Flow (Channel I)

Experiment Number	Figure	Temperature (°K)	Sphere
19		1.32	3
20	3.1	1.69	3
21	3.2	1.32	1
26		1.39	1
27		1.30	1
28		1.30	3
29	3.3	1.39	3
30	3.4	1.50	3
31	3.5	1.66	3
32		1.87	3
33	3.6	2.00	3
46		1.42	2
47	3.7	1.31	2
48		1.37	2
49		1.43	2
50		1.68	2
51	3.8	1.58	2
52	3.8	1.58	2
53		1.37	2
54		1.50	2
55	3.8	1.58	2

Two experiments which are illustrated but not correlated, owing to uncertainty in the heat input:

11	3.15	2.00	2
14	3.16	1.64	2

3.2.4 Cylinders in Heat Flow (Channel III)

Experiment Number	Figure	Temperature (°K)
58		1.32
59		1.46
60		1.67
61		1.67
62		1.67
63	3.9	1.31
64	3.10	1.46
65	3.11	1.69

3.2.5 Sphere in Superflow (Sphere 4 in Channel II)

Experiment Number	Figure	Temperature (°K)
38		1.26
43	3.12	1.35
44	3.13	1.30

3.2.6 Cylinders in Superflow (Channel III)

Experiment Number	Figure	Temperature (°K)
66		1.31
67	3.14	1.31

3.3 CORRECTIONS

3.3.1 General

Corrections have been made to allow for the various factors which affect the drag. In the sphere experiments, it is necessary to allow for the drag on the supporting stem, which is about three times larger per unit area than the drag on the spheres. 'Blockage' correction, to allow for the finite width of the channels is also made, although it turns out to be less significant. Heat loss by evaporation and leakage through the walls is important at large heat current densities. Allowance is made for the effect of temperature on the fibre constant.

In Channels I and II, it is assumed that the velocity profile is effectively flat, so that the velocity at the spheres will be equal to the mean velocity. In the normal flow experiments in Channel III, however, it is shown (3.3.7) that for an ordinary fluid, the velocity profile would be almost parabolic at the cylinder but for the presence of the cylinder, so that the velocity at the centre of the channel would be almost 1.5 x the mean velocity. However, it seems likely that the cylinder will modify the upstream profile to such an extent that the relevant effective velocity will be closer to the average velocity. Because the effect of velocity profile cannot be estimated, no correction has been made for it in the calculations of drag coefficient.

No correction has been made for 'end effects', either in the cylinder experiments, or for the stems in the sphere experiments.

3.3.2 Blockage Factor

Flow past an obstacle is usually considered when any solid boundary is well away from the obstacle. In the case of flow in a channel, the presence of the channel walls will influence the flow since :

(1) The longitudinal velocity averaged over the cross-sectional plane perpendicular to the channel walls, will be greater at the obstacle since the available area is reduced by the cross-sectional area of the obstacle.

(2) The velocity vector must be parallel to the channel wall in the vicinity of the wall.

The magnitude of this effect cannot be calculated at the relevant Reynolds numbers ($R > 5$) since the flow pattern itself cannot be calculated. Experiments on cylinder drag at low Reynolds numbers (10^{-5} to 10^{2}) by White (1945) revealed that at $R = 10^{-4}$, a blockage ratio (cylinder diameter/channel diameter) of 1/500 doubled the drag; however, as the Reynolds number increased, and the inertial effects became more important than the viscous effects, the effect of the channel walls decreased, so that for a blockage ratio of 1/50 and a Reynolds number of unity the effect on the drag was less than a few percent. Perkins and Leppert (1964) measured the effect on velocity distribution round a cylinder of blockage ratios of 0.1 to 0.4 at

Reynolds numbers of 10,000 - 50,000 and compared the corrections to the Reynolds number with those arrived at by other workers. At a blockage ratio of 0.1, the Perkins and Leppert's correction factor of 1.015 x Reynolds number compares with other values of 1.01 for potential flow, 1.03, 1.08 and 1.43. The figure of 1.43 is arrived at by a devious route and is probably wrong. The figure of 1.08 is arrived at by correcting the average longitudinal velocity in the region of the obstacle ('mean area' concept). Thus if the dimension of the obstacle along the direction of flow is c, the total cross-sectional area of the channel is A, and the volume of the obstacle is V,

$$\frac{V_{corrected}}{V} = \frac{A \times c}{A \times c - V}$$

Goldstein (1938, p. 567) shows a calculation by Glauert of the effect of walls on cylinder drag in the region where the wake consists of a Karman vortex sheet ($60 < R < 300$); the fractional increase in the drag is to be found to be approximately 0.9 x the blockage ratio.

Laing and Rorschach (1961) found a drag coefficient correction at $R > 10^4$ for sphere blockage ratios of 0.2 to 0.5 in pipes which agrees with a calculation by Birkhoff; at low blockage ratios the correction is again somewhat less than the blockage ratio.

The 'mean area' correction was chosen as a suitable compromise between the small and large effects occurring at large and small Reynolds numbers; applied as a velocity correction, it enters into the Reynolds number and the drag coefficient, although the drag itself is not corrected.

For a sphere,

$$\frac{v_{corrected}}{v} = \frac{A \times d}{A \times d - \frac{4}{3}\pi\frac{d^3}{8}} = \frac{1}{1 - \frac{\pi d^2}{6A}}$$

= for sphere 1 in channel I 1.007

2 I 1.01

3 I 1.05

For the cylinder in channel II,

$$\frac{v_{corrected}}{v} = \frac{w \times d \times l}{w \times d \times l - \frac{\pi d^2 l}{4}} = \frac{1}{1 - \frac{\pi d}{4w}}$$

= 1.10

3.3.3 Evaporation Correction

For large heat currents, the temperature at the heater end of the channel can reach several millidegrees, and allowance must be made for evaporation. The calculation of the correction is given in Appendix B; it is only necessary to apply it for the ten experiments in which sphere 2 was used.

3.3.4 Heat Leakage through Walls

The rate of loss of heat through the channel walls is determined by the Kapitza conductance of the brass. Taking the Kapitza conductance at 1.3°K to be about 0.2 mW cm^{-2} $mdeg^{-1}$ (Wilks, 1967, p. 424), and considering only the resistance of the inner walls (since the outside of the channel has a larger area), the loss along 1 cm of Channel I will be :

$$\text{Conductance} \times \text{area} = 0.2 \times (2 \times \text{depth} + \text{width})$$

$$= 0.2 \text{ mW mdeg}$$

The rate of loss of heat along 1 cm of Channel by evaporation is (Appendix B) $c \times K \times$ width mW $mdeg^{-1}$ where K is the simple kinetic theory evaporation constant and c is a correction factor. At 1.3°K the loss is 7.6 x c mW $mdeg^{-1}$ or, taking c = 1/9 as in Appendix B, 0.8 mW. Thus at 1.3°K the heat loss by evaporation is about four times greater than the heat loss through the walls. At 1.7°K, the evaporation loss increases by a factor of four, whereas the Kapitza loss increases by a factor of three, so the evaporation loss is five times greater than the Kapitza loss. The heat loss through the walls is thus considerably less than the evaporation loss, and since the evaporation correction is largely empirical, and has a similar temperature dependence, it can be taken to include the loss through the walls.

3.3.5 Stem Correction

All the spheres were supported by wires, and it is necessary to take into account the increase in the drag caused by these wires. Allowance was made by calculating the proportion of drag which would be due to the wires, assuming no surface end effect and no end effect where the wire joined the spheres. To make this correction it is necessary to assume that drag will be essentially classical, an assumption which is later shown to be justified by the experimental results.

For the relevant range of Reynolds numbers,
(R (sphere) = 22 - 1350) it can be seen (Figs. 1.1 and 1.2) that

$$C_D \text{ (cylinder)} \doteq 3 \times C_D \text{ (sphere)}$$

$$\text{if } R \text{ (cylinder)} \doteq \frac{1}{5} \text{ to } \frac{1}{10} \times R \text{ (sphere)}$$

at the same velocity. In other words, the drag on unit cross-sectional area of wire is about three times greater than the drag on unit cross-sectional area of sphere.

The total, or measured, drag on the sphere stem will then be

$$D_{total} = D_{sphere} + D_{stem} = C_{D_{sphere}} \cdot \tfrac{1}{2} \rho v^2 \ (A + 3A')$$

where A' is the submerged cross-sectional area of the stem.

$$\text{Thus } D_{sphere} = D_{total} \ \frac{A}{A + 3A'}$$

The correction factor $\frac{A}{A + 3A'}$ = 0.50 for sphere 1

0.64 for sphere 2

0.78 for sphere 3

In other words, for a small sphere, half the measured drag is caused by the stem.

3.3.6 Temperature Correction to Torsion Constant

McSkimin (1953) measured the shear modulus of fused quarts from 20°C to - 200°C using ultrasonic waves, and found that over this range the shear modulus decreased by about 3.3%. The rate of decrease at -200°C with decreasing temperature was small, so McSkimin's results can be extrapolated with confidence down to -272°C. At this temperature the shear modulus, and hence the torsion constant, of the quarts fibre is reduced by a factor of 1.036; this has been applied as a correction factor to all correlated drag measurements.

3.3.7 Velocity Correction in Channel III

For an ordinary fluid flowing laminarly in a deep channel, the velocity profile will become parabolic after a certain inlet length l_I, and the velocity in the centre of the channel becomes 1.5 x the mean velocity. Schlichting (1960, p. 171) shows that the parabolic profile is almost fully developed after an inlet length $l_I = 0.04\ w\bar{u}_{ch}$, where

w is the channel width and R_{ch} is the Reynolds number referred to the channel width.

For the normal fluid flow experiments in Channel III, when the normal and superfluid velocities are both below any critical values, it should be reasonable to use a Reynolds number for the channel

$$R_{ch} = \frac{\rho_n v_n w}{\eta_n} \quad \text{which gives} \quad l_I = \frac{\rho_n v_n w^2 \times 0.04}{\eta_n}$$

For the experimental values which were correlated, l_I varies between 0.23 cm and 2.1 cm. The cylinder was situated at a distance of 1.4 cm from the heater chamber channel inlet, so that, but for the presence of the cylinder, for most of the range the velocity profile would have been almost fully developed, and the velocity at the cylinder = 1.5 x the mean velocity. However the effective velocity which is relevant to describe the drag on the cylinder seems likely to be closer to the mean velocity, and no correction for profile effect has been made in the drag coefficient calculations.

3.4 CORRELATION AND ANALYSIS

3.4.1 Heat Flow Drag Coefficients

In conventional fluid dynamics (see 1.4) the drag coefficient C_D for an immersed body of frontal area A in a stream velocity v is defined by Drag = $C_D \cdot \frac{1}{2} \rho v^2 A$. For a body of characteristic shape the drag coefficient is a universal function of a Reynolds number defined by $R = \rho vd/\eta$ where d is a characteristic dimension of the body.

The two-fluid picture of heat flow in liquid helium introduces two densities, two velocities and possibly two viscosities as parameters. This leads to an infinite number of possible definitions of C_D and R to describe the flow situation.

If one can ignore the presence of the superfluid then the relevant parameters will be

$$R_{\rho_n} = \frac{\rho_n v_n d}{\eta_n}$$

$$C_D = \frac{D}{\frac{1}{2} \rho_n v_n^2 A}$$

If these representations of drag coefficient and Reynolds number are valid, then there will be a simple functional relationship between C_D and R which will be independent of ρ_n/ρ, i.e. independent of temperature.

Graphs of the variation of C_D with $R_{\rho n}$ are shown for spheres in Figures 3.17 and 3.18 (by spheres) and for the cylinder in Figure 3.19. Corrections have been made for torsion constant temperature dependence, blockage, stem drag and evaporation. The effect of the evaporation correction in the sphere experiments is also shown (Figure 3.20).

It is shown later (3.4.2) that at velocities greater than a critical velocity, the superfluid appears to exert a negative drag causing a decrease in net drag of about 25% at temperatures between 1.6 and 1.7°K. The effect of correcting the sphere drag coefficient for superfluid drag is shown in Figure 3.17 for the relevant points between 1.6 and 1.7°K.

Although there is considerable scatter, the drag coefficient does not deviate significantly from the classical value for spheres. For cylinders, the values of C_D appear slightly too high at low Reynolds numbers and slightly too low at higher Reynolds numbers; this may be partly due to using a constant blockage correction factor rather than one which increases with decreasing Reynolds number.

Graphs are also shown for the dependence of C_D on a Reynolds number $R_\rho = \frac{\rho v_n d}{\eta_n}$ (Figures 3.21 and 3.22).

To test for temperature dependence, the following procedure was adopted. The $\log_{10} C_D$ and $\log_{10} R$ points were fitted by a quadratic curve using the least squares criterion. A correlation coefficient r was then computed for the deviations of $\log C_D$ from the curve, comparing these with temperature, normal fluid density and (in the case of the sphere experiments) diameter, respectively.

The correlation coefficient r is defined (Young 1962, p.130) by

$$r = \frac{N\Sigma x_i y_i - \Sigma x_i \Sigma y_i}{(N\Sigma x_i^2 - (\Sigma x_i)^2)^{\frac{1}{2}} (N\Sigma y_i^2 - (\Sigma y_i)^2)^{\frac{1}{2}}}$$

The probability P of a non-zero correlation coefficient arising purely by chance can be calculated (Fisher, 1950, p.193 and p.174). P_1 is calculated by assuming that the number of degrees of freedom equals the number of points correlated (84 in the case of the spheres, 32 in the cylinder experiments); P_2 is calculated by assuming that the number of degrees of freedom equals the number of experiments (21 and 8 respectively). Correlations using $R_{\rho n} = \frac{\rho_n v_n d}{\eta_n}$ and $R_\rho = \frac{\rho v_n d}{\eta_n}$ are compared overleaf.

	Correlated against	Using R_ρ	Using $R_{\rho n}$	P_1 Using R_ρ	P_1 Using $R_{\rho n}$	P_2 Using R_ρ	P_2 Using $R_{\rho n}$
Spheres	T	0.555	0.0005	< 1%	> 90%	1%	> 90%
	ρ_n	0.458	0.036	< 1%	74%	3%	88%
	d	0.447	0.146	< 1%	18%	4%	53%
Cylinder	T	0.756	0.597	< 1%	< 1%	2%	10%
	ρ_n	0.731	0.564	< 1%	< 1%	3%	14%

This shows clearly that the use of R_{ρ_n} gives rise to a much weaker correlation between C_D and T, ρ_n and d than the use of R_ρ; in other words R_{ρ_n} is very much more suitable than R_ρ to describe the flow pattern round a sphere or cylinder.

On the other hand, it is not completely clear just how suitable R_{ρ_n} is. There appears to be evidence of some correlation with sphere diameter; this may be connected with stem drag correction, which may well be different from the 50% which is assumed for sphere 1. There appears to be a significant correlation with T and ρ_n in the cylinder experiments, although it is possible that this is fortuitous.

3.4.2 Apparent Critical Effects in Normal Fluid Drag/Velocity Graphs for Spheres

In experiments above 1.6°K, it was usually found that at a certain velocity, the drag decreased with increasing velocity for a small range. The effect was sometimes not clear owing to the scatter, but perfectly definite on a number of occasions. It was checked by decreasing the heat again; the readings involved were always taken with the torsion head fixed. Examples are shown in Figures 3.1, 3.5, 3.15 and 3.16.

The decrease in drag was such that the actual value at the local minimum was some 30% below the extrapolated value in the most clear cut cases. The most likely explanation for this effect is the onset of superfluid turbulence; the superfluid will acquire an eddy viscosity and will exert some drag in the opposite direction to that of the normal fluid.

The velocities mid-way between the local maxima and minima for a number of experiments are shown below. In the first two, the presence of an intermittent short circuit in the heater, led to a large uncertainty in the velocities.

Experiment Number	Figure	Temperature °K	Decrease in Drag	v_n cm sec^{-1}	v_s cm sec^{-1}	$R_{\rho\,ch}$
11	3.15	2.00	40%	.35	.44	1800
				to	to	to
				.70	.88	3600
14	3.16	1.64	36%	.45	.11	2100
				to	to	to
				.90	.22	4200
20	3.1	1.69	30%	.80	.21	3700
31	3.5	1.66	25%	1.04	.27	4800
		Less well defined examples:-				
24		1.69	20%	0.90	0.25	4200
32		1.87	20%	0.70	0.45	3300

$R_{\rho\,ch}$ is a Reynolds number defined as $\frac{\rho v_n d}{\eta_n}$ where d is the channel hydraulic diameter defined by $d_H = \frac{4 \times A}{p}$ where A is the area and p the perimeter. Since there is a free surface in the channel, the effective depth has been taken as 1.5 x the actual depth. This gives, for Channel I, d = 4.2 mm.

Describing these velocities now as 'critical velocities', the average magnitude of the superfluid critical velocity in the region of 1.68°K is 0.24 cm/sec^{-1}. The experiments of Chase (1962) in a tube of 0.08 cm diameter, yield v_{sc} = 0.60 cm sec^{-1} at 1.68°K.

At higher temperatures, however, the rate of increase of v_{sc} with temperature appears to be greater than that found by Chase, whose v_{sc} only increases by about 20% between 1.7 and 2.0°K.

The magnitude of the decrease in drag to be expected from superfluid turbulence can be estimated by assuming that the turbulent superfluid behaves like an independent fluid with a homogeneous eddy viscosity η_s. Various estimates have been made of this eddy viscosity (1.3.4); it is believed to lie between 10 and 100 micropoise (Vinen, 1961). Writing D_n for the normal fluid drag and D_s for the superfluid drag,

$$D_n = C_{D_n} \cdot \tfrac{1}{2} \rho_n v_n^2 A$$

$$D_s = C_{D_s} \cdot \tfrac{1}{2} \rho_s v_s^2 A$$

$$\frac{D_s}{D_n} = \frac{C_{D_s}}{C_{D_n}} \cdot \frac{v_s}{v_n} \doteq .22 \frac{C_{D_s}}{C_{D_n}} \quad \text{at } 1.68^\circ K$$

The ratio of Reynolds numbers is

$$\frac{R_s}{R_n} = \frac{\rho_s v_s d / \eta_s}{\rho_n v_n d / \eta_n} = \frac{\eta_n}{\eta_s}$$

The percentage drop in net drag to be expected from the appearance of the eddy viscosity can be estimated for the relevant range of Reynolds numbers for different values of eddy viscosity.

η_s (micropoise)	R_n/R_s	C_{D_s}/C_{D_n}	Expected Decrease
10	0.763	0.85	19%
30	2.26	1.2	26%
40	3.04	1.6	35%
100	7.63	2.0	44%

Comparing the percentage decrease in drag which occurs with that expected for different values of η_s suggests a value of about 35 micropoise for η_s, although the experimental uncertainty and dubious validity of this simple argument do not allow any reliance to be placed on this figure: 10 or 100 micropoise are only slightly less likely to be correct.

3.4.3 Superfluid Drag

By assuming a superfluid eddy viscosity η_s (1.3.4) it is possible to attempt a Reynolds number - drag coefficient correction for the superflow experiments, similar to that which was carried out for the heat flow results in section 3.3.1. Because $\rho_s >> \rho_n$ at the temperatures of the superfluid experiments, it makes no significant difference whether ρ_s or ρ is used in the Reynolds number: ρ_s is in fact used.

Figure 3.23 shows two values of drag coefficient from each of the sphere experiments 43 and 44 assuming η_s = 10, 35 and 100 micropoise respectively. Figure 3.24 shows two points from the cylinder experiment 67 for the same viscosities. If one can justifiably compare this situation with a classical one, then from the sphere experiments, an eddy viscosity of around 35 micropoise seems suitable, while the cylinder experiment implies a somewhat larger value.

3.4.4 Subcritical Superflow and Superfluid Critical Velocity

In two experiments with superflow with the cylinder in Channel III (experiments 66 and 67) there was a range of velocity over which the drag appeared to be precisely zero, as near as could be measured. This is shown in Figure 3.14. There is some doubt about the actual velocity, especially in the low velocity region (Appendix C), but the very approximate method of counting drips emerging from the superfluid overflow pipe tends to confirm the velocities deduced from calibration: at a calibration velocity of 0.62 mm sec^{-1} on Figure 2.7, the method of counting drips gave a velocity of 0.3 mm sec^{-1} within a factor of about 2. Since the relationship between actual velocity and heater power is probably non-linear in the very low velocity region, this agreement is as good as can be expected.

The critical velocity at which drag appears lies between 2.5 and 3 mm sec^{-1} on the calibrated scale. Because of the calibration uncertainties, all that can be said is that the real critical velocity is likely to be between 1 and 3 mm sec^{-1}.

3.5 ACCURACY OF HEAT FLOW RESULTS

3.5.1 Experimental Accuracy

The more important sources of experimental error are listed below, together with a rough estimate of the standard error associated with each, for sphere 3 experiments below 1.6°K at moderate velocities.

Torsion constant of fibre	3%
Alignment of spheres or cylinder	2%
Levelling of channels (sphere experiments)	2%
Location of correct level	4%
Temperature fluctuations	1%
Convection and stray forces	6%
Level fluctuations	5%
Accuracy of measurement	3%

These lead to a predicted standard deviation of 10%. Larger percentage deviations are to be expected for :

low velocities (less drag)

sphere 1 experiments (less drag)

higher temperatures (less drag, more heat)

sphere 2 experiments at large heat currents

(evaporation correction, less control).

3.5.2 Correction Factors

The blockage correction factor is not large and therefore not important except perhaps at low Reynolds numbers in the cylinder experiments. The stem correction is more important, and inaccurate estimation may lead to significant error in the case of sphere 1. The temperature correction for the torsion constant is not large and is probably accurate.

Evaporation correction is very important in some of the experiments with sphere 2; the empirical correction which has been made probably does not add greatly to the inaccuracies already present.

The lack of allowance made for velocity profile effect in Channel III could lead to significant error. For example, if the effective velocity is 1.2 x the mean velocity, then the drag coefficients would be less by 44%, and the Reynolds numbers would be increased by 20%.

3.5.3 Consistency of Correlated Results

Most heat flow results correlated with a Reynolds number using the normal fluid density are adequately self-consistent. The largest deviations coincide with high temperatures and low velocities. These deviations are partly due to the difficulties in measuring small drags accurately, and partly due to the breakdown at higher temperatures of the validity of the correlation, which takes no account of the critical effects above 1.6°K or of the failure of the two fluid model near the λ-point.

3.6 RELIABILITY OF THE SUPERFLOW RESULTS

The superflow results are less reliable than the heat flow ones partly because of uncertainty about the superfluid velocity, and partly because of the possibility of normal fluid back flow. The latter could be caused either by direct leakage of normal fluid past the filter or by indirect heating by conduction through the brass. In Channel II only one fifth of the heat is accounted for by superfluid flow, and it might be supposed that up to two fifths would find its way down the channel as normal fluid flow. It is shown in 2.3.3 that the calculated superfluid velocity $v_s = \frac{\rho}{\rho_s} v_n$, where v_n is the normal fluid velocity which would correspond to the same power flow. At the temperatures which were used in the superfluid experiments ($\sim 1.3^{\circ}K$) $\rho_s \simeq \rho$, so the normal fluid velocity might be up to about twice the superfluid velocity in Channel II.

If the normal fluid velocity is 2 cm sec^{-1} in Expt. 44 when $v_s = 1$ cm sec^{-1}, the normal fluid drag would be about 100 microdynes, compared to the measured drag of 350 microdynes, so that the true superfluid drag would be about 450 microdynes. A correction of this order would have little significant effect on the rough estimate of effective superfluid viscosity: it would increase $\log_{10} C_D$ in Figure 3.23 by 0.11 and this would imply that 60 micropoise would be more likely than 35 micropoise.

In the cylinder experiments in Channel III only half the heat input is accounted for, and it seems unlikely that more than half of this would be converted into normal fluid flow down the channel. If all of it were converted, the normal fluid velocity would be almost the same as the superfluid velocity. The ratio of normal to superfluid drag would be $\frac{C_{D_n}}{C_{D_s}} \frac{\rho_n}{\rho_s}$, which is not greater than 10%, and the effect on the viscosity estimate would be negligible.

4. DISCUSSION

4.1 HEAT FLOW

4.1.1 Normal Fluid Drag

The results for sphere and cylinder drag at temperatures between 1.3 and 1.6°K show that the two fluid theory can be used even in this complex flow situation. The drag exerted by the normal fluid agrees within experimental error with that exerted by a classical fluid if the Reynolds number $R = \frac{\rho_n v_n d}{\eta_n}$ is used. At temperatures greater than 1.6°K, if the superfluid velocity exceeds a critical value, account must be taken of the negative drag from the turbulent superfluid, which becomes comparable with that of the normal fluid.

This situation can be interpreted in terms of Vinen's ideas on superfluid vorticity. At low enough velocities, when superfluid turbulence is small or absent, it might be expected that the effect of the superfluid on the normal fluid flow pattern or on the drag on an obstacle could be ignored. At higher flow velocities, when mutual friction and probably shear forces in the superfluid become important, the justification for considering the two fluids as independent in their contributions to drag lies in the decrease of the relative velocity in the vicinity of the sphere or cylinder. Since the two components only interact directly through mutual friction, which is proportional to the relative velocity for a given degree of superfluid vorticity, then the interaction will be greatly diminished in the boundary layer where the normal fluid and probably the superfluid are retarded.

The use of the Reynolds number $R = \frac{\rho v d}{\eta_n}$ to describe critical velocities in channels in terms of the onset of classical turbulence, and its justification by Tough (see 1.3.3) is consistent with the use of the Reynolds number $R = \frac{\rho_n v d}{\eta_n}$ to describe drag. The onset of turbulence is determined by instability of a flow to velocity fluctuations, and Tough proposes that these fluctuations will affect the whole flow as a result of coupling through mutual friction. The characteristic flow round an obstacle, however, is determined by the ratio of inertial and viscous forces; the drag will only be affected by mutual friction in so far as the mutual friction modifies this characteristic flow, and it is suggested that this modification is not significant.

4.1.2 Higher Temperatures

At a temperature of 2.00°K, where $\rho_s \doteq \rho_n$ and $v_s \doteq v_n$, the predicted ratio of drags is $\frac{D_s}{D_n} \doteq \frac{C_{D_s}}{C_{D_n}}$;

if $\eta_s \gtrsim \eta_n$

then $R_s \lesssim R_n$

and $C_{D_s} \gtrsim C_{D_n}$

so that $D_s \gtrsim D_n$;

in other words one might expect the net drag to be zero or negative. The fact that this is not so (Fig. 3.6) implies either that a smaller value of η_s should be used at high temperatures, or that the two fluid picture cannot be used in this manner close to the λ-point.

In fact the drag coefficient calculated from the experiment at 2.00°K, while less than the classical value at low velocity, becomes greater than the classical value at high velocity, as can be seen in Figure 3.17. This may be partly caused by extra torsional forces on the suspended system resulting from excessive evaporation near the heater. One experiment at a temperature of 2.08°K ($v_s = 2.5 \times v_n$) did in fact show irregular but repeatable negative

drag when the superfluid velocity was in the region between about 1 and 10 cm sec^{-1}; at higher velocities the drag became clearly positive. Later experiments at similar temperatures, however, showed only zero drag becoming positive at higher velocities. It seems possible that the results of the experiment which showed negative drag values were genuine but caused by some highly non-uniform flow pattern as was found by Ricci and Vicentini-Missoni (1967).

Experiment 32 at a temperature of 1.87°K gave a drag coefficient which was greater than the classical value at low velocity and decreased to closer to the classical value at high velocity (Figure 3.17).

Thus the experiments above 1.8°K are not truly consistent with the scheme outlined in the previous section, nor are they satisfactorily self-consistent (some show a distinct critical effect, others do not). The explanation may lie partly in the increased experimental difficulties at high temperatures, where the heat input required for a given normal fluid velocity is greater.

4.1.3 Turbulence of the Normal Fluid

If the flow becomes classically turbulent at a critical normal fluid velocity, as suggested by Chase (1962) and Tough (1966), given by $R_c = \frac{\rho v_{nc} d}{\eta_n}$, where d is the hydraulic diameter of the channel, then for Channels I and III this critical velocity will be of the order of 0.5 cm sec^{-1}. Except at high temperatures, most of the experimental points for Channel I are at velocities greater than this. For Channel III many of the experiments show values above and below 0.5 cm sec^{-1}; no distinct change in the relationship between drag and velocity is discernable in this region.

The drag on a sphere is sometimes used as a measure of the degree of turbulence in wind tunnels (Schlichting, 1960, p. 471). The 'critical' Reynolds number at which the drag decreases owing to turbulence in the boundary layer decreases from 380 000 for very low tunnel turbulence to about 50 000 for a turbulent intensity in which the RMS velocity fluctuations in the tunnel were 5%, and probably never drops below 6 000. However the sphere Reynolds numbers in the work described here did not exceed 2 000, so that this critical velocity is never reached.

Goldstein (1938, p. 419) shows measurements of cylinder drag in two wind tunnels where the turbulence differs enough to cause a factor of 2 change in the critical velocity, but below the critical velocity the drag coefficient is the same. It is certainly reasonable to expect that free stream turbulence will not have a large effect on drag where the boundary layer is laminar, since the RMS velocity fluctuations in fully developed pipe turbulence are only of the order of 10%.

4.1.4 Compressibility of the Normal Fluid

In classical fluid dynamics it sometimes becomes necessary to take account of the effect of compressibility on drag when the Mach number (the ratio of flow velocity to velocity of sound) is greater than 0.3 (Schlichting, 1960, p.18). The relevant velocity of sound in the case of the normal fluid is that of second sound, which is at the temperatures of interest about 20 metres sec^{-1}, though falling to zero at the λ-point. A Mach number of 0.3 is thus equivalent to 600 cm sec^{-1}, so that compressibility effects can be ignored in the experiments described here.

4.2 SUPERFLUID DRAG

4.2.1 Subcritical Flow

The results of experiment 67 show that below a superfluid velocity of about 2 mm sec^{-1} there is no measurable drag: these results are also found in the previous experiment, 66.

The sensitivity of the torsion system should have made possible the detection of a force of between 50 and 100 microdynes. A classical fluid flowing at 2 mm sec^{-1} would have produced a force on the cylinder depending on the viscosity as follows:

Force (microdynes)	Viscosity (micropoise)
100	0.01
90	0.1
100	1
250	30
350	100

In other words, there was probably no effective viscosity in the classical sense below the critical velocity.

No region was found in experiments in Channel II where the drag was zero while liquid was seen to be flowing. It is probable that the seal was sufficiently leaky to allow a certain flow of superfluid to pass unobserved, so that by the time the flow was visible the velocity was greater than critical.

The cylinder experiments provide direct evidence of the potential nature of the superfluid flow, and complement the lift measurements of Craig and Pellam (1957).

4.2.2 Superfluid Critical Velocities

The superflow critical velocity of 2 ± 1 mm sec^{-1} in a channel 1.6 mm (x 2 cm) at $1.31^{\circ}K$ compares with a value found by Peshkov and Stryukov (1962) of about 0.25 mm sec^{-1} in a tube 3.85 mm in diameter (detected by second sound), and a value of 1.3 mm sec^{-1} found by Kidder and Fairbank (1959) in a tube 1.1 mm in diameter (pressure measurement). This comparison is not out of line with the sort of agreement found amongst superfluid critical velocities in general (see e.g. Atkins, 1959, p. 199, Wilks, 1967, p. 391); it is conceivable, nevertheless, that the channel value is high because the total length of the channel (2.4 cm) is short enough to increase the critical velocity through an inlet length effect.

The heat flow experiments between 1.6 and 1.7°K also show evidence of a critical superfluid velocity of about 2 mm sec^{-1} in channel I which has a hydraulic diameter of 4.2 mm; this compares with values found by Chase (1962) of 6 mm sec^{-1} in tubes of diameter 0.8 mm by measurement of the temperature gradient. Most other observations of critical superfluid velocity in heat flow have been carried out at lower temperatures.

At higher temperatures, the critical superfluid velocity in heat flow appears to increase, but the experimental evidence is not good enough to say anything more definite.

The corresponding normal fluid velocities in the range 1.6 - 1.7°K are of the order of 0.8 cm sec^{-1}, so it is possible to suppose that the critical effects are caused by classical turbulence of the normal fluid or the whole fluid, especially since the short length of the channel might lead to a higher classical critical normal fluid velocity than 0.5 cm sec^{-1}. On the other hand, the effect of the onset of classical turbulence on, for example, pressure gradient is gradual, and it is unlikely that it would have such a marked effect on drag; hysteresis was ruled out by repeating the measurements with decreasing heat flow. While it is possible that the critical effect is associated with some kind of normal fluid turbulence, it seems likely that the decrease in net drag is caused by a marked increase in superfluid vorticity.

4.2.3 Supercritical Flow

If it is permissible to regard the turbulent superfluid as a laminarly flowing viscous fluid, then the heat flow experiments on spheres and the superfluid experiments on spheres and cylinders imply that the relevant viscosity is probably in the range 20 - 100 micropoise (3. .2 and 3. .3).

For a classical turbulent fluid flowing in a pipe, the eddy viscosity is invoked to describe the total increase in friction at a given velocity for a given pipe, is not homogeneous across the pipe, and cannot be defined locally. In superfluid turbulence, however, an eddy viscosity can be defined in an element of volume which contains a sufficient length of vortex line. If the eddy viscosity is reasonably homogeneous across the channel, then it can be regarded as a classical viscous fluid. It will be homogeneous if the level of vorticity is maintained mostly by the normal fluid velocity through mutual friction. In fact, a decrease in vorticity in the boundary layer on the sphere or cylinder might occur as a result of the proximity of the wall and the decrease in relative velocity.

Vinen's (1957) theory gives the average spacing between lines in heat flow as $\frac{0.011}{(v_n - v_s)}$ cm, where the velocities are in cm sec^{-1}, at 1.3°K, and $\frac{0.005}{(v_n - v_s)}$ cm at 1.7°K. In the sphere drag experiments in heat flow at around 1.7°K this gives a mean spacing of about 0.005 cm at the critical velocity, or about $\frac{1}{20}$ th of the diameter of the sphere 3. In the superflow experiments the spacing at 1 cm sec^{-1}, if the above formula is true, will be 0.011 cm, which compares with a cylinder diameter of 0.018 cm. This suggests that it might be reasonable to talk about a homogeneous eddy viscosity for sphere drag, but in the case of the cylinder it is doubtful whether the concept is valid.

5. CONCLUSION

Between 1.3°K and about 1.8°K, the drag exerted by the normal fluid in heat flow on spheres or cylinders is the same as that exerted by a classical fluid of the same density and viscosity, and the appropriate Reynolds number to describe the drag is $\rho_n v_n d/\eta_n$.

The use of the Reynolds number $\rho v_n d/\eta_n$ to characterise the critical velocity in heat flow in a channel of dimension d is considered to be compatible with the use of $\rho_n v_n d/\eta_n$ to characterise the flow round an obstacle, and the arguments used to justify the former cannot be considered less valid as a result of the present work. The drag exerted by the normal fluid probably does not depend appreciably on whether or not normal fluid or the superfluid is turbulent.

The turbulent superfluid also exerts a drag on spheres and cylinders, both in heat flow and superflow. In heat flow the superfluid drag is only large enough to become noticeable against the normal fluid drag at temperatures greater than 1.6°K. The drag exerted by the turbulent superfluid is the same as would be exerted by a laminarly flowing classical fluid with the same density and a viscosity in the range 20 to 100 micropoise. It is probably justifiable to regard the turbulent superfluid as having the same properties as a laminar viscous fluid when a large enough volume is being considered; however, in the case of the superflow experiment with the cylinder, the predicted separation of vortex lines is of the same order of magnitude as the cylinder diameter at the lower supercritical velocities, so the concept is no longer valid.

In heat flow, the superfluid turbulence between 1.6 and 1.7°K occurs at a critical velocity which is compatible with that found by Chase (1962).

It is not possible to deduce whether the normal fluid is turbulent, or if it is so, whether the turbulence of the both components is precipitated by a critical normal fluid velocity or a critical superfluid velocity. Chase's analysis suggests that there is a changeover from the first mechanism to the second as the temperature increases through the region of 1.7°K.

In pure superflow, a critical velocity of 2 ± 1 mm sec^{-1} in a channel 1.6 mm wide is found. This is slightly higher than found by other workers.

Below this critical velocity, no drag is measured on the cylinder. This may be taken as good evidence that the bulk superfluid obeys ideal fluid theory; in particular the fluid velocity at the cylinder wall must be similar to that of the bulk flow without tangential force being exerted on the wall. This is believed to be the first experimental demonstration of D'Alembert's paradox.

APPENDIX A - DEVELOPMENT OF APPARATUS

First Constant Level Bath

In the first apparatus the constant level bath was an open glass beaker which was high enough to be clear of the liquid level in the dewar. Two fountain pumps were used to raise and lower the level as required.

A brass tube rising above the cryostat cap contained the torsion head (a stainless steel $\frac{1}{8}$" rod passing through an O-ring seal), the fibre, and the top of a long glass rod which carried the suspended system.

A conventional system was used to observe deflection; a light beam passed through a window in the brass tube, and was reflected by a front-silvered mirror on the glass rod onto a scale.

The long glass rod (diameter 0.7 mm) was manufactured by drawing out molten glass, and straightened beyond reasonable doubt by hanging it in an annealing oven with a weight on the bottom and allowing it to lengthen somewhat, over the course of several hours.

To render it free of suspicion of harbouring electrostatic charges, all non-metallic parts of the suspended system were painted with Aquadag or Silver Dag. Any net charge should be lost by contact with earthed parts of the apparatus. During the first run, there were torsional forces on the system at least an order of magnitude larger

than those it was hoped to measure. An indication of the strength of these spurious forces was given by comparing the natural period of oscillation, 27 secs, with that occurring at low temperatures, which varied between 2 and 10 secs. The effective torsion constant is proportional to the inverse square of the period and was thus at times 180 times too big.

The effect was reproduced at room temperatures by applying a tesla coil to the constant level bath for a few seconds. This tended to confirm the suspicion that the spurious forces were electrostatic, probably resulting from a charge distribution on the inner wall of the bath. At room temperatures the effect died away in a few minutes, as the charge leaked away, but at low temperatures in helium it cannot leak away.

The inside of the bath was painted, apart from windows, with Silver Dag and this seemed to be successful at room temperature. At low temperature, however, the spurious forces, though considerably diminished were still present. A semi-transparent coating of aluminium was evaporated onto the inside of the bath, but no improvement resulted. It was discovered, however, that shutting off the pump line caused the effect to disappear in a few seconds; this suggested that the forces were in some way connected with convection.

In fact, a sensible explanation was not forthcoming; but it was thought the difficulty might be overcome by shielding the suspended system from convection currents in the main dewar. The glass rod was then enclosed in a tube which belled out at the bottom as a loose-fitting roof over the bath. When this failed to help, the suspended system was made cylindrically symmetrical by removing the cross arms and fitting a horizontal disc. Since this was now essentially the same as an arrangement which had been used before (Osborne, 1962) it was surprising to find that the spurious forces were still there. The only part of the suspended system which was still obviously cylindrically asymmetrical was the mirror. This was encased in a small cylinder, and a glass tube was inserted inside the brass tube, to isolate the window, but no improvement resulted.

Second Constant Level Bath

At this stage it was decided to build a constant level bath which was as completely isolated as possible from the rest of the dewar. Internally conducting glass tubing (60 ohms per square), supplied by Joblings, was made into a beaker. The thin lip of an annealed copper annulus was araldited onto the glass. A stainless steel annulus was soft-soldered (Woods metal) onto the copper. This assembly was then sealed demountably onto a stainless steel top-plate by means of an

indium ring ($\frac{1}{16}$" diameter) washer and eight 4 B.A. bolts. The bath top-plate was rigidly supported by a 15 mm diameter stainless steel tube which was attached by means of a flange and bolts to the dewar top-plate. The bath was now at the bottom of the dewar vessel and was connected with the dewar space through four holes - the emptying fountain pump, the raised funnel for filling fountain pump, and two $\frac{3}{32}$" holes in the top of the stainless steel support tube to prevent the possibility of gas oscillations with catastrophic heat transfer.

When this failed to dispose of the spurious forces, the long glass rod was dispensed with and the fibre was hung inside the bath, carrying only about 3 cm of glass rod and the disc. After some troubles with leaks in the bath and mechanical noise had been dealt with, the suspended system was now found to be behaving sensibly and continued to do so after arms had been attached to it.

No convincing explanation for the spurious forces was ever found. The copper-glass araldite seal in the second bath started to leak after a few runs, apparently because of lack of plasticity in the araldite. The third and final design of constant level bath had a different type of seal (see 2.2.2) but was otherwise similar to the second.

APPENDIX B - EVAPORATION CORRECTION (CHANNEL I)

For large heat current densities the excess temperature near the heater can reach several millidegrees and it becomes necessary to allow for loss of heat by evaporation.

Simple kinetic theory (Atkins, Rosenbaum and Seki, 1959) gives

$$\frac{dm}{dt} = c\sqrt{\frac{M}{2\pi RT}}\ (pl - pg)\ \text{gms sec}^{-1}\ \text{cm}^{-2}\ \text{deg}^{-1}$$

net evaporation, where pl - pg is the pressure difference corresponding to a temperature difference of one degree at the surface; c is a correction factor, which takes account of the blurring of the temperature discontinuity at the surface and consequent reduction of evaporation rate: its value will lie between 0 and 1. The heat loss associated with this evaporation will be

$$L\frac{dm}{dt} = cK \qquad \text{where} \qquad K = L\sqrt{\frac{M}{2\pi RT}}\ (pl - pg)$$

K is the evaporation constant. Its temperature dependence is given below.

T(°K)	K (joules sec^{-1} cm^{-2} deg^{-1})
1.3	15.6
1.4	23.6
1.5	33.8
1.6	66.3
1.7	61.0

Assuming perfect vertical conduction and constant c, it is possible to calculate the variation of v_n along the channel:

Notation:- b - breadth of channel (cm)

d - depth (cm)

x - co-ordinate for position along channel, = 0 at mouth of channel, = l at heater (cm)

W - heat current density (watts cm^{-2}) along channel

A - b x d = cross-sectional area of flow.

The heat loss along the channel, (AW), will then be given by CKbdx ΔT where ΔT is the local excess temperature. Chase (1962) gives $\nabla T^* = DW^{3.4}$; using this relation and his values of D (and ignoring the difference between ∇T^* and ∇T, namely the contribution of the normal fluid viscosity to the temperature gradient),

$$\frac{d(AW)}{dx} = bcKD \int W^{3.4}\, dx$$

$$\text{or} \quad \frac{d^2W}{dx^2} = \frac{CKD}{d} W^{3.4}$$

Solving,

$$\frac{dW}{dx} = \left(\frac{CKD}{2.2d}\right)^{\frac{1}{2}} (W^{4.4} - W_o^{4.4})^{\frac{1}{2}}$$

where W_o is the heat current density at x = o

$$\text{or} \quad x = \alpha \int_{v_{no}}^{v_n} \frac{dv}{(v^{4.4} - v_{no}^{4.4})^{\frac{1}{2}}} \qquad \text{(1)}$$

where v_{no} is the velocity at $x = 0$

and $\alpha = \left(\frac{vn}{W}\right)^{1.2} \left(\frac{2.2d}{cKD}\right)^{\frac{1}{2}}$

Numerical integration leads to a relation between v_n and x for a given value of v_{no}, where v_{no} is the velocity at the mouth of the channel. x/α was graphed against v_n for several values of v_{no} (Fig. B.1). The value of v_n at l/α was then equivalent to the value of v_n calculated from the heat input, and the value v_n' at $l/2\alpha$ gave the velocity half-way along the channel, which is where the sphere was. The variation of v_n' with v_n for various temperatures with $c = \frac{1}{9}$ is shown in Fig. B.2.

The evaporation correction with $c = \frac{1}{9}$ was applied to the experiments using sphere 2; for all other experiments it was negligible. The value of $\frac{1}{9}$ was chosen as leading to reasonably consistent values of drag coefficient. In fact it is likely that c is not constant but decreases with increasing rate of evaporation, when a considerable flow of vapour must be set up. The whole correction is thus very approximate; its main purpose is to show that the apparent temperature correlation appearing at large Reynolds numbers in the $C_D v_s R_n$ graph (Fig.3.20) is spurious.

Mention is made in Appendix C of the possibility that in the superfluid experiments heat leakage through the brass may be comparable with evaporation. In the normal fluid situation the ratio of area of wall to area of free surface is less by a factor of about 5, but c may also be much smaller since the evaporation rate is greater, so it is again possible that heat loss through the walls is an important mechanism. The Kapitza resistance of most metals falls by a factor of approximately 2 or 2.5 between 1.3 and 1.7°K (Wilks, 1967), and the evaporation constant rises by a factor of 4; so the dependence on temperature of the two mechanisms of heat loss is fairly similar and the argument about the temperature correlation still applies.

APPENDIX C - SUPERFLUID CALIBRATION DISCREPANCY

This Appendix contains a brief discussion of the discrepancies in the superflow experiments between the calculated superfluid velocity and that measured by calibration.

There are five possible factors contributing to the discrepancy in the superflow experiments between the calculated superfluid velocity and that measured by calibration.

(a) Heat loss through brass.

(b) Leakage of normal fluid past the filter.

(c) Heat loss by evaporation.

(d) Liquid loss by evaporation.

(e) Heating of liquid above ambient temperature.

All of these mechanisms, except (b), depend on the excess temperature of the liquid in the heater. Assuming for present purposes that (b), at least in Channel III, was negligible, it is easily shown that (d) and (e) were less than (c) by a factor of about 100, so they need not be considered.

Three principal features are noticeable on the superfluid calibration graphs (Figs. 2.6 and 2.7).

(1) A finite amount of heat must be input before any fluid emerges.

(2) The discrepancy between the calculated and measured flows increases with flow.

(3) The amount of heat required to start flow increases with temperature.

These features are discussed in turn below.

(1) In the particular case of the calibration of superfluid flow in Channel III (1.31°K), no liquid was seen to emerge until the heat input reached 1.2 mW, the drag experiment at the same temperature, the heat input required was 2.7 mW. The temperature difference necessary to raise the liquid the required height of about 3 mm is 0.3 millidegrees. Using the simple kinetic theory (see Appendix B) the heat loss by evaporation at 1.31°K is 17 watts deg^{-1} cm^{-2} or 5 mW cm^{-2}. The cross-sectional area of the emptying tube is only a few square millimetres, but the effective area available for evaporation might easily be increased to something of the order of a square centimetre by film flow, so that the initial heat required

could all be lost by evaporation. The lower heat input figure in the calibration experiment is probably due to the fact that the outflow pipe fitted fairly snugly into the calibration bucket mouth so that a slight excess gas pressure would be maintained, and evaporation reduced.

If one assumes that the Kapitza resistance of the brass is 5 deg cm^2 $watt^{-1}$, then ignoring the resistance at the outside wall (owing to the larger area) and assuming an inside wall area of 10 cm^2 and a temperature difference of 0.3 m the heat loss through the brass will be 10 x 0.3/5 or 0.6 mW; so clearly this could be a significant source of heat loss if the Kapitza resistance is much smaller.

(2) As the heat input is increased, so the apparent rate of loss of heat increases. This may be partly due to an increase in effective area for evaporation, but this should cause only a relatively small extra loss. It seems likely that the loss results from an increase in the temperature in the heater chamber, but it is not clear why this should come about: a calculation of the excess temperature due to frictional forces in the channel or pipe shows this to be negligible.

(3) At higher temperatures, more heat has to be supplied before any liquid emerges. The evaporation constant increases by a factor of 4 between 1.3 and 1.7 (see Appendix B), but the temperature difference necessary to sustain the level decreases by the same amount, so no net change is expected from this source. The Kapitza resistance decreases, however, with increasing temperature, and this may be the cause of the extra heat loss.

REFERENCES

Allen, J. F., Griffiths, D. J., and Osborne, D. V. (1965)
Proc. Roy. Soc. A 287, 328.

Atkins, K. R. (1959) Liquid Helium, Cambridge University Press.

Atkins, K. R., Rosenbaum, B. and Seki, H. (1959) Phys. Rev. 113, 751.

Brewer, D. F. and Edwards, D. O. (1961) Phil. Mag. 6, ~~775~~, 1173

Chase, C. E. (1962) Phys. Rev. 127, 361.

Chase, C. E. (1963) Phys. Rev. 131, 1898.

Corke, H. E. and Hildebrandt, A. F. (1968) Phys. Rev. Fluids 11, 465.

Craig, P. P. and Pellam, J. R. (1957) Phys. Rev. 108, 1109.

Dowley, M. W. and Hollis-Hallet, A. C. (1960) Proc. 7th International
Conference on Low Temperature Physics,
University of Toronto Press, p. 464.

Feynman, P. P. (1955) Prog. Low Temp. Phys., Vol. I, p. 36.
Amsterdam : North-Holland Publishing Co.

Fisher, R. A. (1950) Statistical Methods for Research Workers,
11th Edition. Edinburgh : Oliver and Boyd.

Goldstein, S. (Ed.) (1938) Modern Developments in Fluid Dynamics,
Oxford : Clarendon Press.

Goner, R. (1953) Rev. Sci, Instr., 24, 993.

Griffiths, D. J. (1965) Thesis, University of St. Andrews.

Hussey, R. G. and Reynolds, J. M. (1965) Phys. Fluids, 8, 1213.

Kidder, J. N. and Fairbank, W. M. (1962) Phys. Rev. 127, 987.

Kochler, T. R. and Pellam, J. R. (1962) Phys. Rev. 125, 791.

Laing, R. A. and Rorschach, H. E. (1960) Proc. 7th International Conference on Low Temperature Physics, University of Toronto Press, p. 461.

Landau, L. D. (1941) J. Phys., Moscow, 5, 71.

McSkimin, H. J. (1953), J. Appl. Phys. 24, 988.

Onsager, L. (1949) Nuovo Cim. 6, Suppl. 2, 249.

Osborne, D. V. (1962) Proc. Phys. Soc. 80, 1343.

Perkins, H. C. and Leppert, G. (1964) Int. J. Heat Mass Transfer, 7, 143.

Peshkov, V. P. and Stryukov, V. B. (1962) J. Exp. Theor. Phys. (USSR) 14, 1031

Schlichting, H. (1960) Boundary Layer Theory, 4th Edition. New York : McGraw-Hill.

Staas, F. A., Taconis, K. W. and Van Alphen, W. M. (1961) Physica 27, 893.

Strong, J. (1938) Modern Physical Laboratory Practice. London: Blackie.

Tough, J. T. (1966) Phys. Rev. 144, 186.

Tough, J. T., McCormick, W. D. and Dash, J. G. (1965) Phys. Rev. 140, 1524.

Van Dyk, H., Durieux, M., Clement, J. R. and Logan, J. K. (1960) National Bureau of Standards Monograph 10.

Vicentini-Missoni, M. and Gunsolo, S. (1966) Phys. Rev. 144, 196.

Vinen, W. F. (1957a) Proc. Roy. Soc. A240, 114.

Vinen, W. F. (1957b) Proc. Roy. Soc. A240, 128.

Vinen, W. F. (1957c) Proc. Roy. Soc. A242, 493.

Vinen, W. F. (1957d) Proc. Roy. Soc. A260, 218.

Vinen, W. F. (1961) Prog. Low Temp. Phys. Vol III, p. 1. Amsterdam : North-Holland Publishing Co.

Wilks, J. (1967) The Properties of Liquid and Solid Helium. Oxford : Clarendon Press.

White, C. M. (1945) Proc. Roy. Soc. A186, 472.

Young, H. D. (1962) Statistical Treatment of Experimental Data. New York : McGraw-Hill.

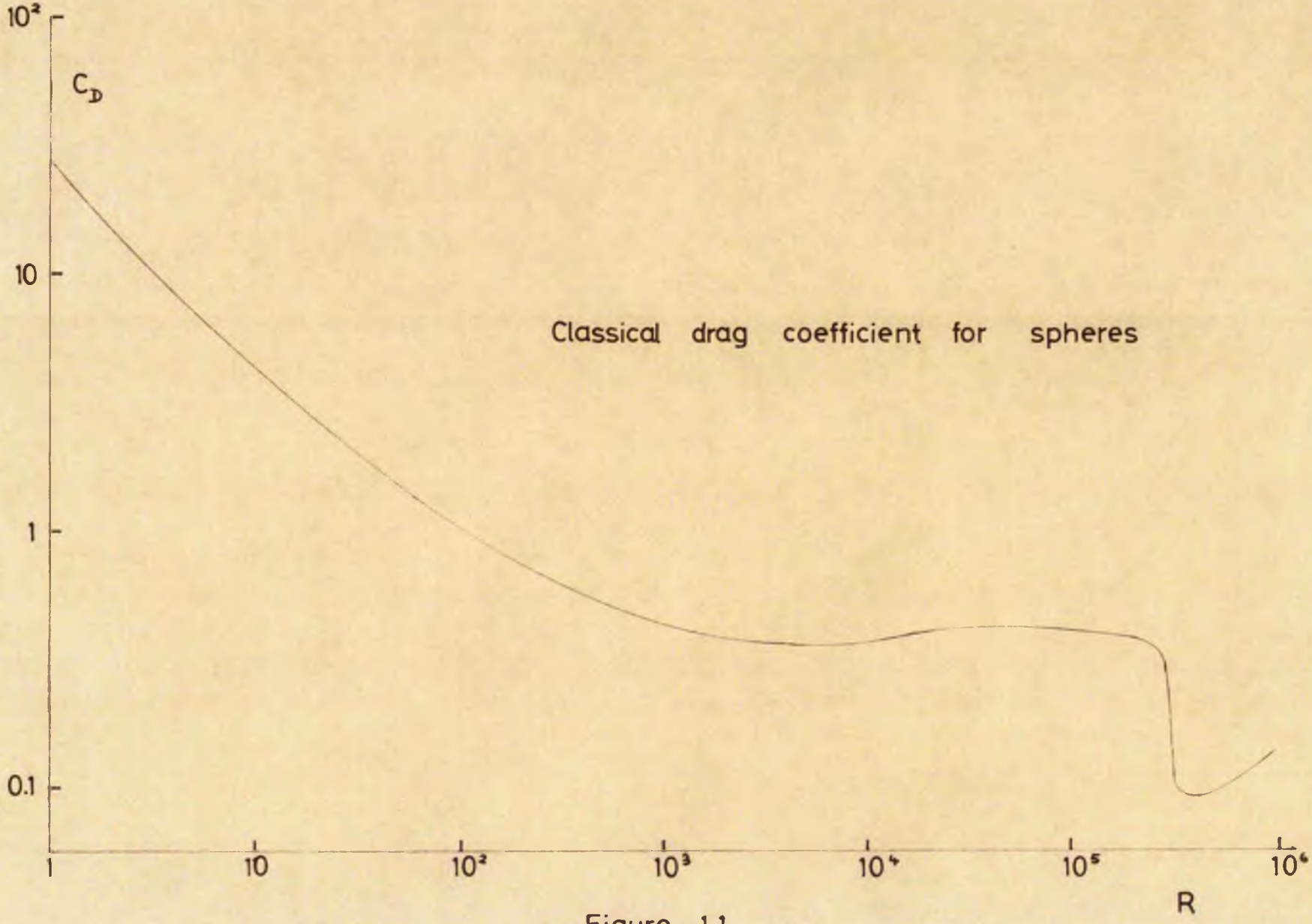
10^2
C_D
10
1
0.1
Classical drag coefficient for spheres
1
10
10^2
10^3
10^4
10^5
10^6
R

Figure 1.1

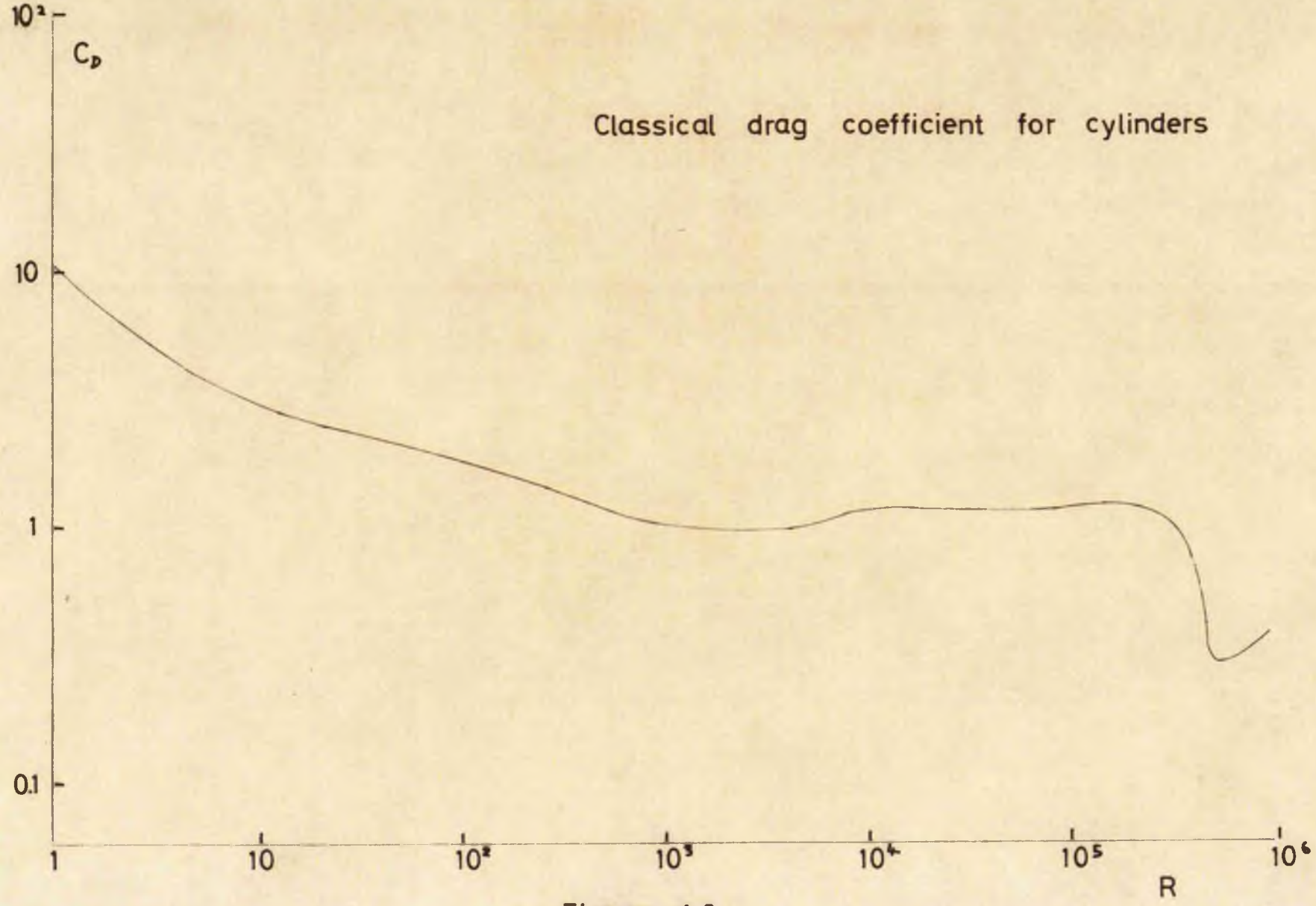
Classical drag coefficient for cylinders
10^2
C_D
10
1
0.1
1
10
10^2
10^3
10^4
10^5
10^6
R

Figure 1.2

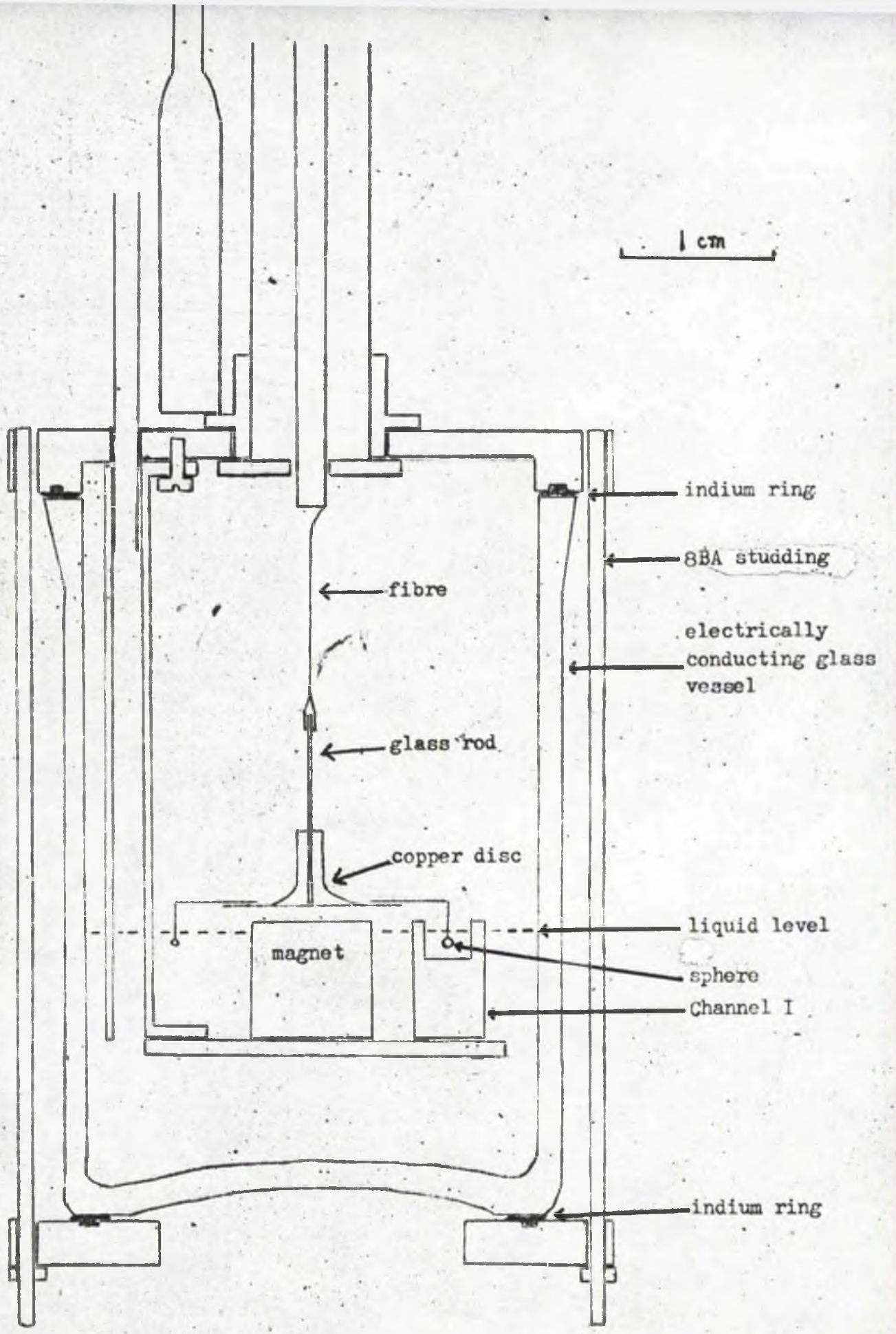

FIGURE 2.1 CONSTANT LEVEL BATH

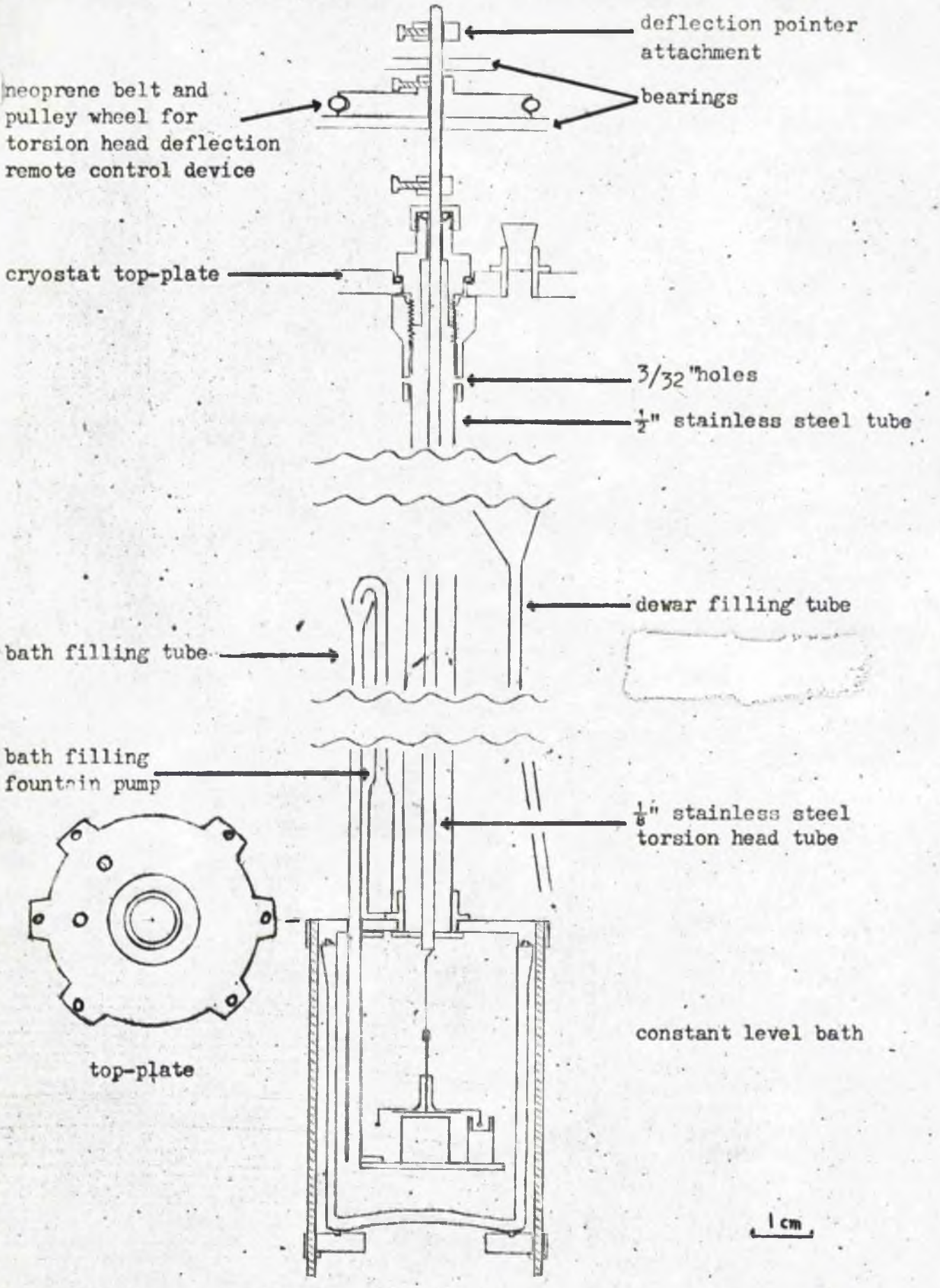

FIGURE 2.2 MAIN APPARATUS

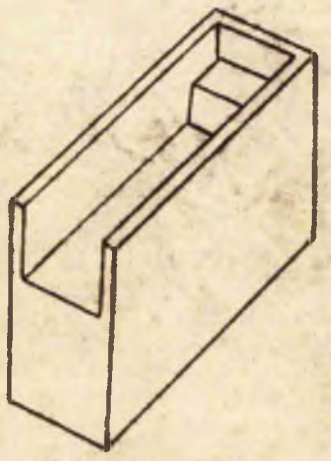

CHANNEL I

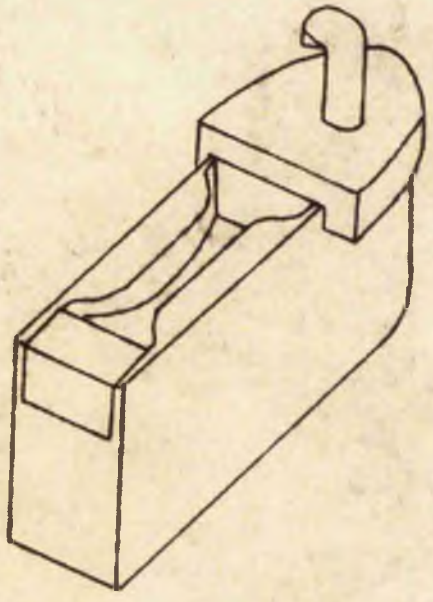

CHANNEL II

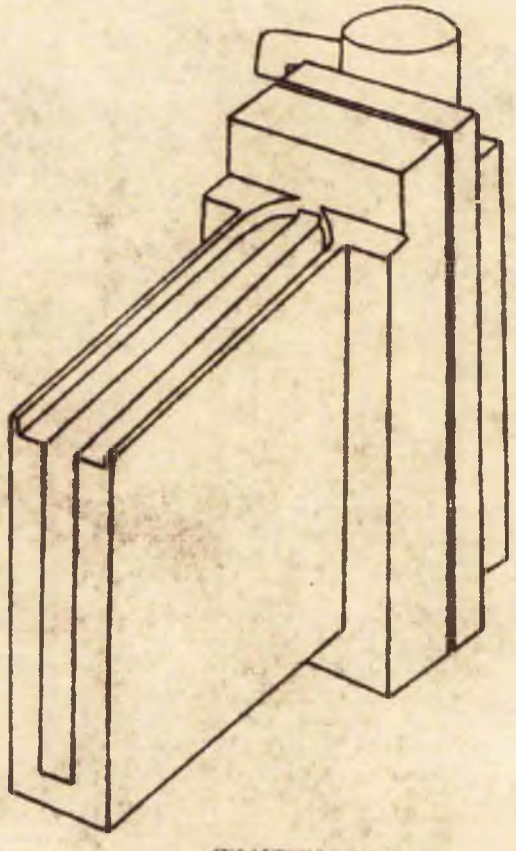

CHANNEL III

FIGURE 2.3

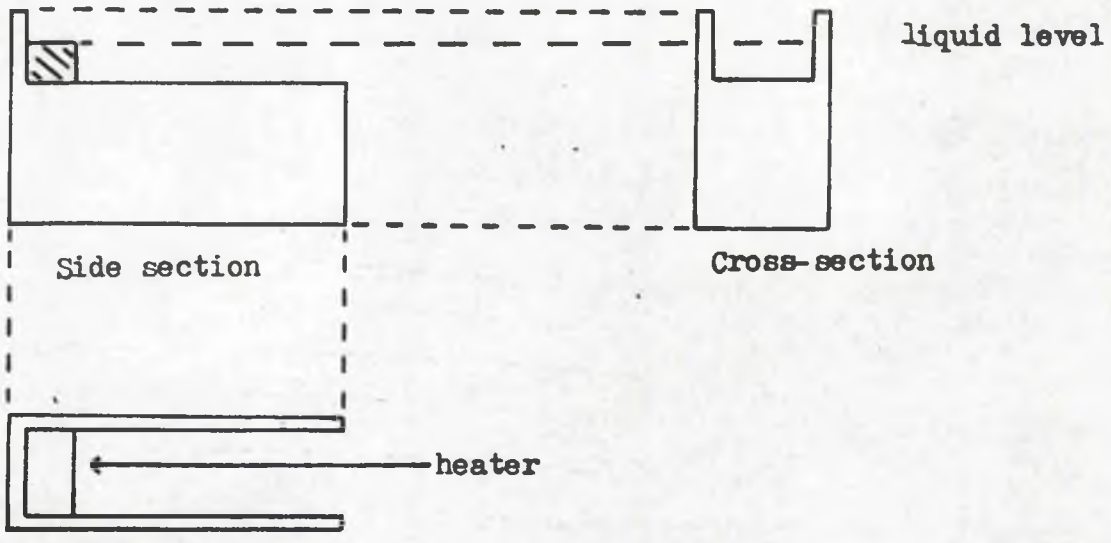

CHANNEL I

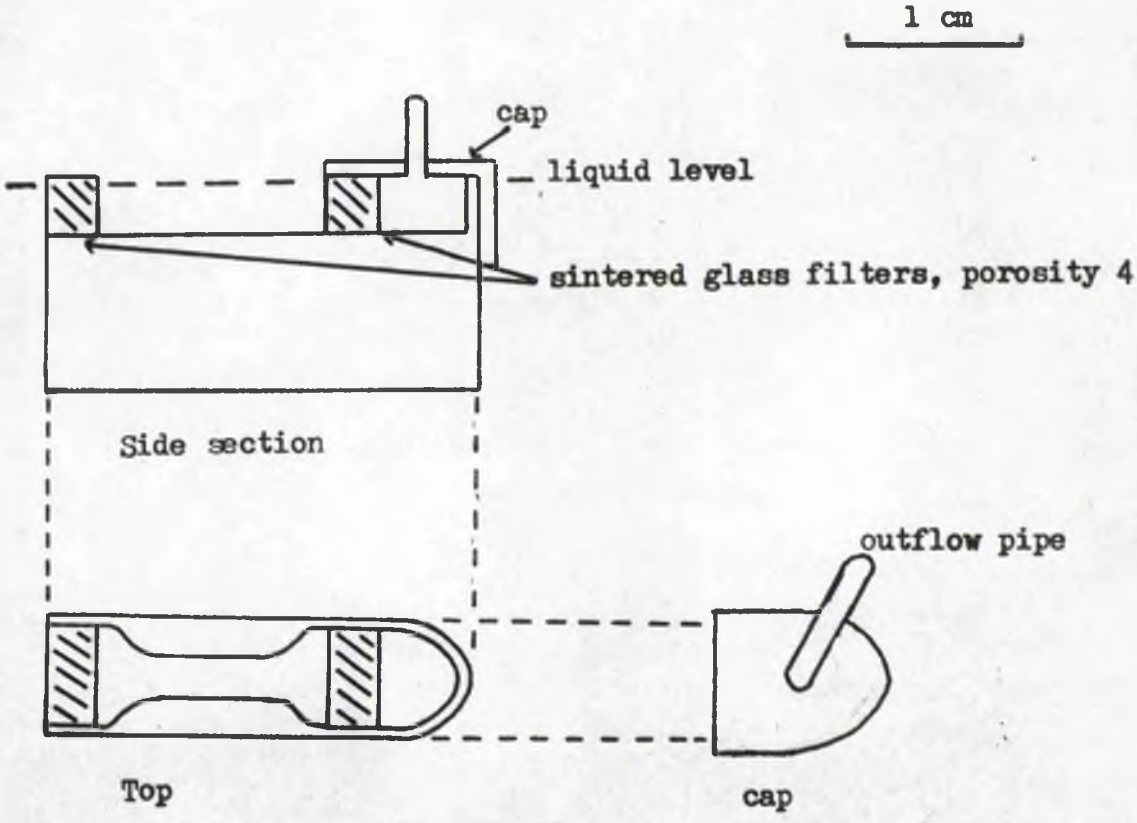

CHANNEL II

FIGURE 2.4

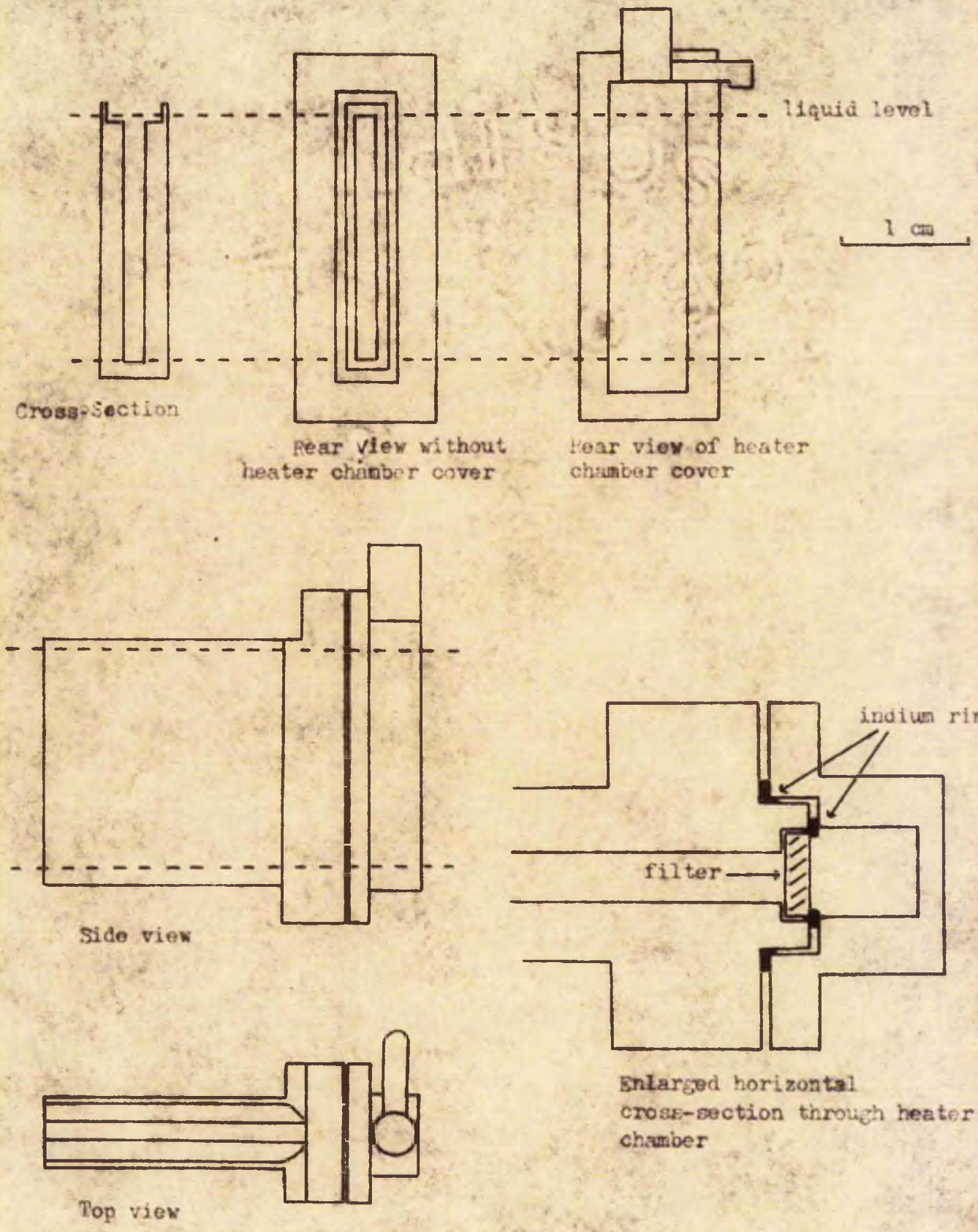

FIGURE 2.5 CHANNEL III

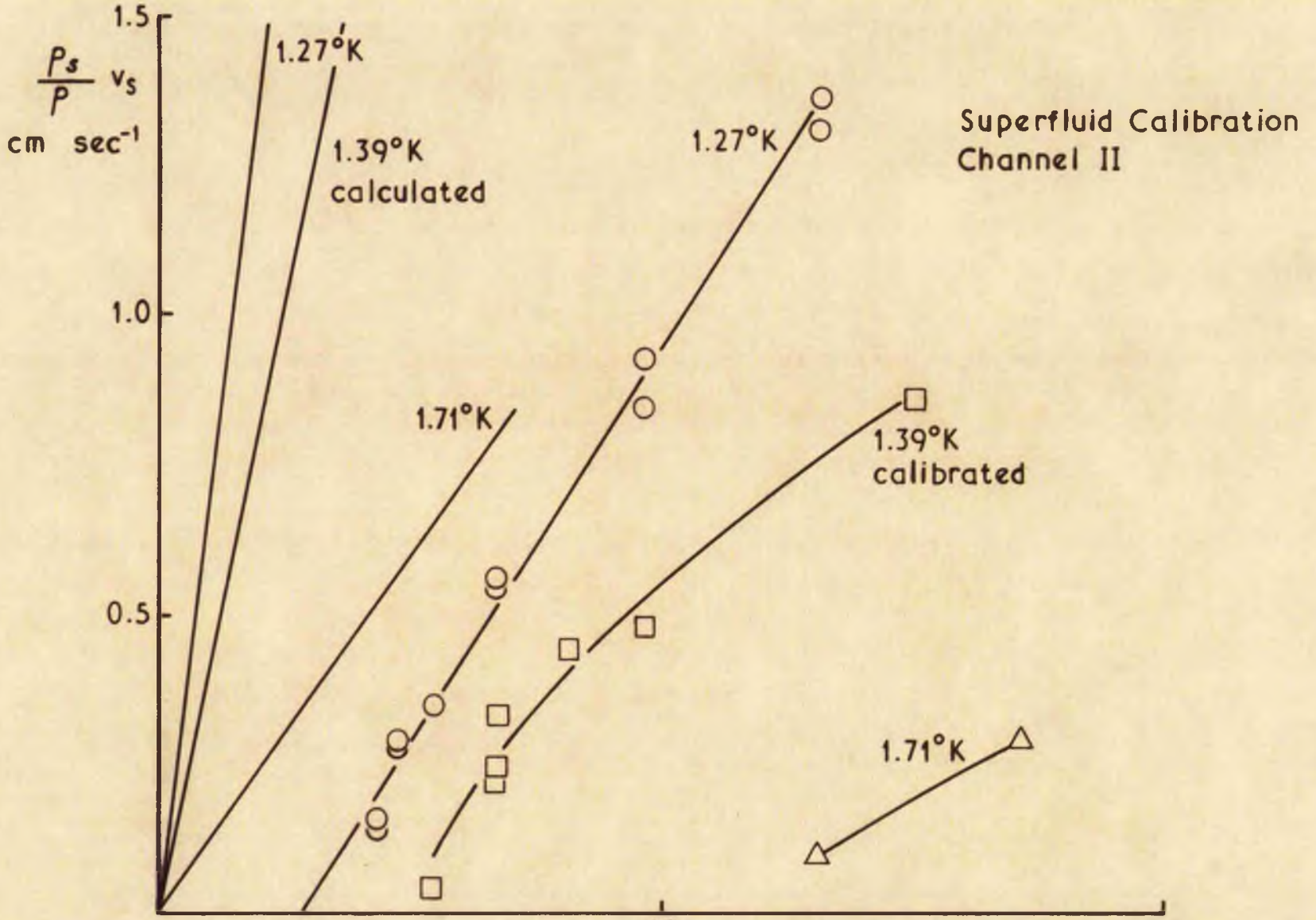
1.5
1.0
0.5
$\frac{P_s}{P}$ v_s
cm sec^{-1}
1.27°K
1.39°K
calculated
1.71°K
1.27°K
1.39°K
calibrated
1.71°K
Superfluid Calibration
Channel II
10
20
Total heater power mW

Figure 2.6

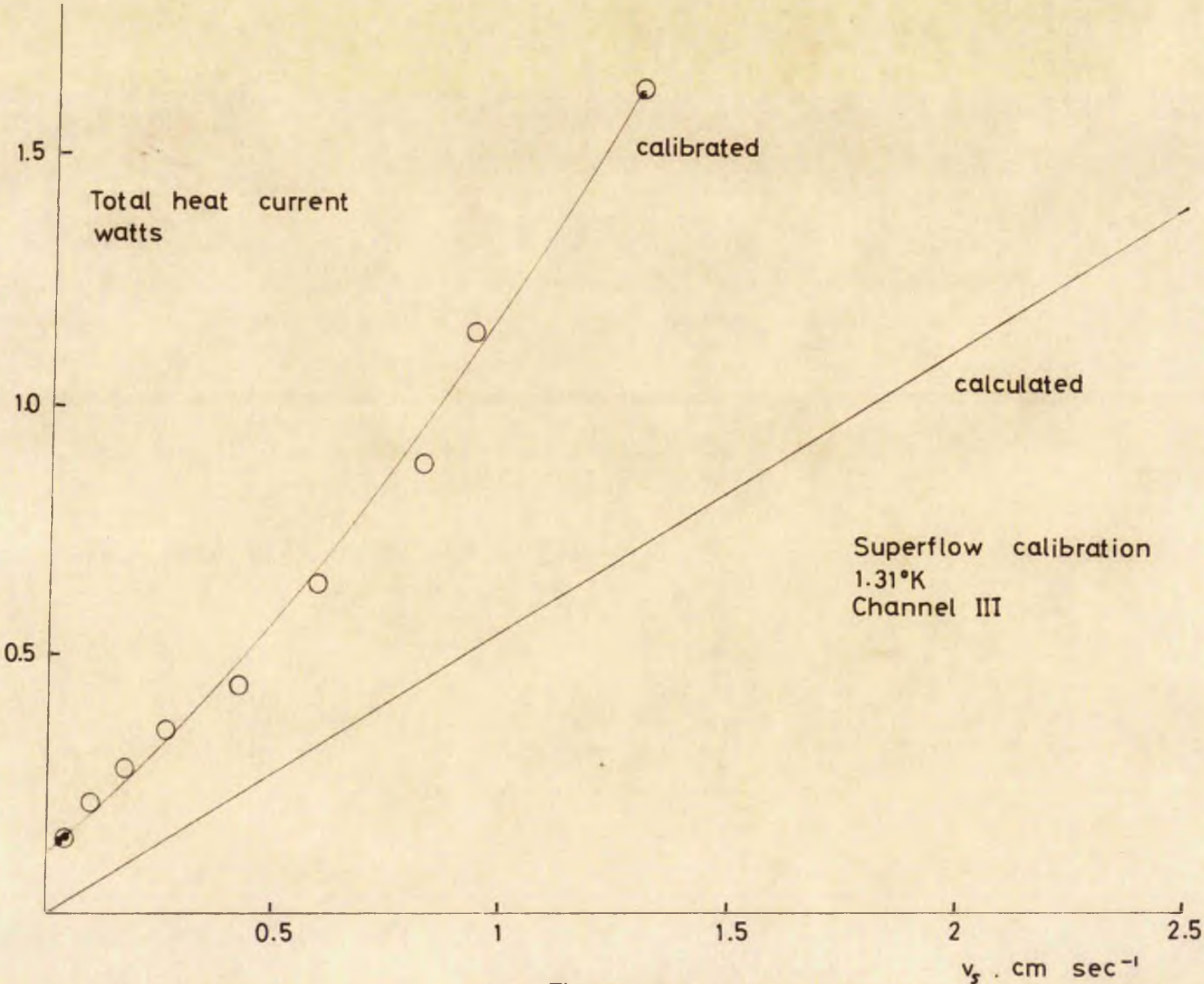
1.5
1.0
0.5
Total heat current
watts
calibrated
calculated
Superflow calibration
1.31°K
Channel III
0.5
1
1.5
2
2.5
v_s . cm sec^{-1}

Figure 2.7

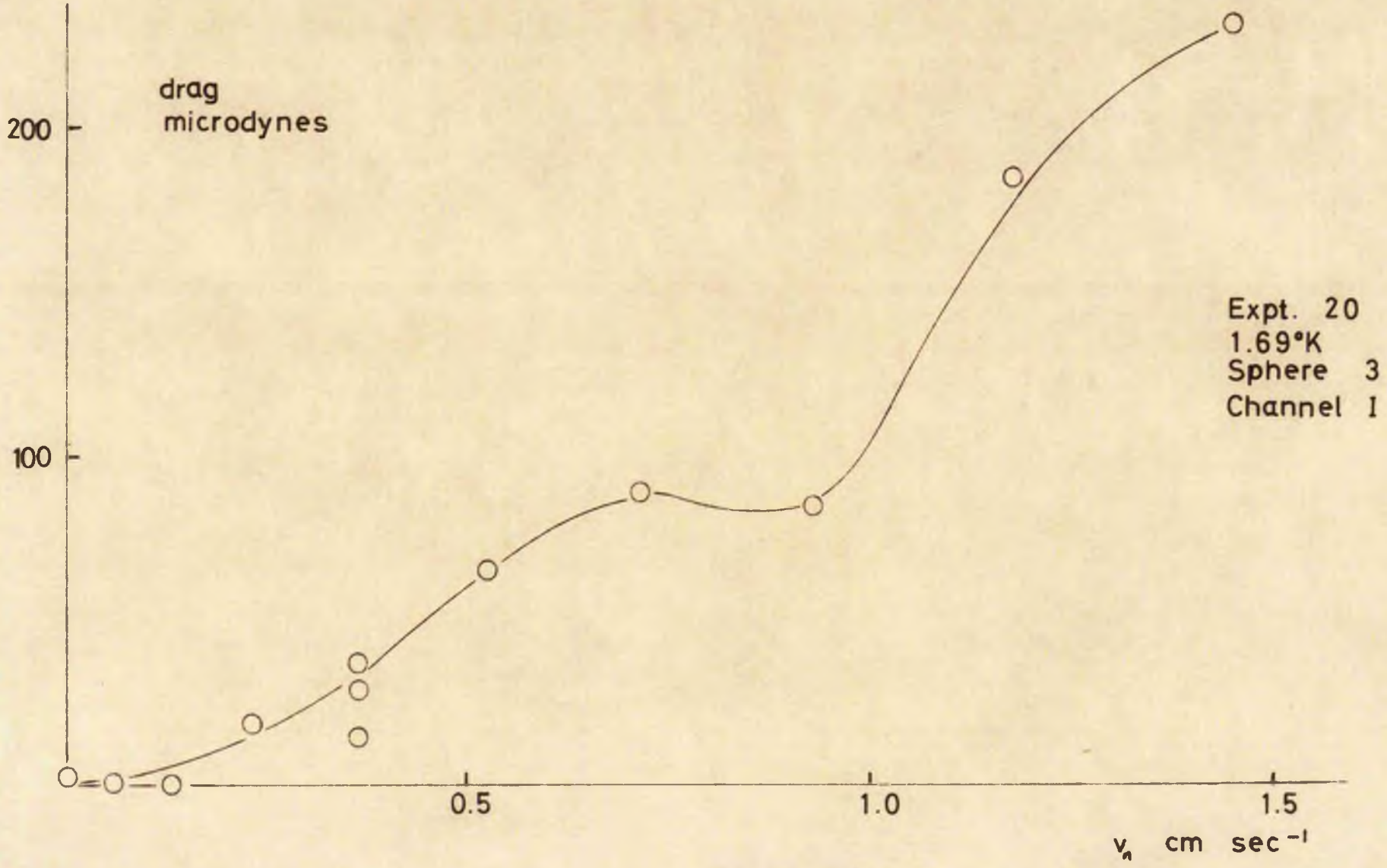
drag
microdynes
200
100
Expt. 20
1.69°K
Sphere 3
Channel I
0.5
1.0
1.5
v_n cm sec^{-1}

Figure 3.1

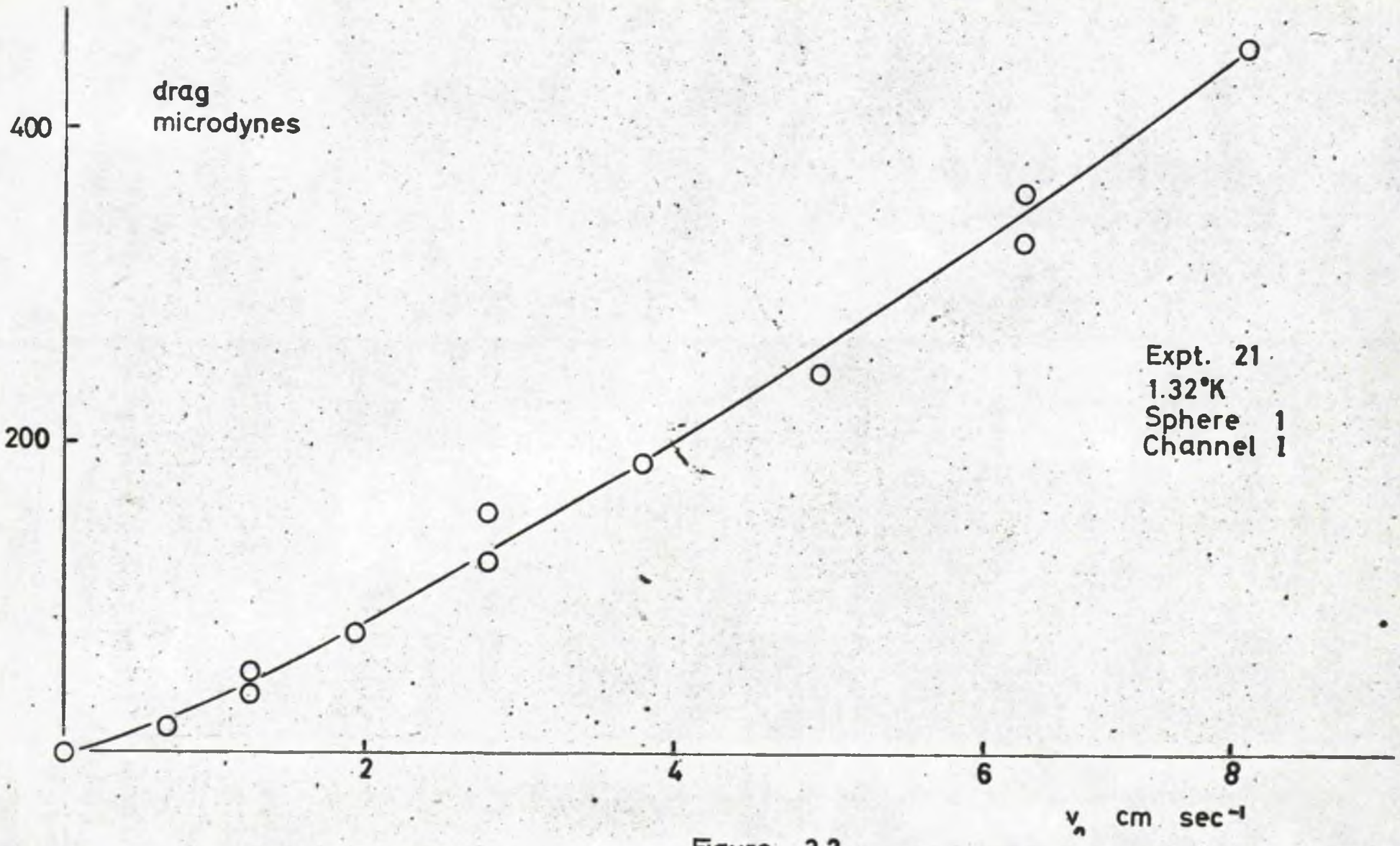
drag
microdynes
400
200
2
4
6
8
v_n cm sec^{-1}
Expt. 21
1.32°K
Sphere 1
Channel 1

Figure 3.2

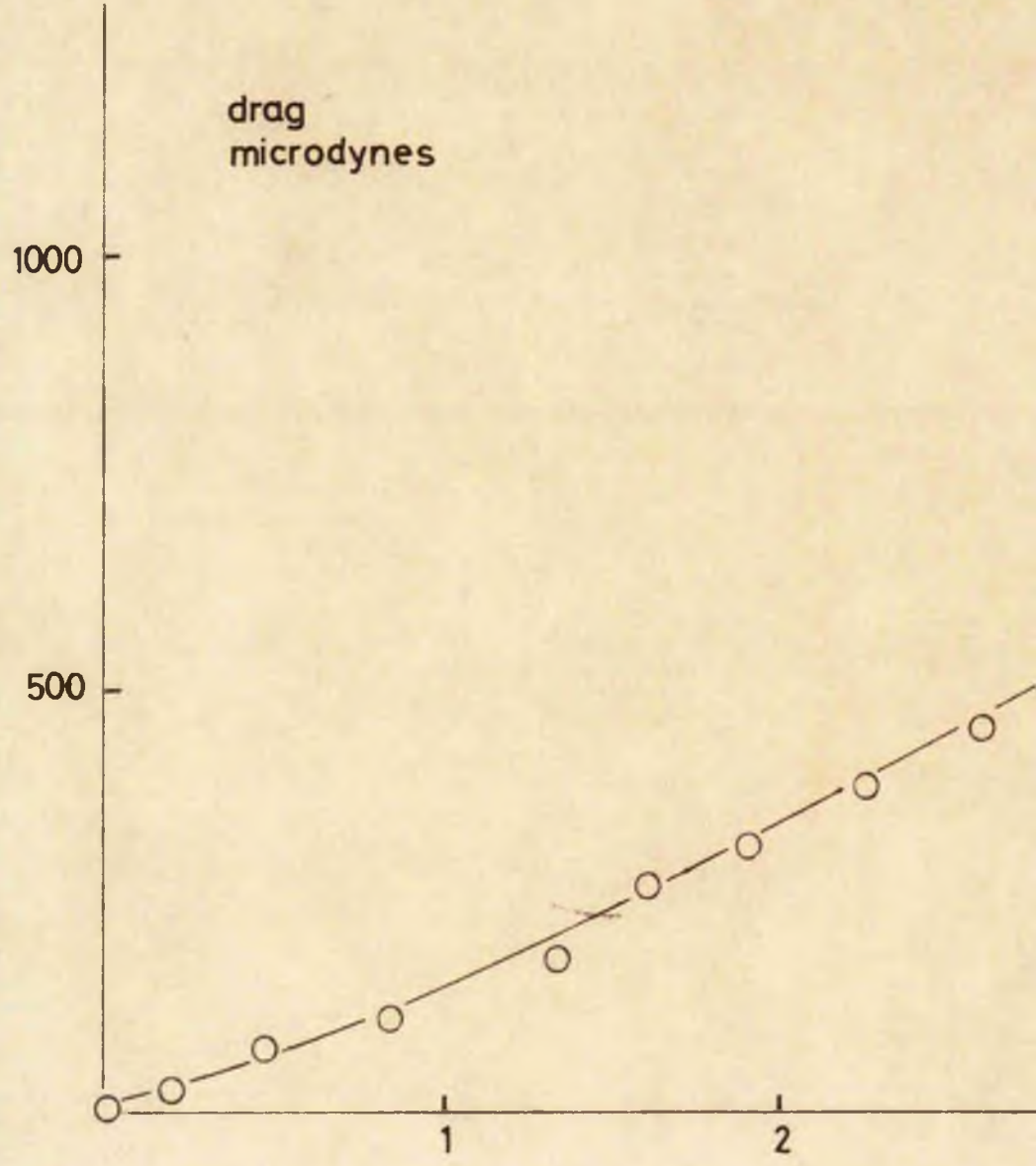

Figure

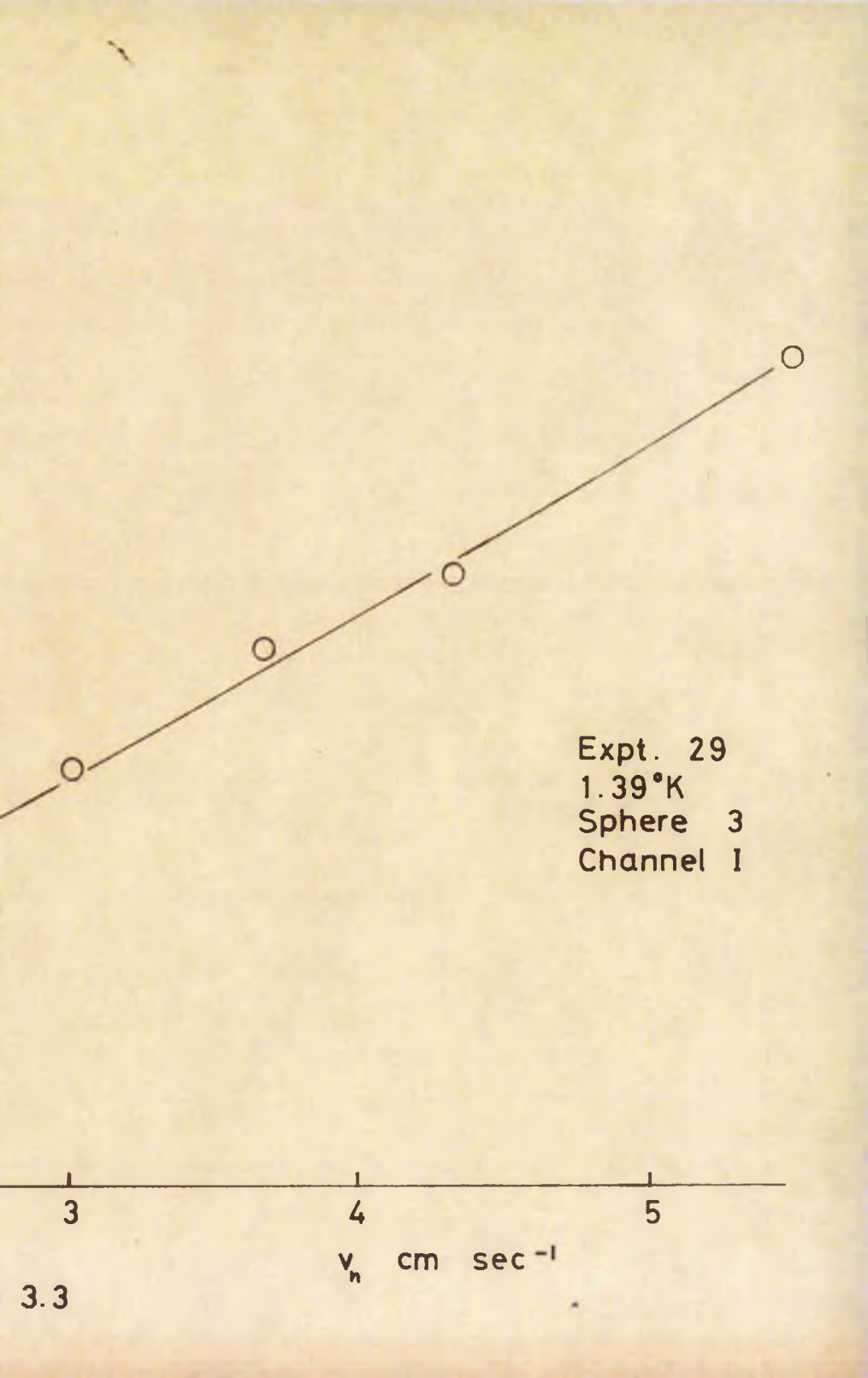

3.3

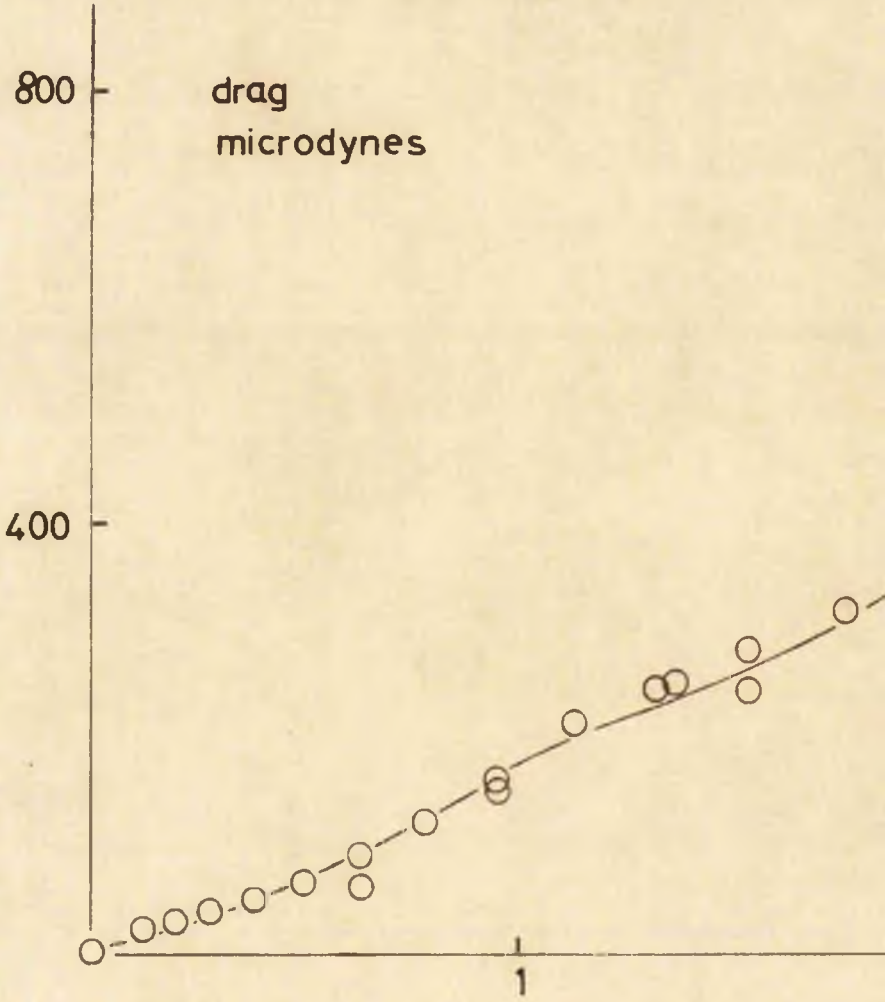
800
drag
microdynes
400
1

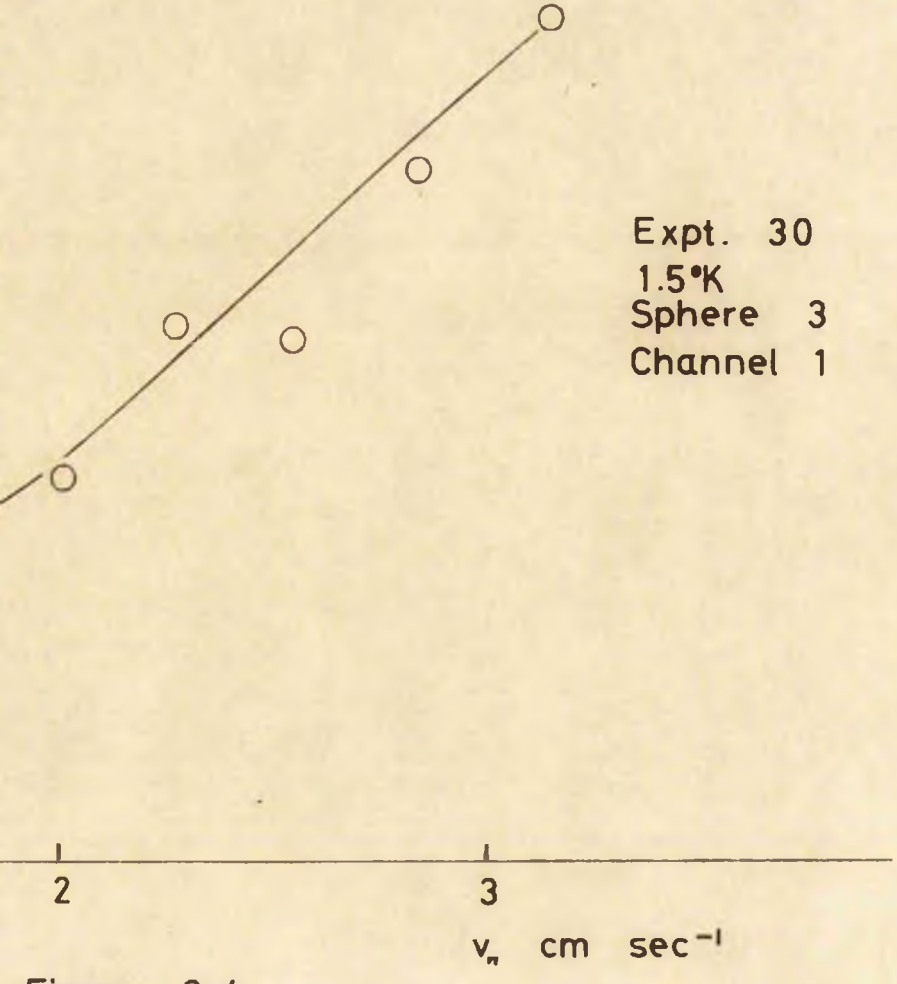

Figure 3.4

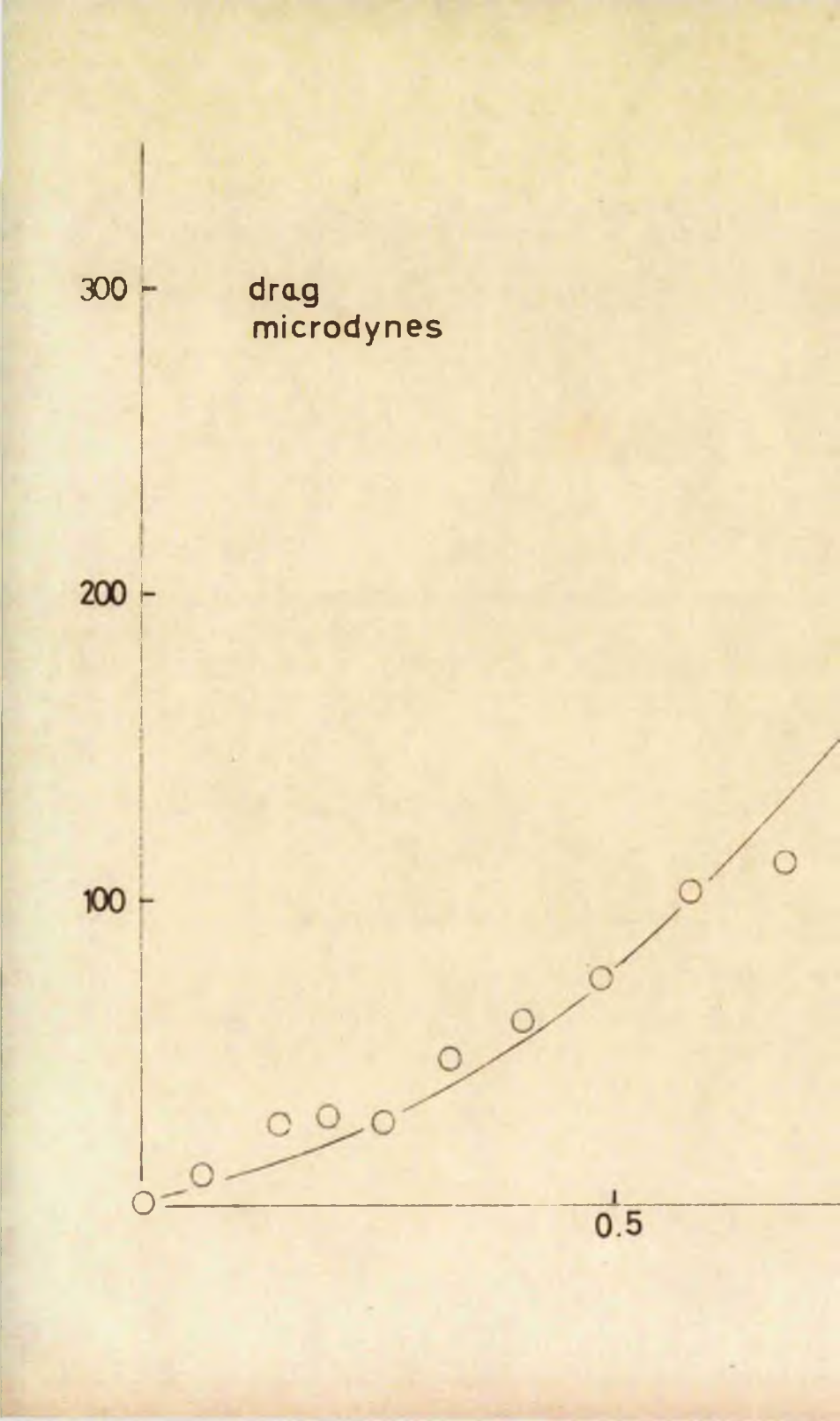
300
drag
microdynes
200
100
0.5

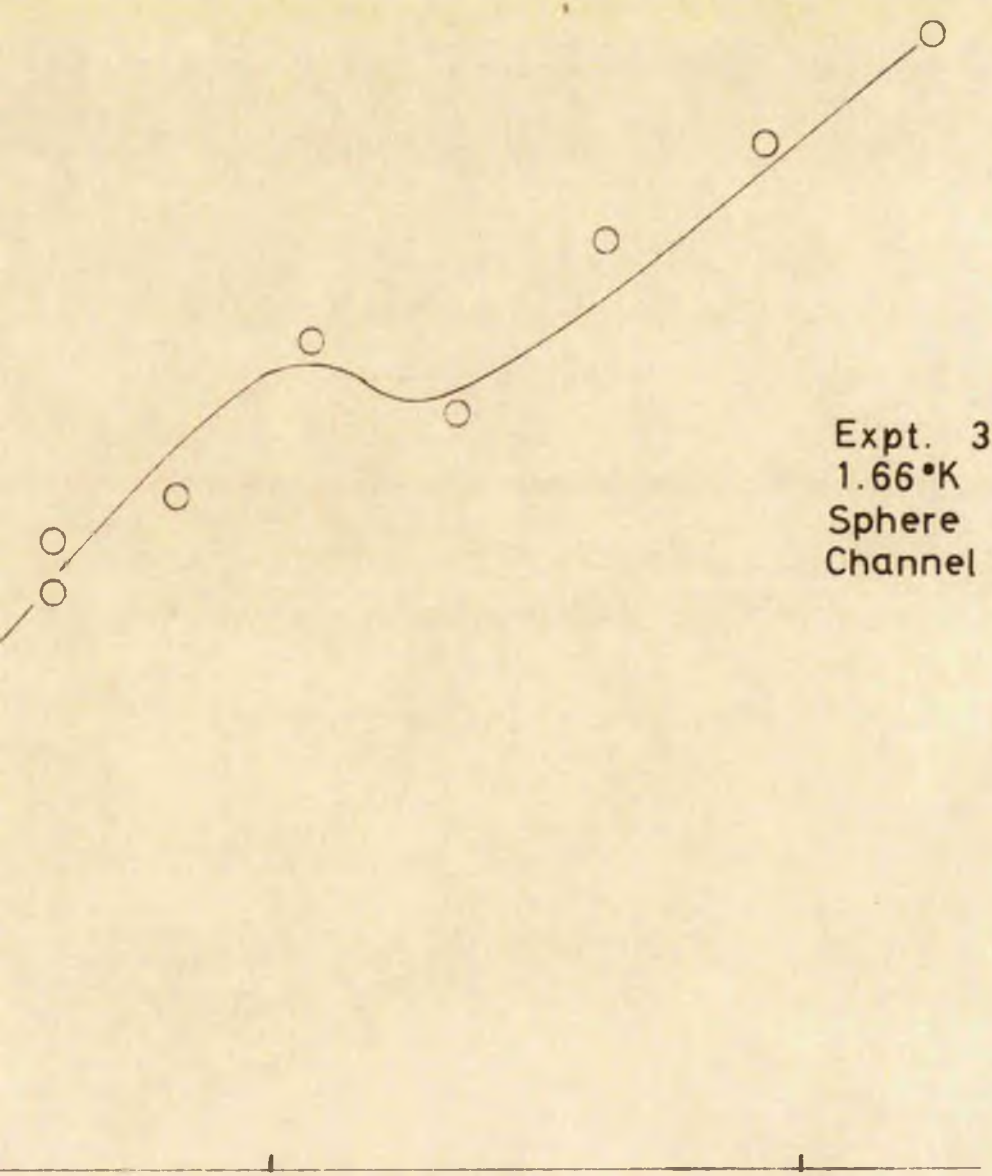

Figure 3.5

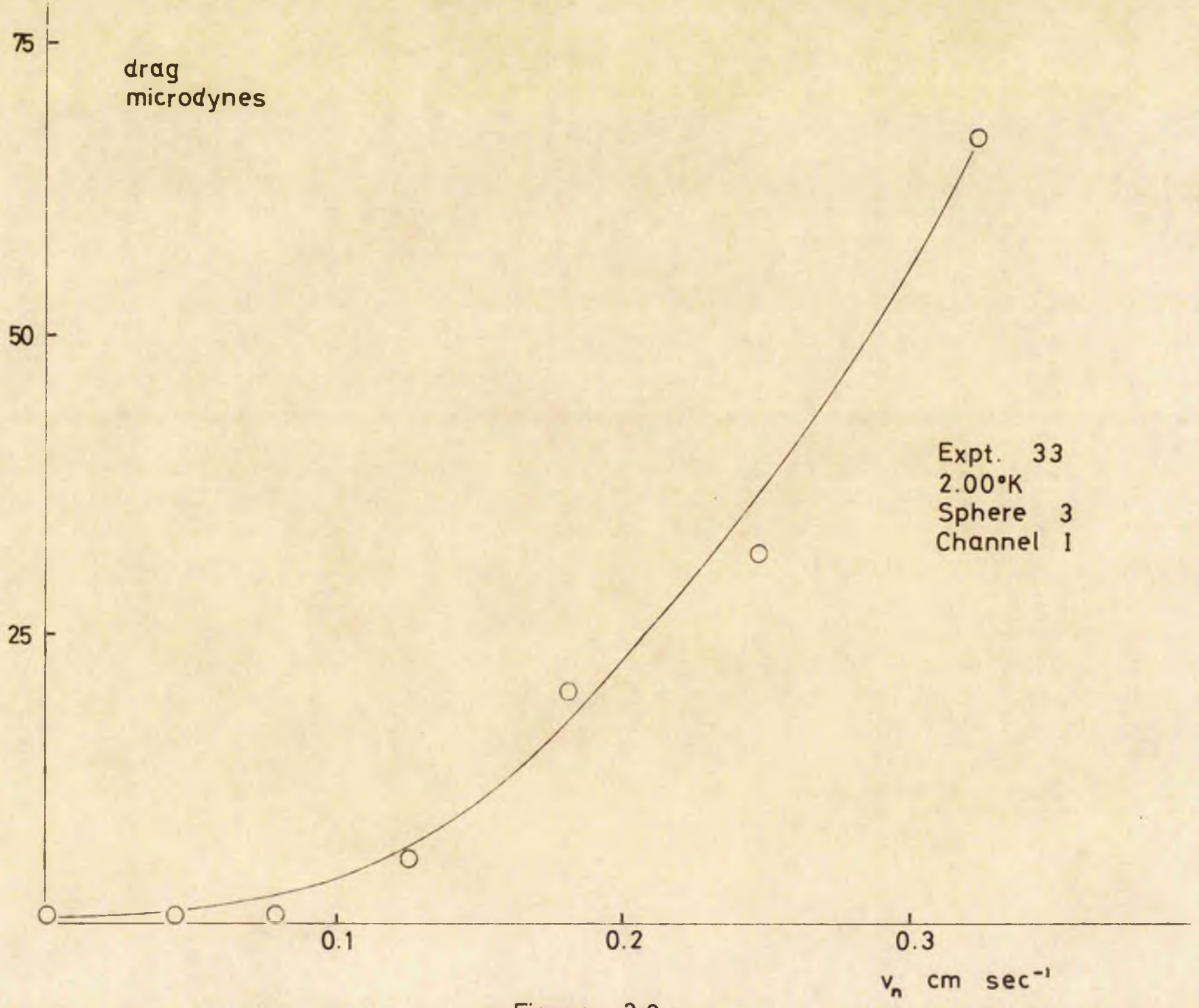
75
drag
microdynes
50
25
Expt. 33
2.00°K
Sphere 3
Channel 1
0.1
0.2
0.3
v_n cm sec^{-1}

Figure 3.6

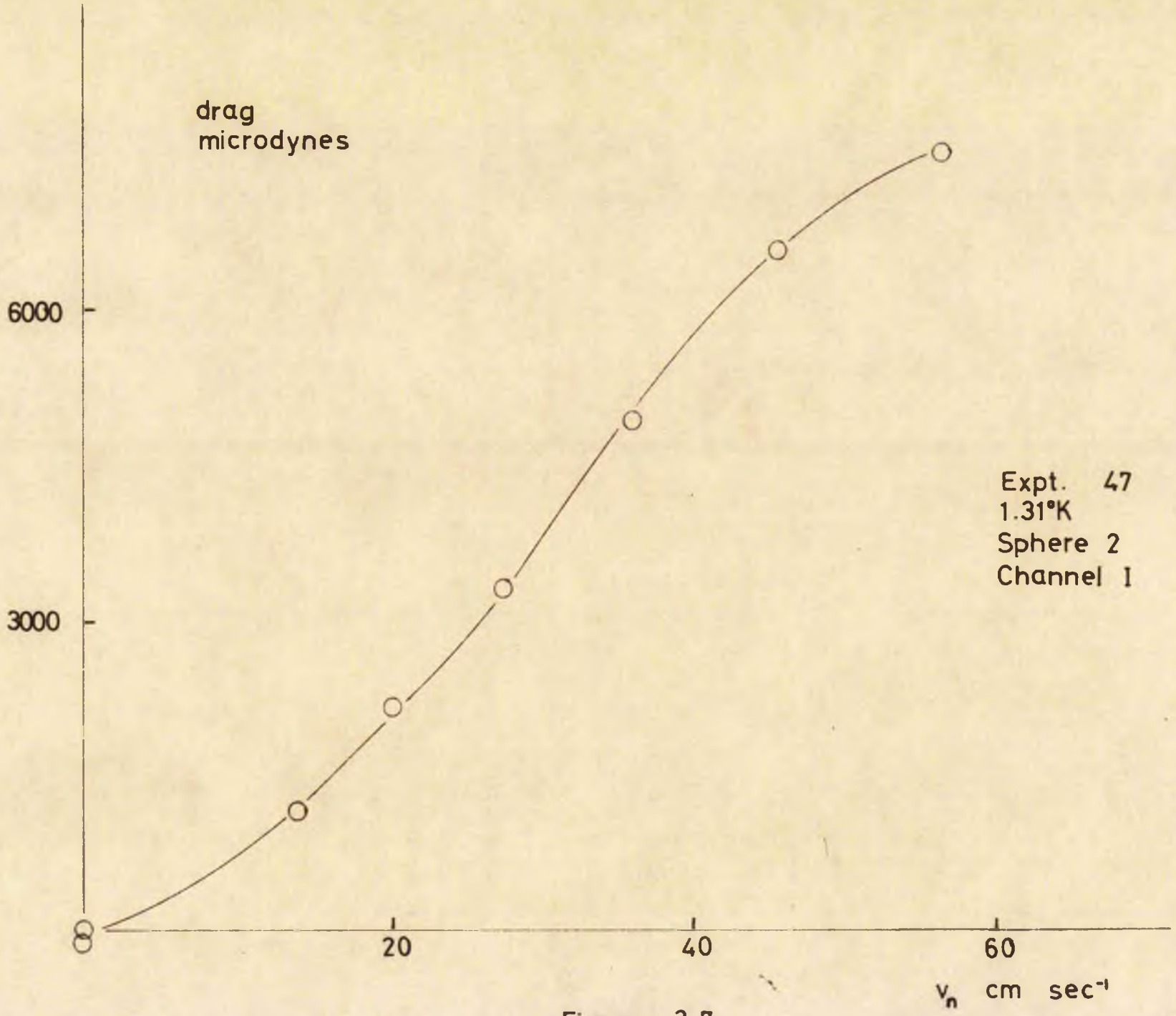
drag
microdynes
6000
3000
0
20
40
60
v_n cm sec^{-1}
Expt. 47
1.31°K
Sphere 2
Channel 1

Figure 3.7

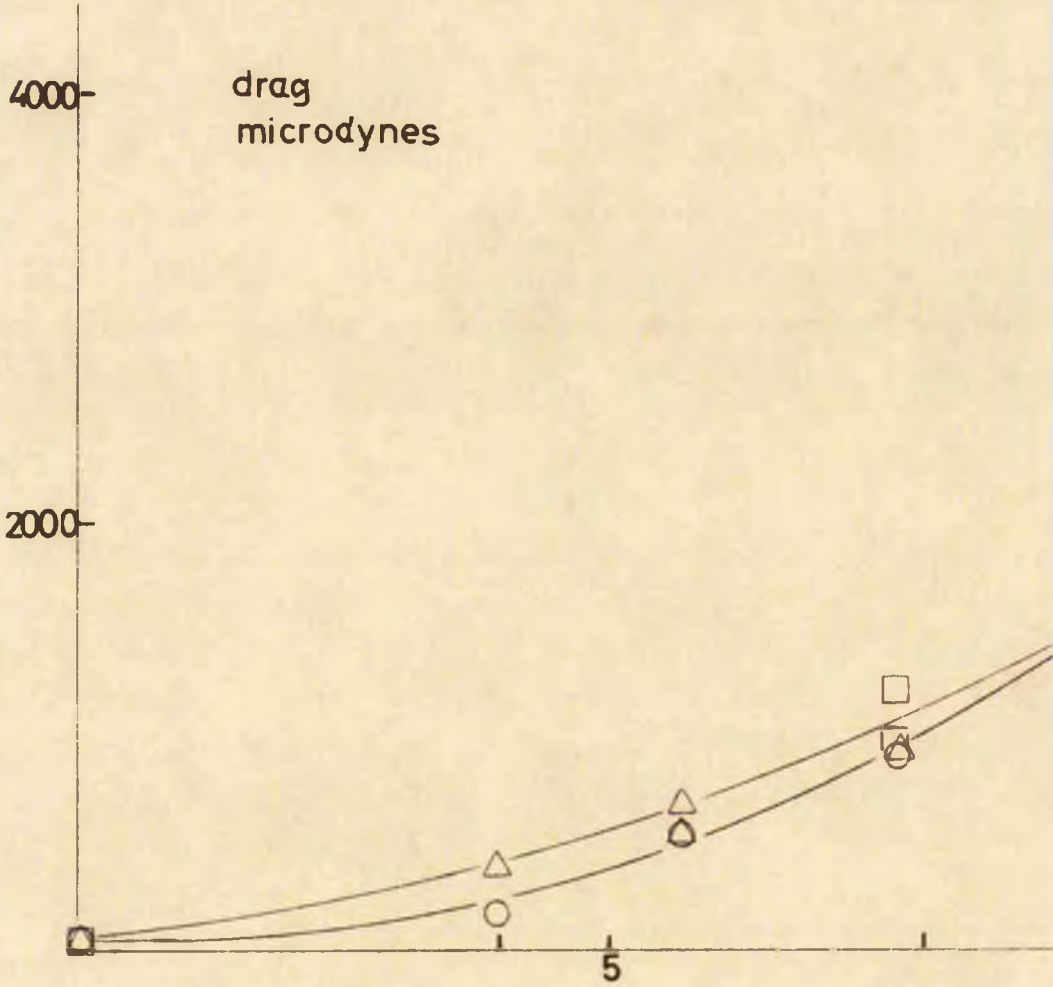

Figure

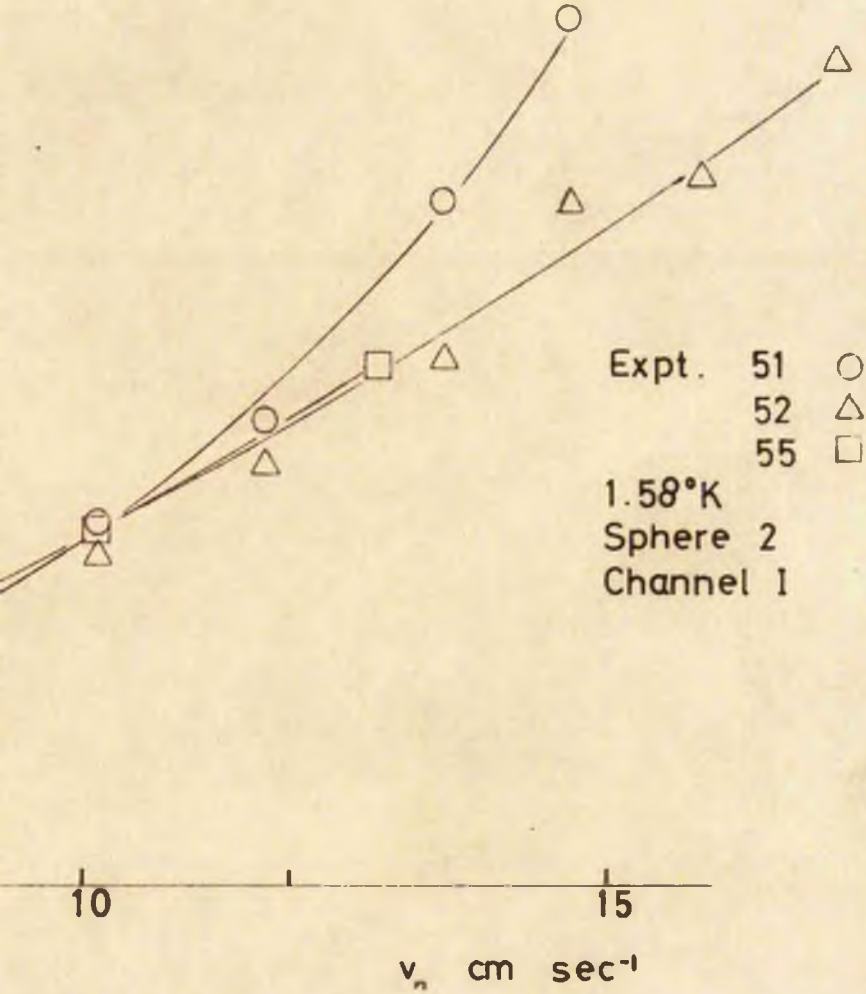

3.8

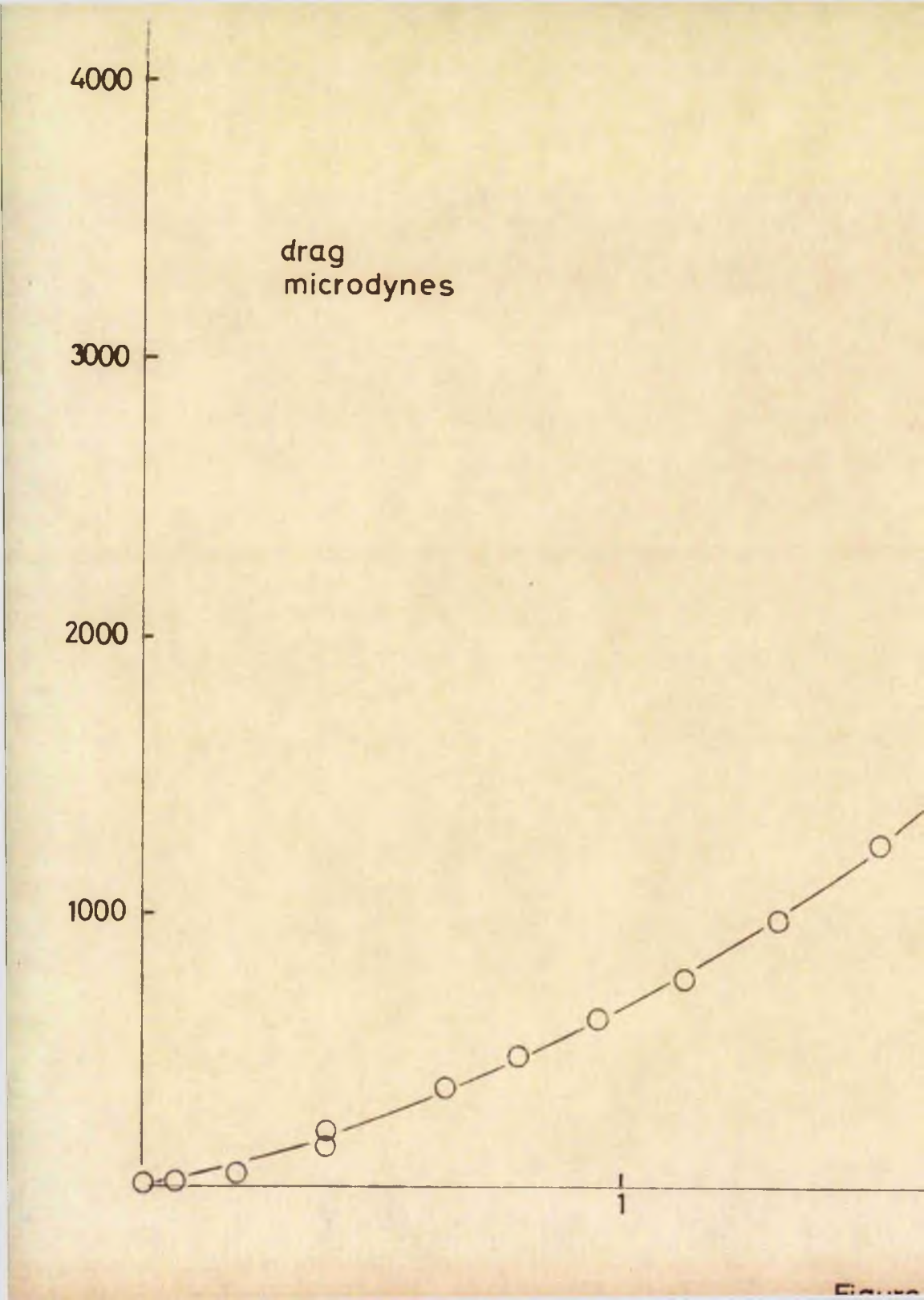
4000
drag
microdynes
3000
2000
1000
1

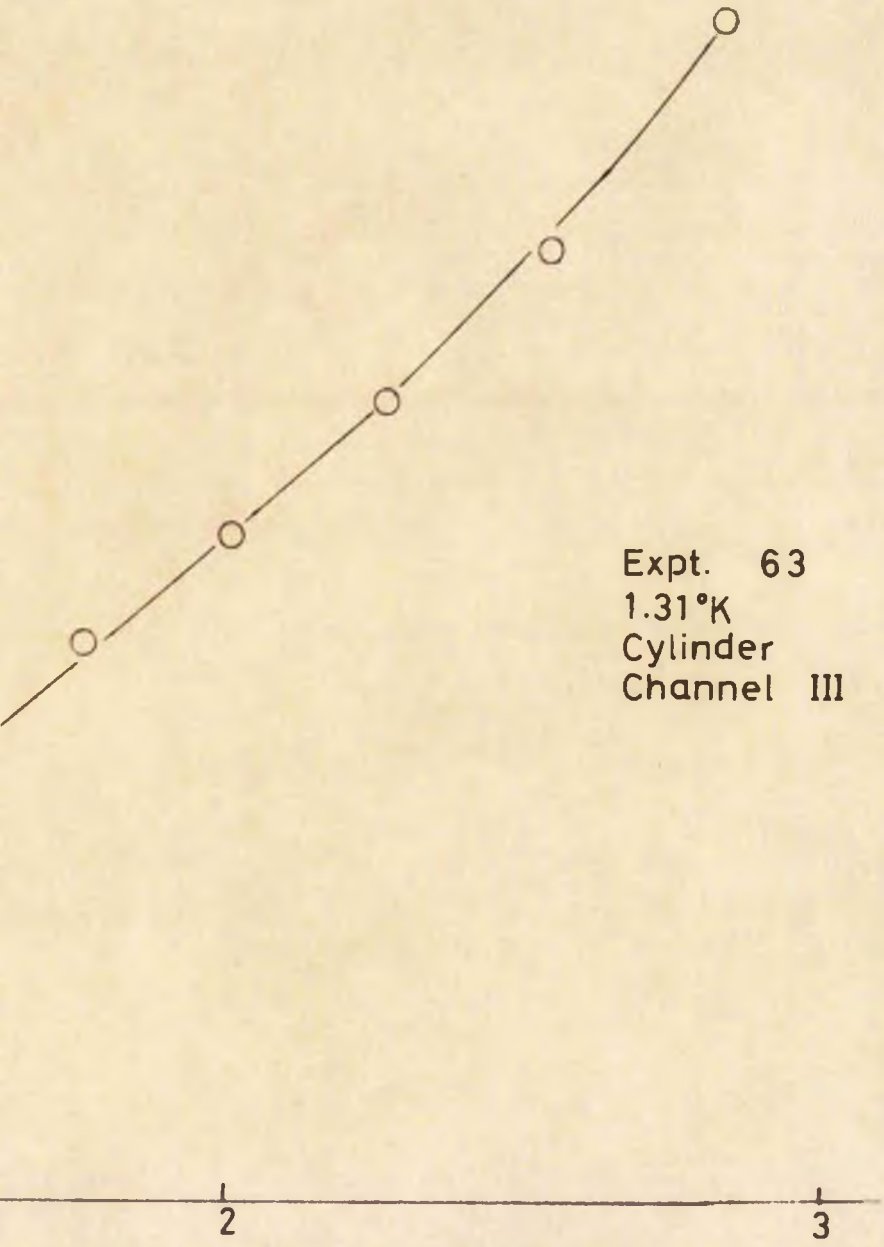
Expt. 63
1.31°K
Cylinder
Channel III
2
3
v_n cm sec^{-1}

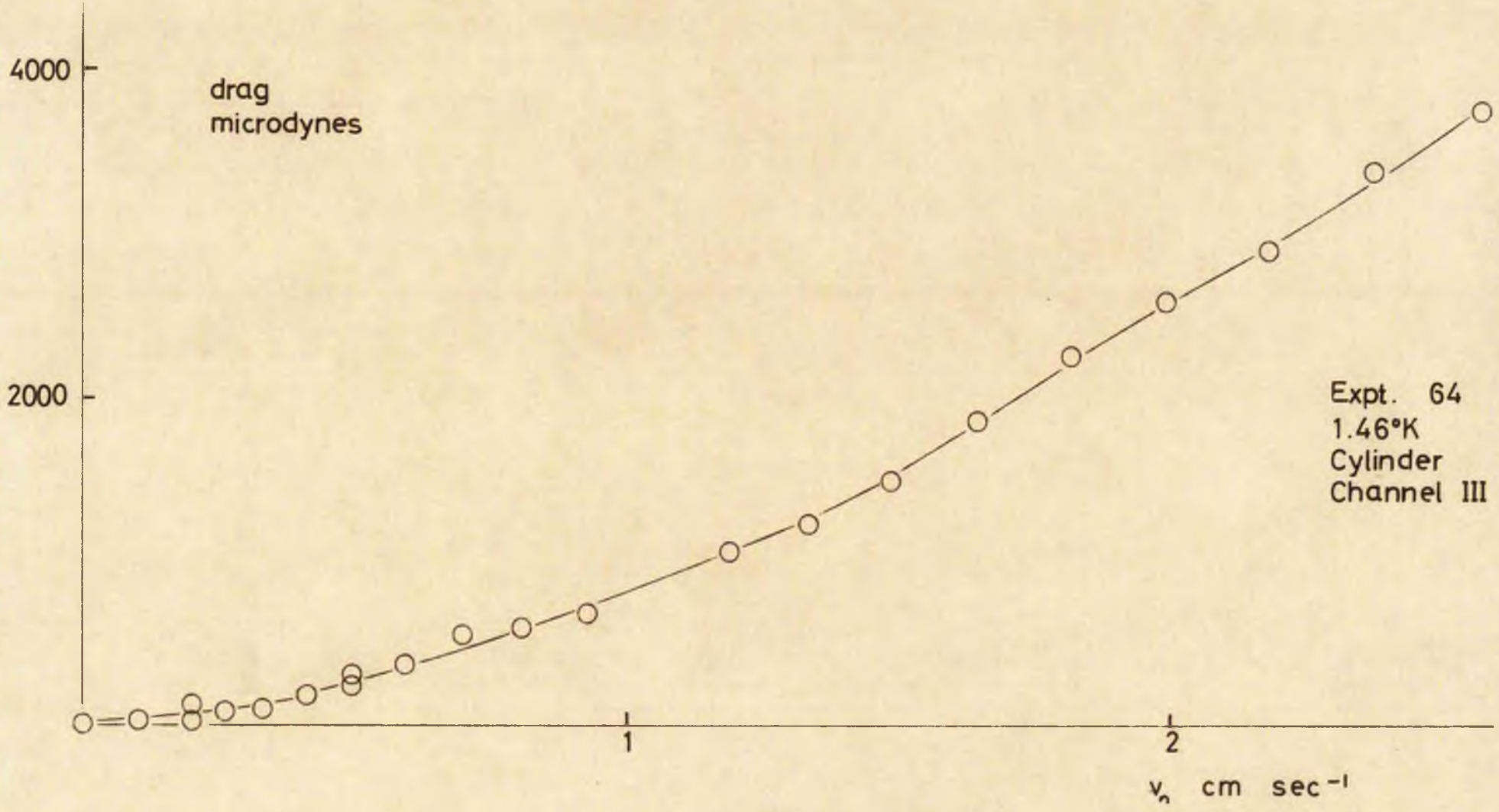
4000
drag
microdynes
2000
Expt. 64
1.46°K
Cylinder
Channel III
1
2
v_n cm sec^{-1}

Figure 3.10

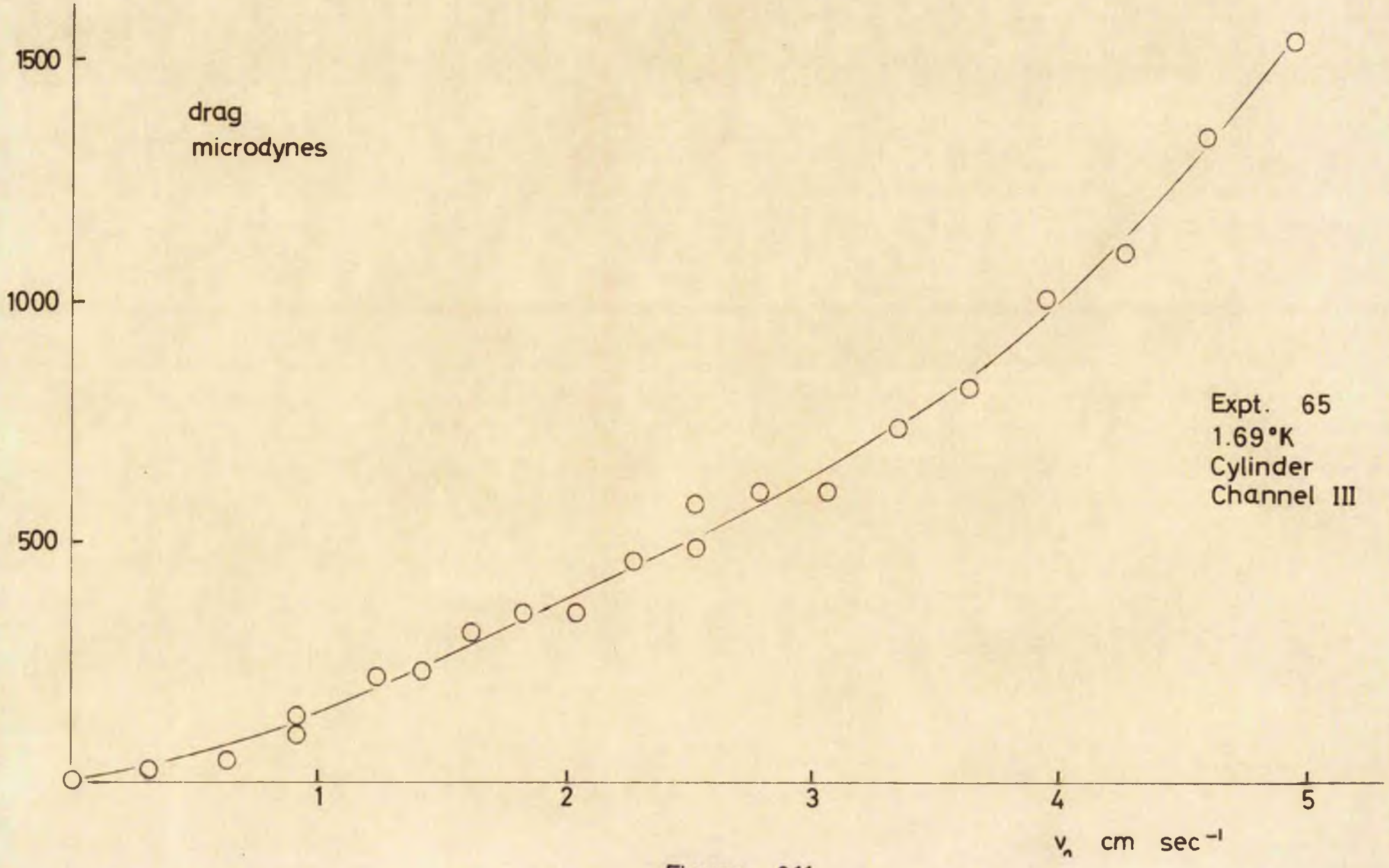
1500
1000
500
drag
microdynes
Expt. 65
1.69°K
Cylinder
Channel III
1
2
3
4
5
v_n cm sec^{-1}

Figure 3.11

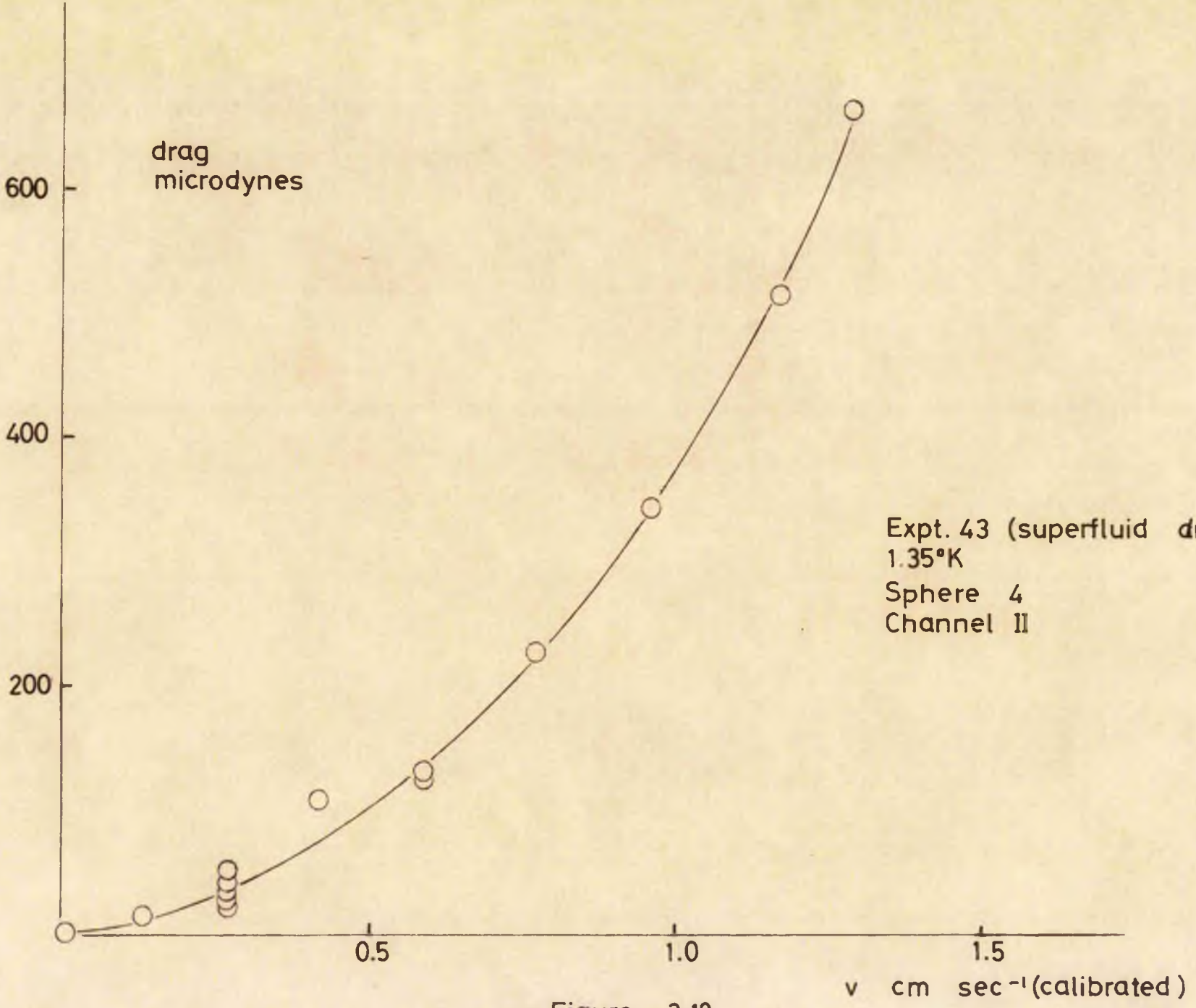
drag
microdynes
600
400
200
0.5
1.0
1.5
v cm sec⁻¹ (calibrated)
Expt. 43 (superfluid drag)
1.35°K
Sphere 4
Channel II

Figure 3.12

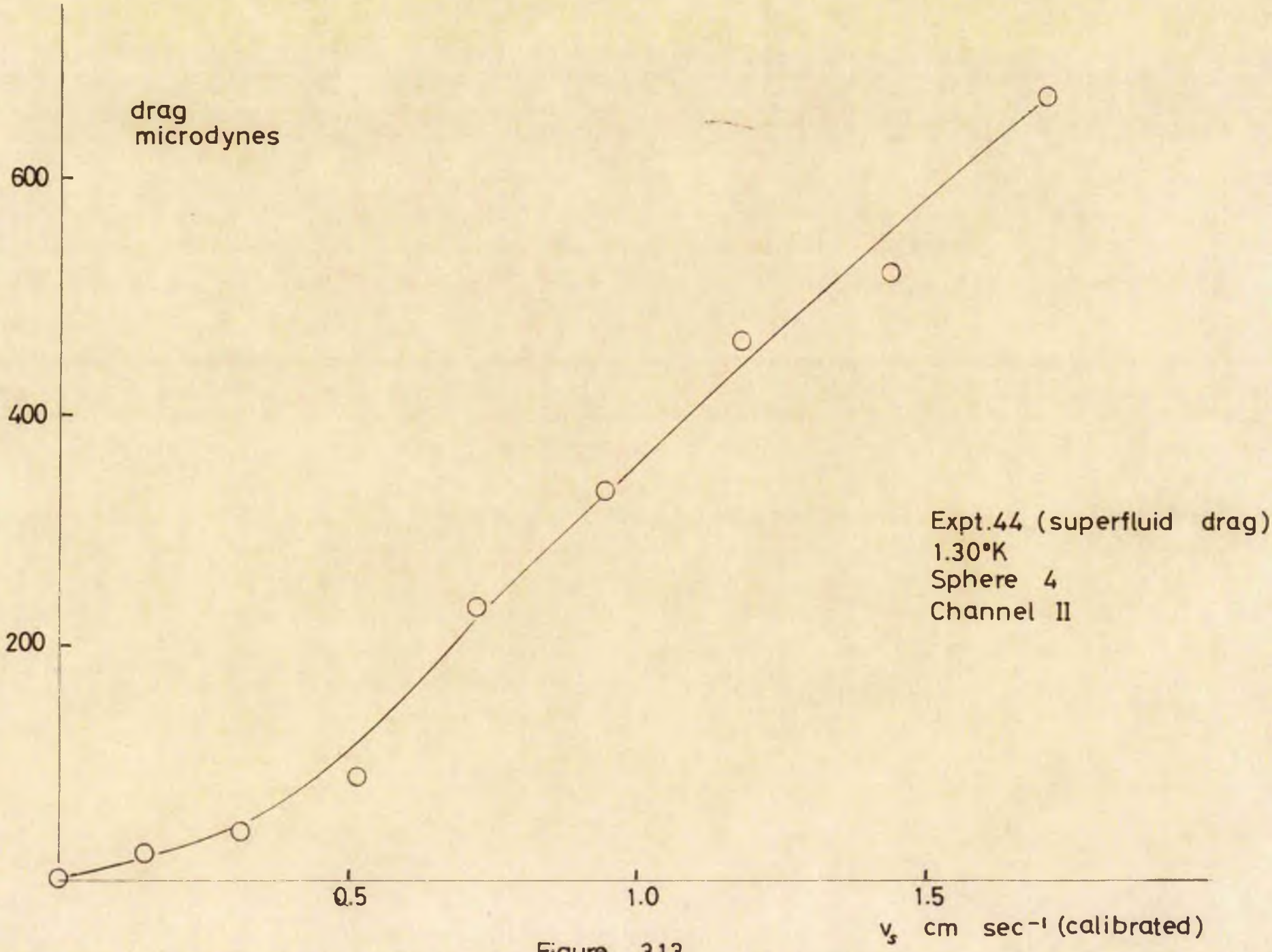
drag
microdynes
600
400
200
0.5
1.0
1.5
v_s cm sec^{-1} (calibrated)
Expt.44 (superfluid drag)
1.30°K
Sphere 4
Channel II

Figure 3.13

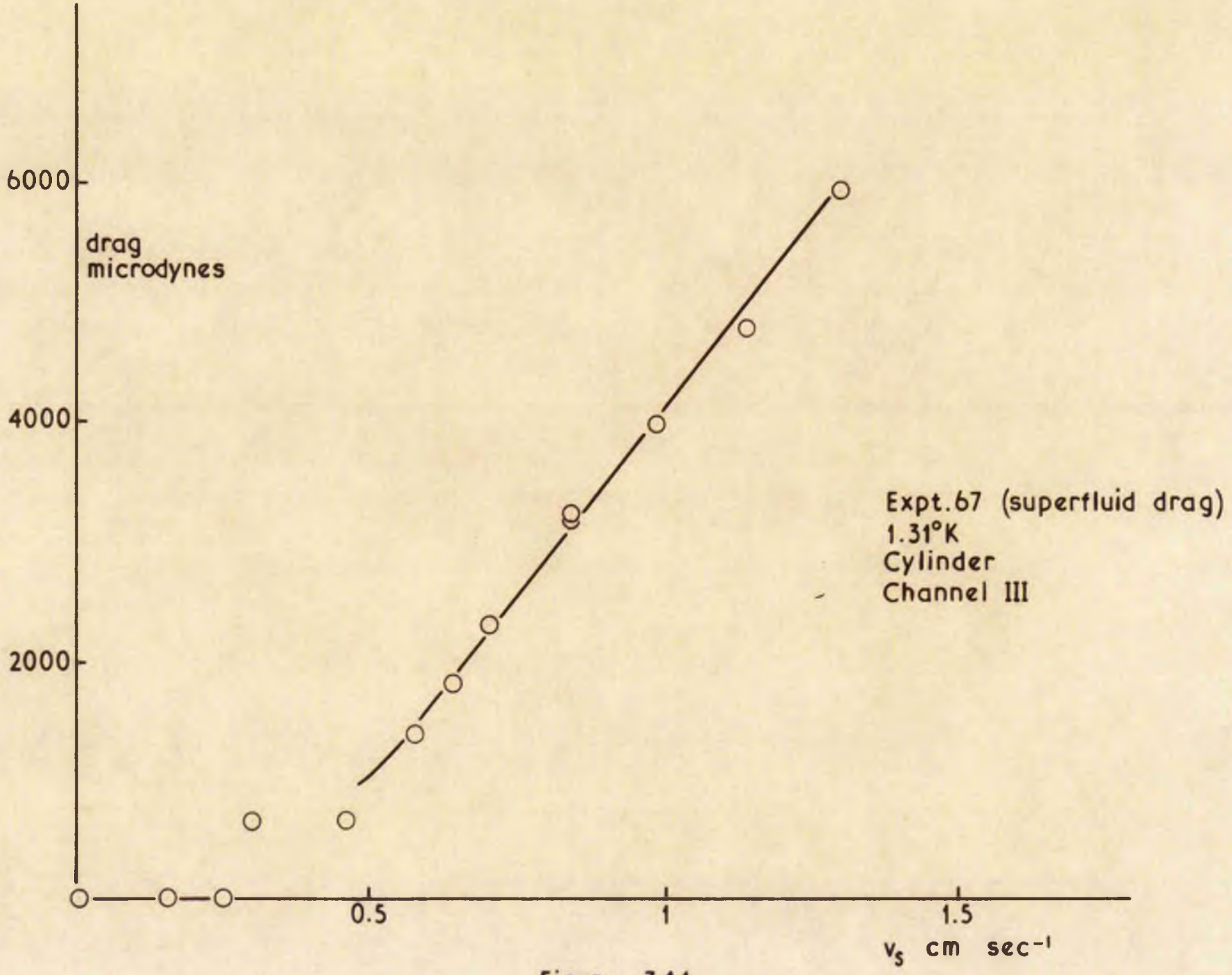
6000
4000
2000
drag
microdynes
0.5
1
1.5
v_s cm sec^{-1}
Expt.67 (superfluid drag)
1.31°K
Cylinder
Channel III

Figure 3.14

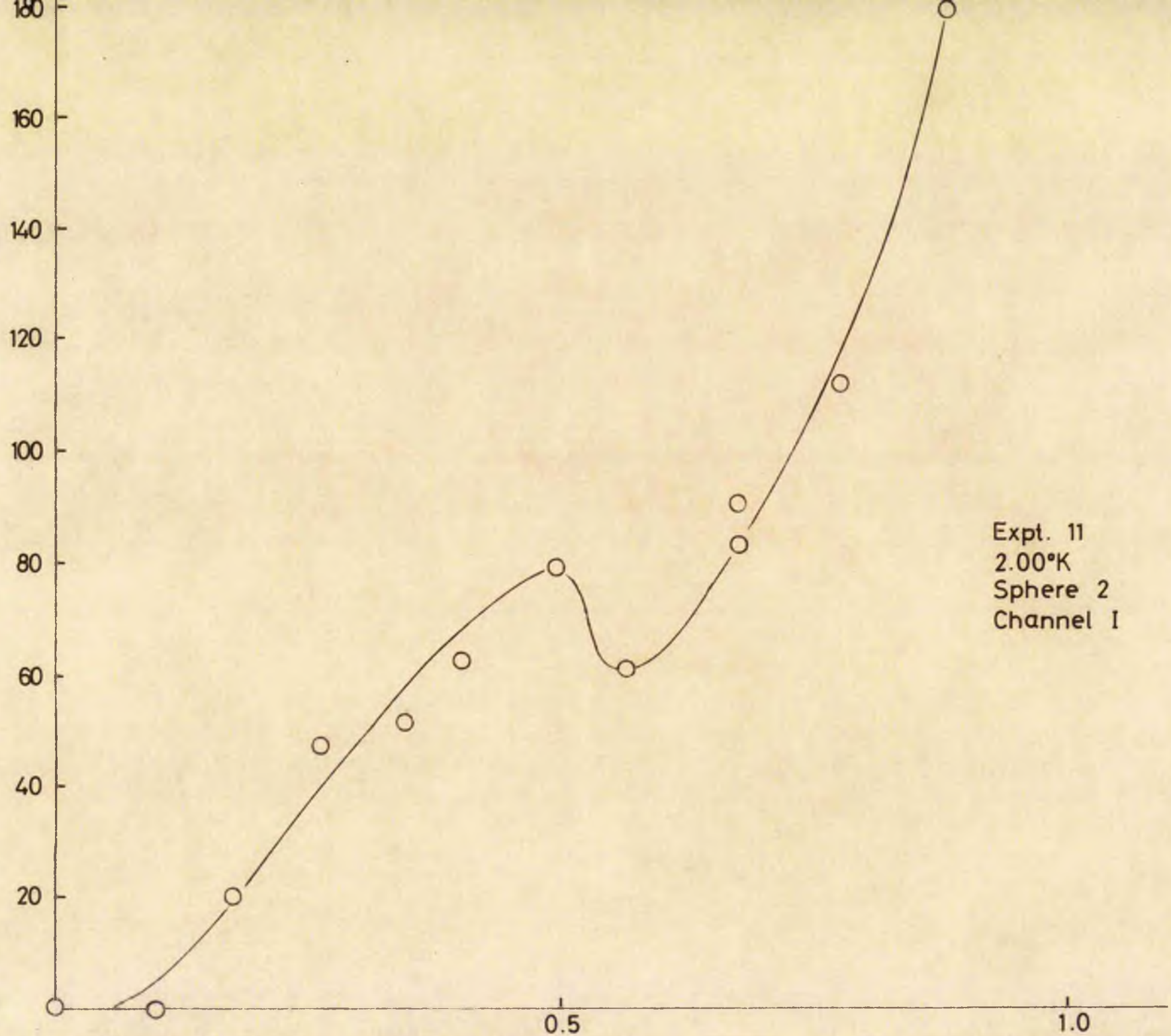

Figure 3.15 v cm sec^{-1}(approx.)

Figure

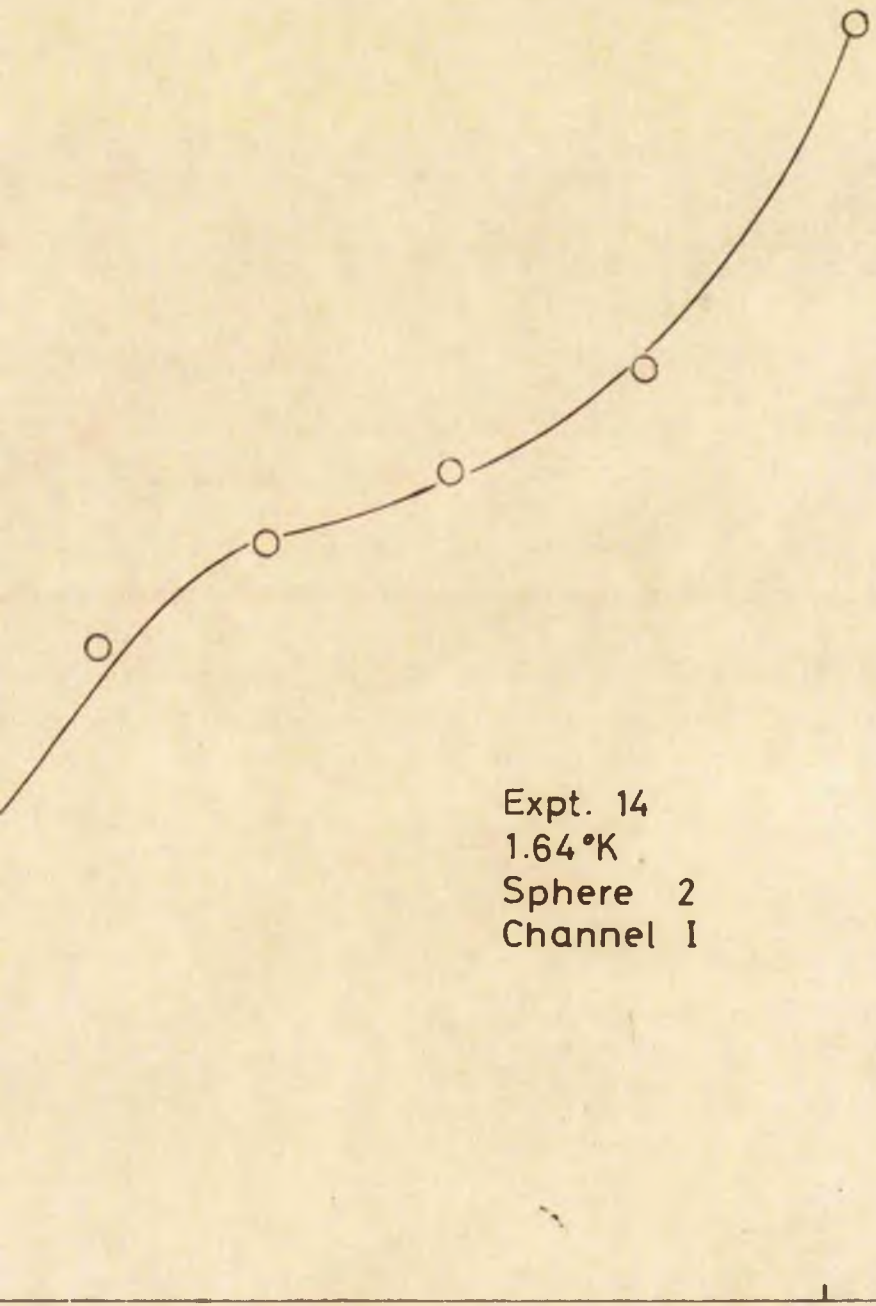
Expt. 14
1.64°K
Sphere 2
Channel I
2
v_n cm sec^{-1} (approx.)

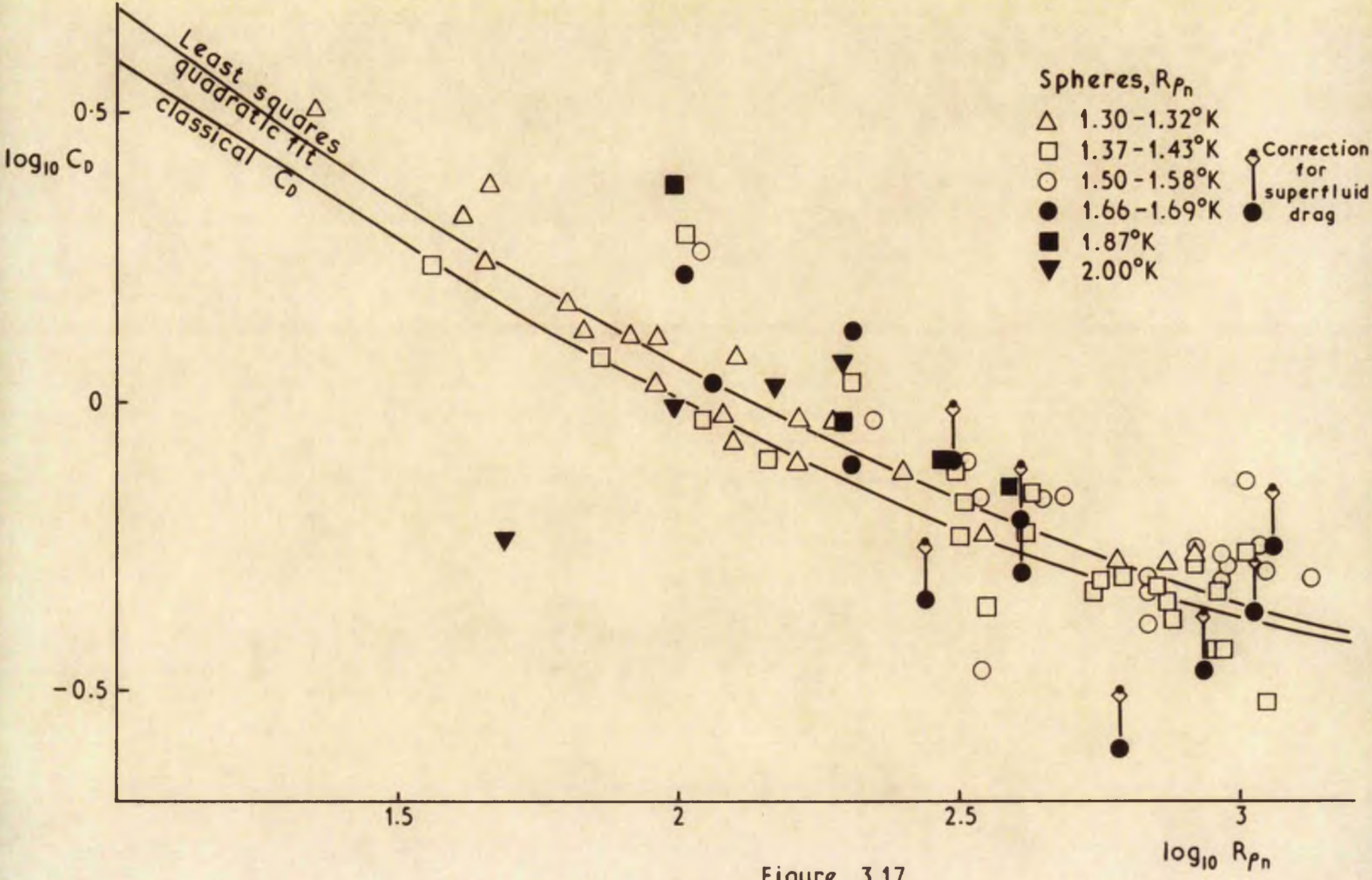
Least squares quadratic fit
classical C_D
$\log_{10} C_D$
0·5
0
−0.5
1.5
2
2.5
3
$\log_{10} R_{\rho n}$
Spheres, $R_{\rho n}$
1.30 - 1.32°K
1.37 - 1.43°K
1.50 - 1.58°K
1.66 - 1.69°K
1.87°K
2.00°K
Correction for superfluid drag

Figure 3.17

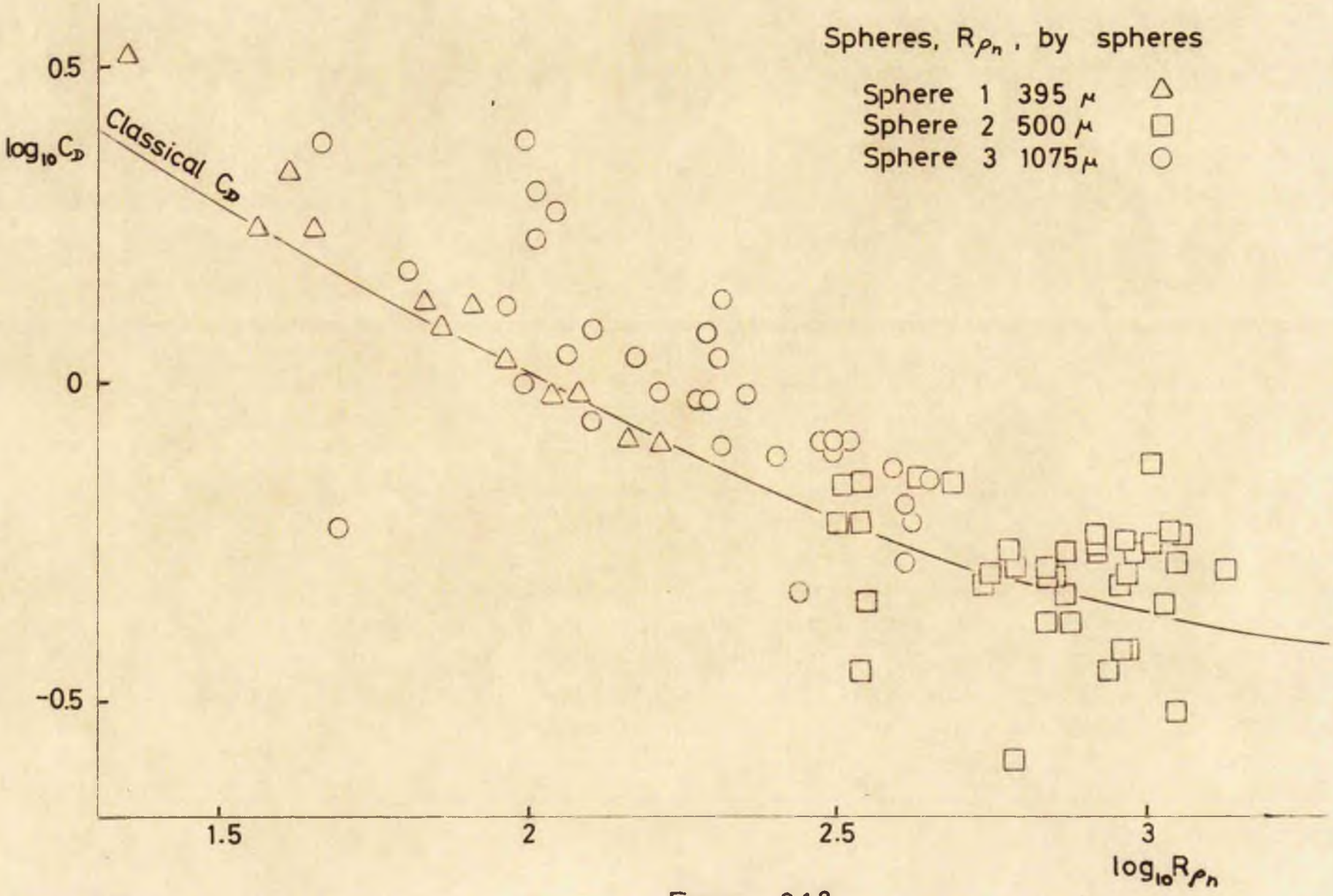
Spheres, R_{ρ_n}, by spheres
Sphere 1 395 μ
Sphere 2 500 μ
Sphere 3 1075 μ
Classical C_D
$\log_{10} C_D$
0.5
0
-0.5
1.5
2
2.5
3
$\log_{10} R_{\rho_n}$

Figure 3.18

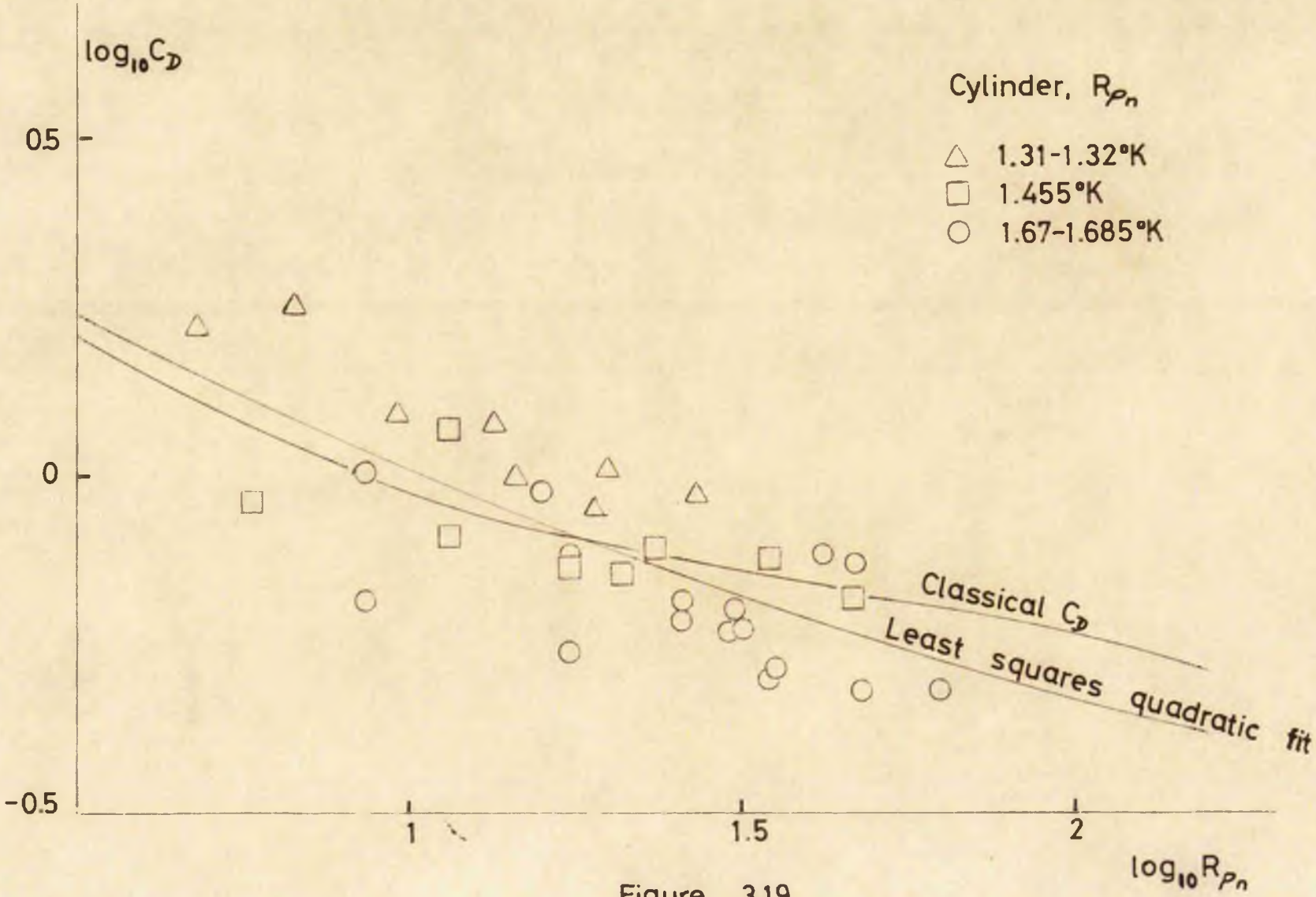
log10CD
0.5
0
-0.5
1
1.5
2
log10Rρn
Cylinder, Rρn
1.31-1.32°K
1.455°K
1.67-1.685°K
Classical CD
Least squares quadratic fit

Figure 3.19

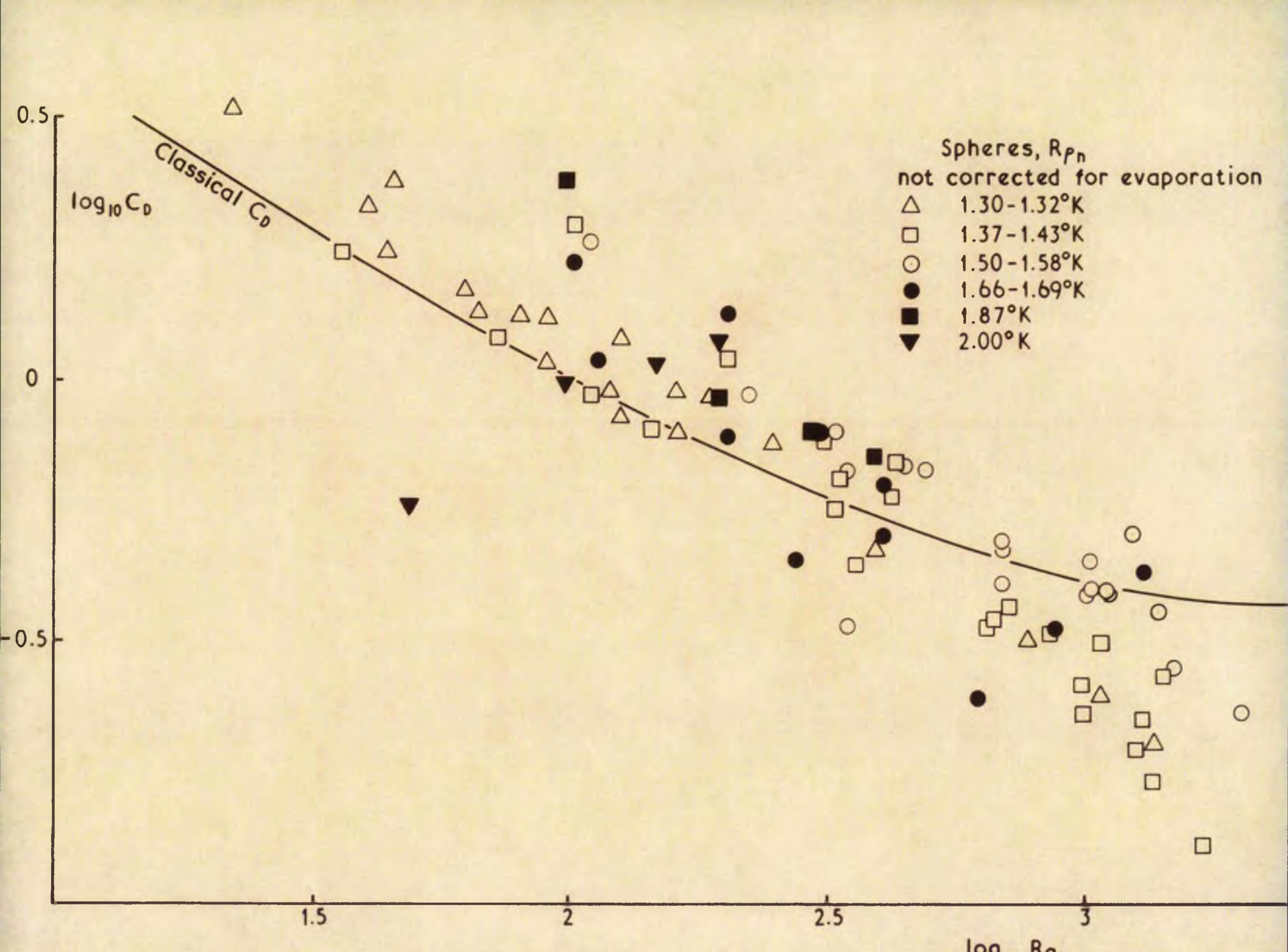
0.5
0
-0.5
$\log_{10} C_D$
Classical C_D
Spheres, $R_{\rho n}$
not corrected for evaporation
1.30-1.32°K
1.37-1.43°K
1.50-1.58°K
1.66-1.69°K
1.87°K
2.00°K
1.5
2
2.5
3
$\log_{10} R_{\rho n}$

Figure 3.20

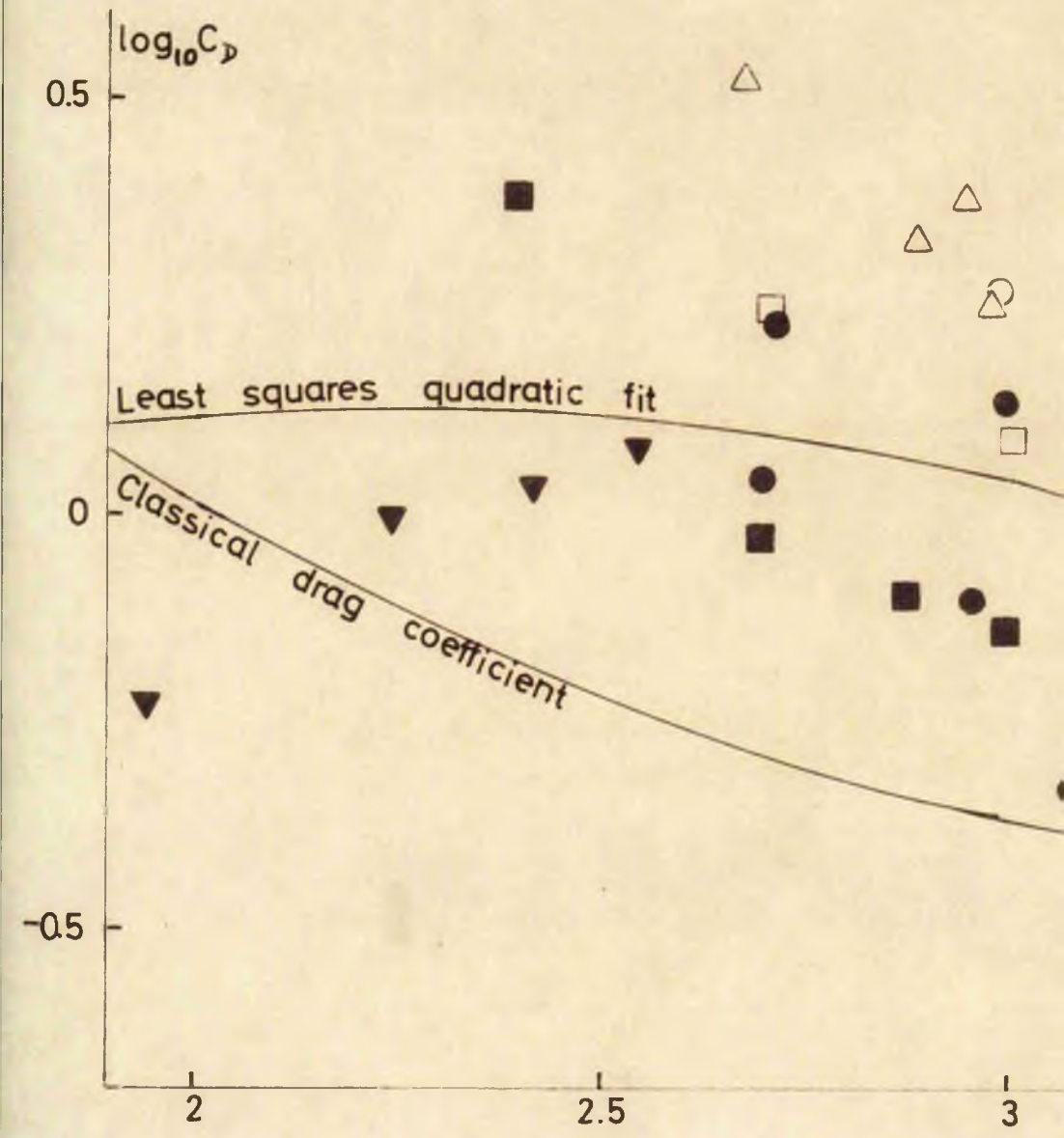
$\log_{10} C_D$
0.5
0
-0.5
Least squares quadratic fit
Classical drag coefficient
2
2.5
3

Figure

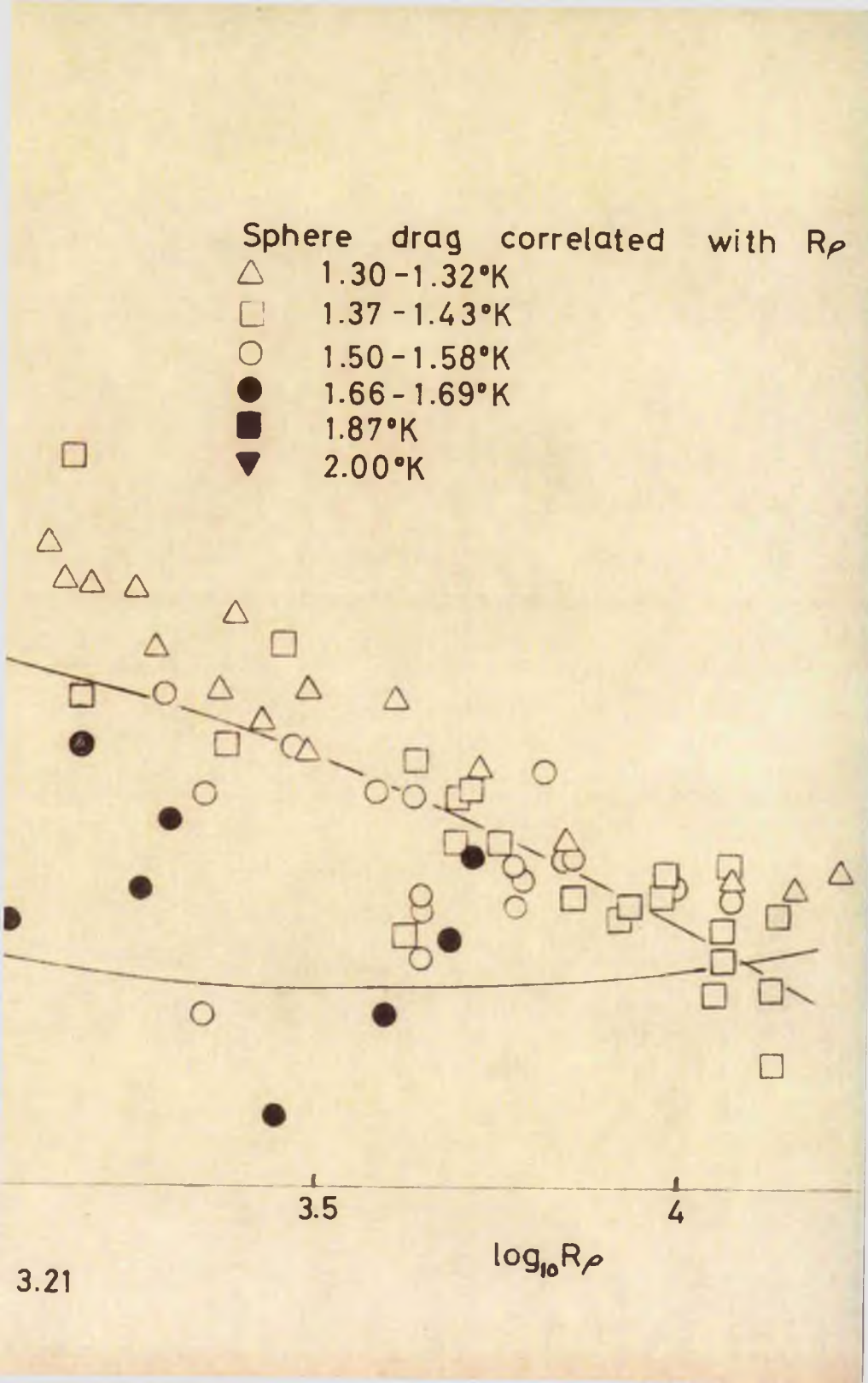
Sphere drag correlated with R_ρ
1.30 - 1.32°K
1.37 - 1.43°K
1.50 - 1.58°K
1.66 - 1.69°K
1.87°K
2.00°K
3.5
4
$\log_{10} R_\rho$

3.21

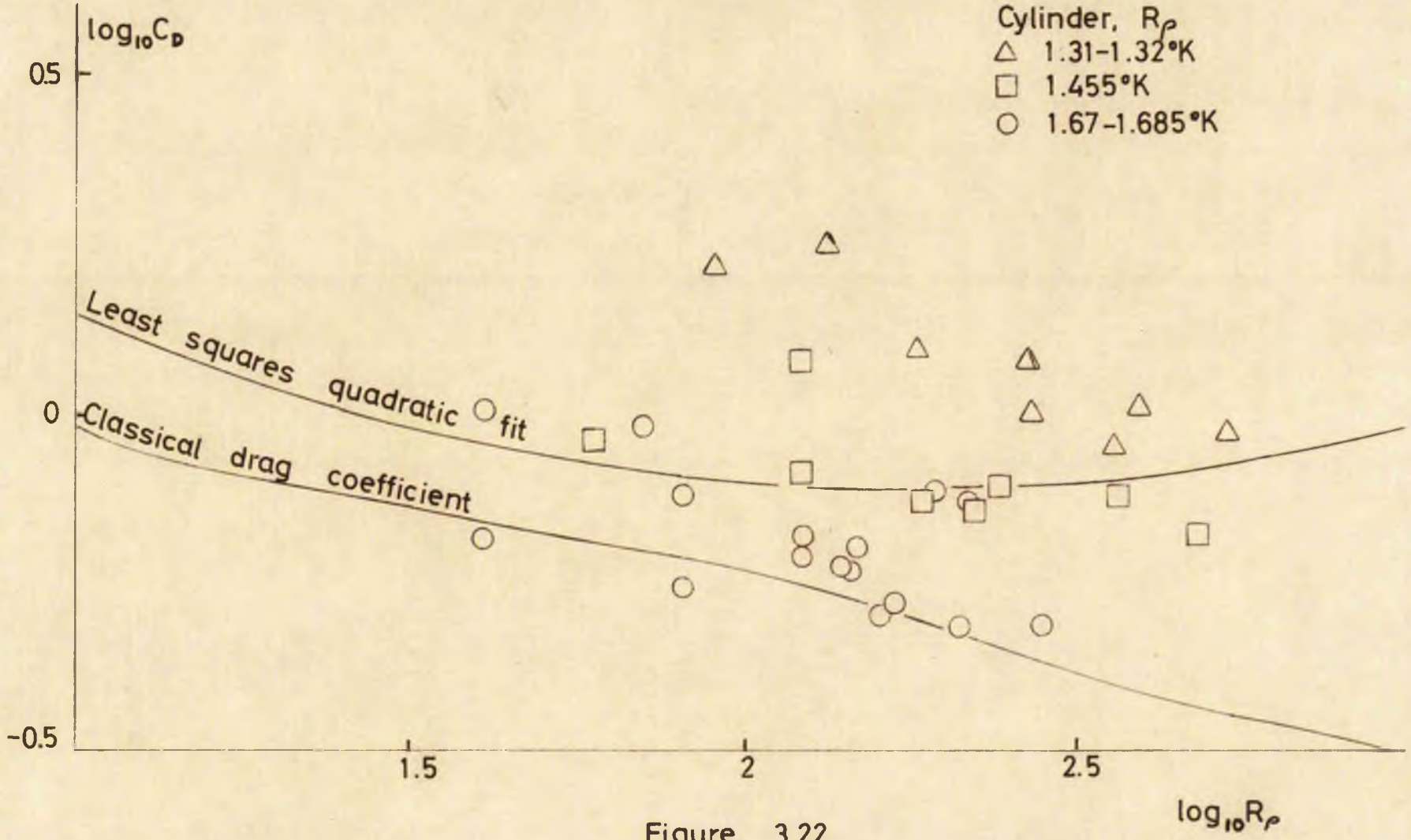
log10CD
0.5
0
-0.5
1.5
2
2.5
log10Rρ
Cylinder, Rρ
△ 1.31-1.32°K
□ 1.455°K
○ 1.67-1.685°K
Least squares quadratic fit
Classical drag coefficient

Figure 3.22

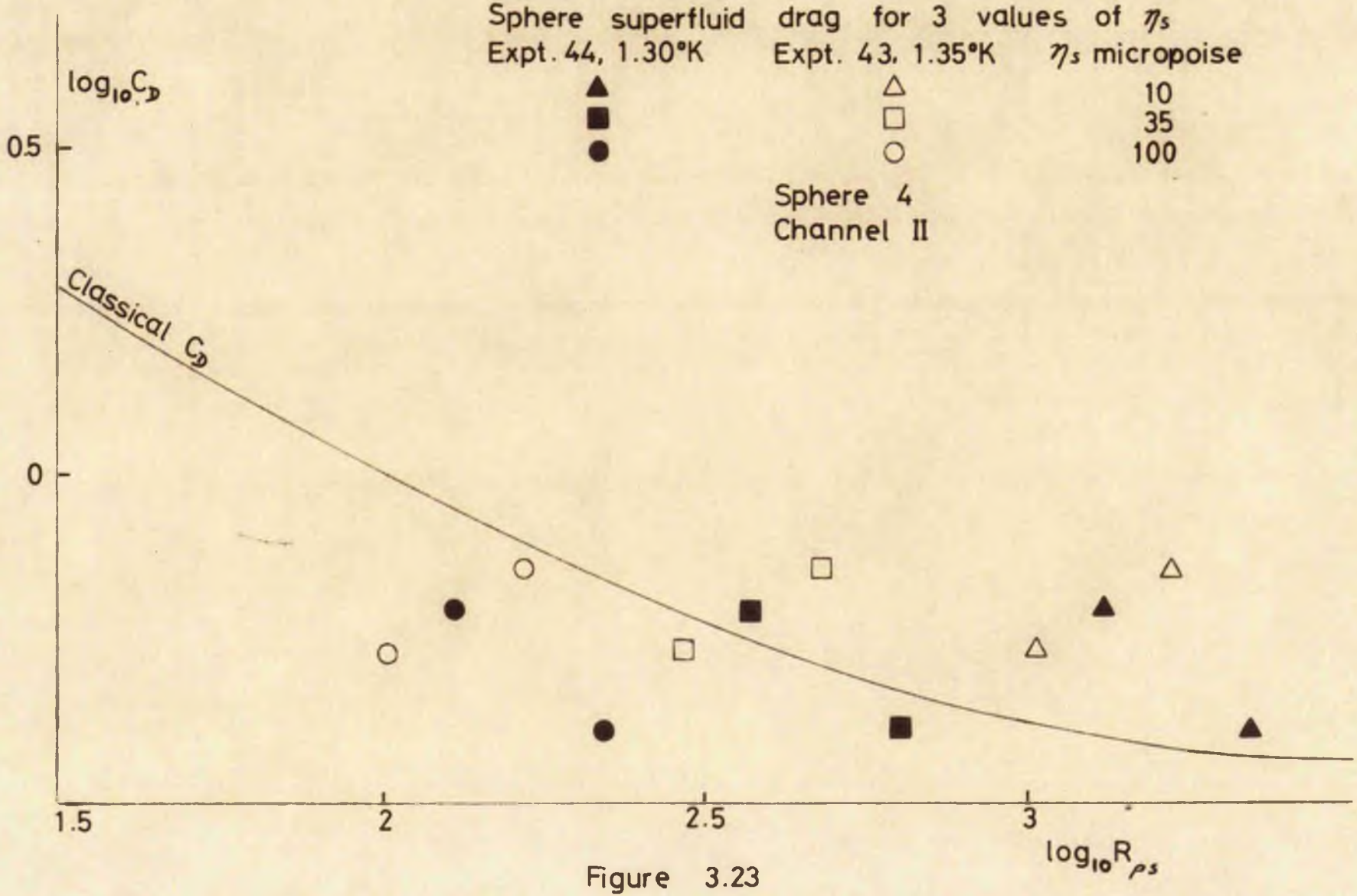
Sphere superfluid drag for 3 values of η_s
Expt. 44, 1.30°K
Expt. 43, 1.35°K
η_s micropoise
10
35
100
Sphere 4
Channel II
$\log_{10} C_D$
0.5
0
Classical C_D
1.5
2
2.5
3
$\log_{10} R_{ps}$

Figure 3.23

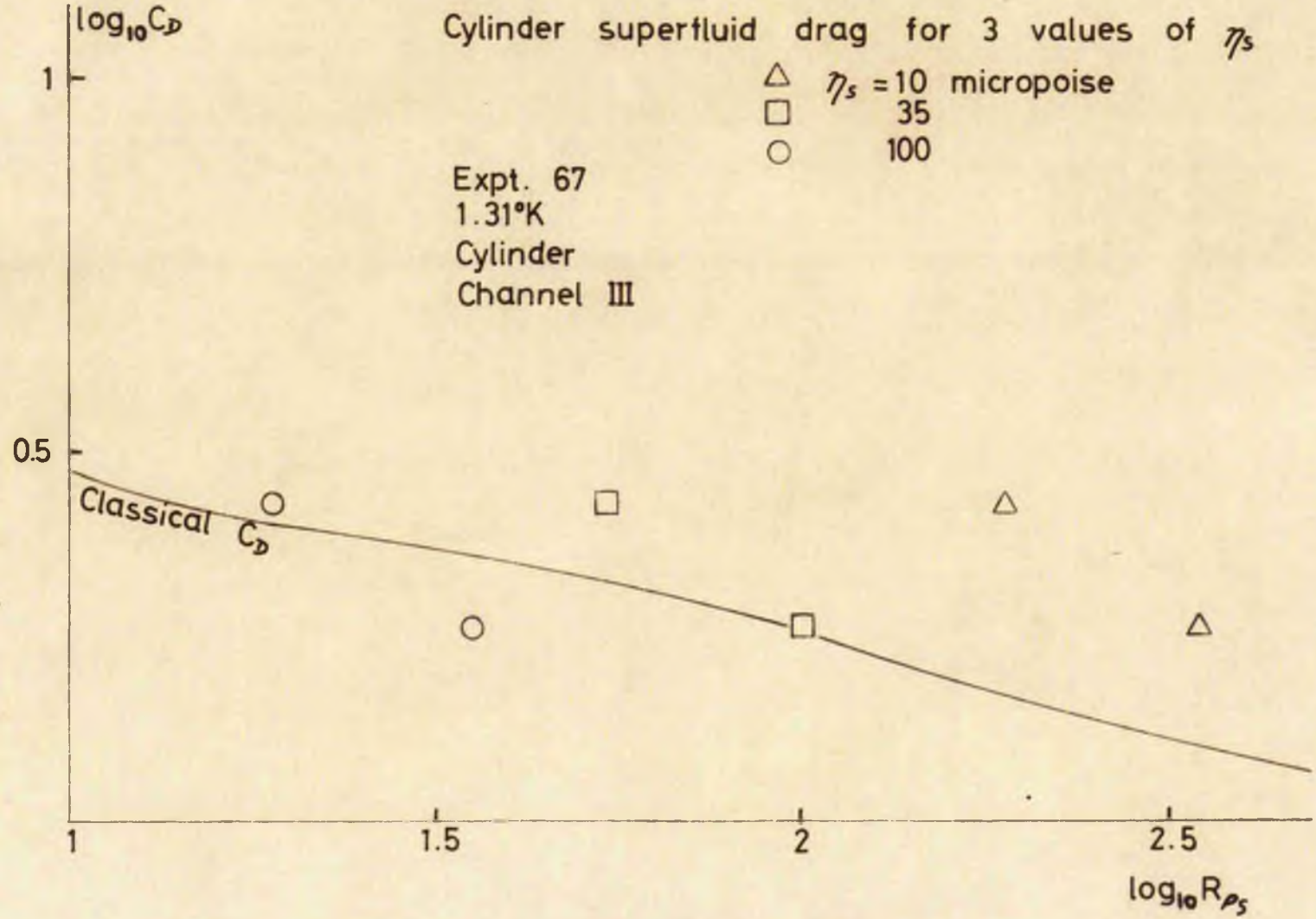
$\log_{10} C_D$
Cylinder superfluid drag for 3 values of η_s
η_s = 10 micropoise
35
100
Expt. 67
1.31°K
Cylinder
Channel III
1
0.5
Classical C_D
1
1.5
2
2.5
$\log_{10} R_{\rho_s}$

Figure 3.24

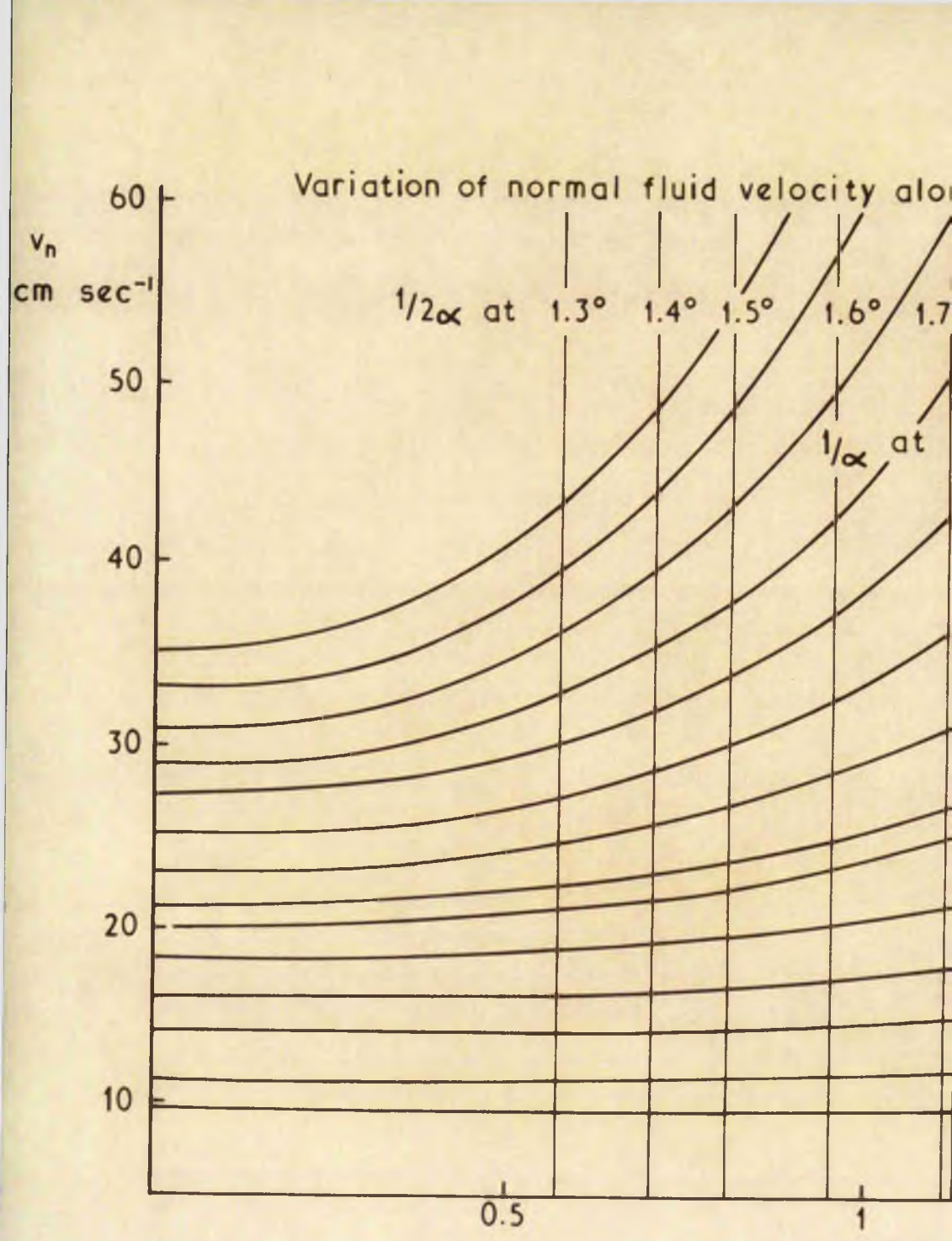
Variation of normal fluid velocity alo
v_n
cm sec^{-1}
60
50
40
30
20
10
$1/2\alpha$ at 1.3° 1.4° 1.5° 1.6° 1.7
$1/\alpha$ at
0.5
1

Figu

ng Channel I, $c = 1/9$

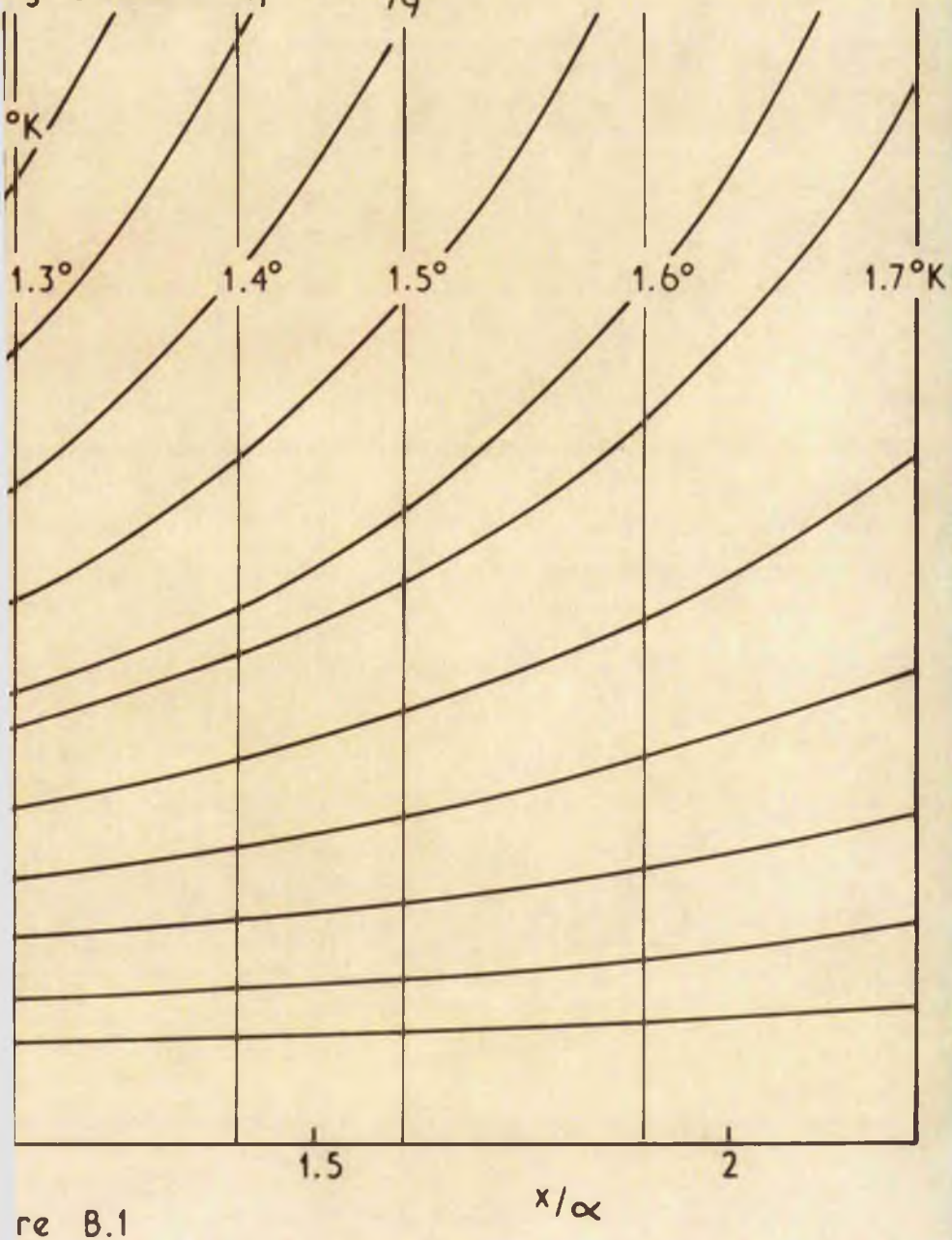

re B.1

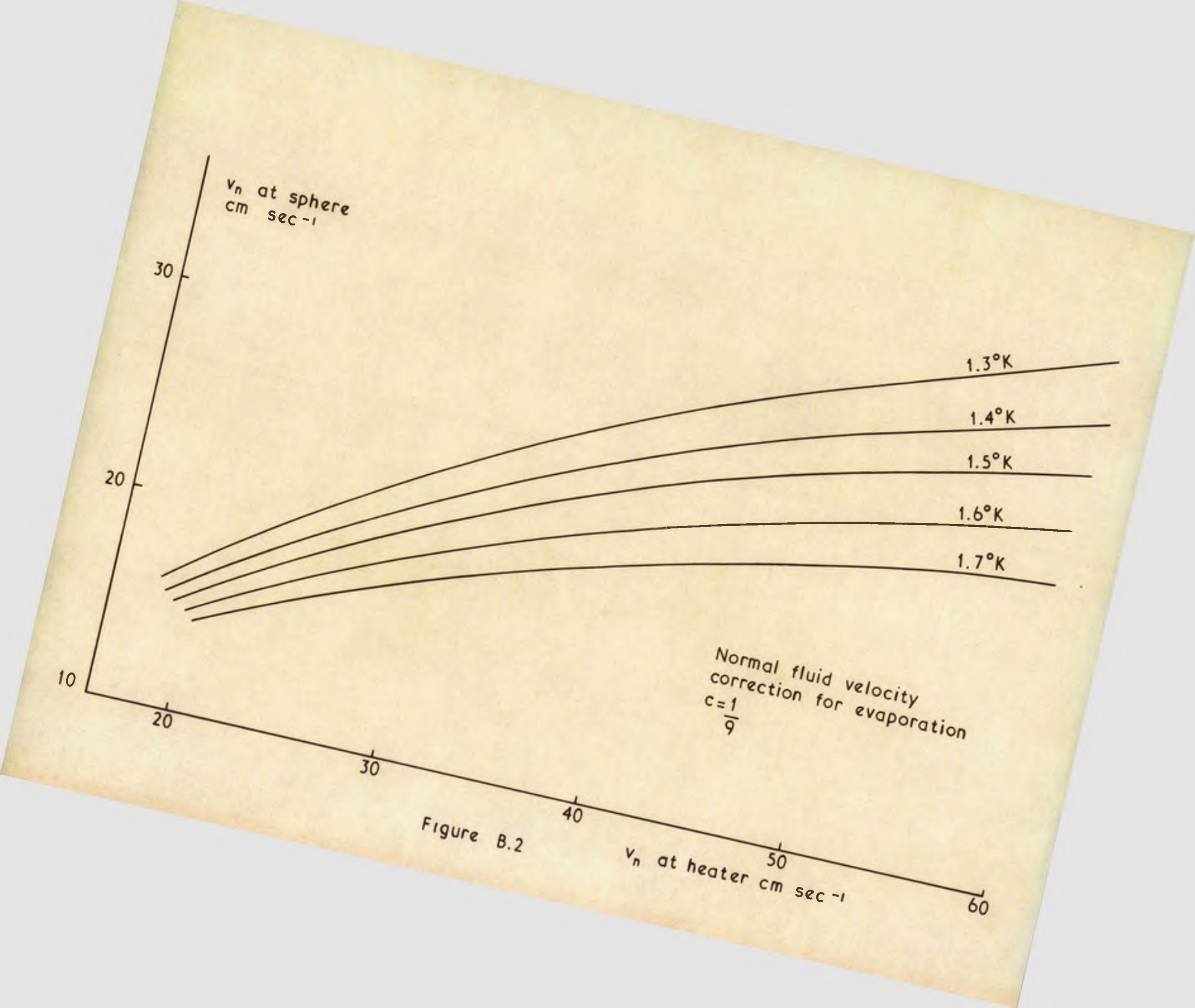
v_n at sphere
cm sec^{-1}
30
20
10
1.3°K
1.4°K
1.5°K
1.6°K
1.7°K
Normal fluid velocity
correction for evaporation
$c = \frac{1}{9}$
20
30
40
50
60
v_n at heater cm sec^{-1}

Figure B.2